Interferometry in Diffusive Systems: Theory, Limitations to Its Practical Application, and Its Use in Bayesian Estimation of Material Properties

Sharmin Shamsalsadati

Dissertation submitted to the faculty of the Virginia Polytechnic Institute and State University in partial fulfillment of the requirements for the degree of

Doctor of Philosophy
in
Geosciences

Chester J. Weiss, Chair
John A. Hole
Martin C. Chapman
Robert Weiss

April 2nd, 2013
Blacksburg, VA

Keywords: Interferometry, Green's function, Bayesian, Electromagnetics, Diffusion

Interferometry in Diffusive Systems: Theory, Limitations to Its Practical Application and Its Use in Bayesian Estimation of Material Properties

Sharmin Shamsalsadati

ABSTRACT

Interferometry in geosciences uses mathematical techniques to image subsurface properties. This method turns a receiver in to a virtual source through utilizing either random noises or engineered sources. The method in seismology has been discussed extensively. Electromagnetic interferometry at high frequencies with coupled electromagnetic fields was developed in the past. However, the problem was not addressed for diffusive electromagnetic fields where the quasi-static limit holds. One of the objectives of this dissertation was to theoretically derive the impulse response of the Earth for low-frequency electromagnetic fields.

Applying the theory of interferometry in the regions where the wavefields are diffusive requires volumetrically distributed sources in an infinite domain. That precondition imposed by the theory is not practical in experiments. Hence, the aim of this study was to quantify the important areas and distribution of sources that makes it possible to apply the theory in practice through conducting numerical experiments. Results of the numerical analysis in double half-space models revealed that for surface-based exploration scenarios sources are required to reside in a region with higher diffusivity. In contrast, when the receivers straddle an interface, as in borehole experiments, there is no universal rule for which region is more important; it depends on the frequency, receiver separation and also diffusivity contrast between the layers and varies

for different scenarios. Time-series analysis of the sources confirmed previous findings that the accuracy of the Green's function retrieval is a function of both source density and its width. Extending previous works in homogenous media into inhomogeneous models, it was found that sources must be distributed asymmetrically in the system, and extend deeper into the high diffusivity region in comparison to the low diffusivity area.

The findings were applied in a three-layered example with a reservoir layer between two impermeable layers. Bayesian statistical inversion of the data obtained by interferometry was then used to estimate the fluid diffusivity (and permeability) along with associated uncertainties. The inversion results determined the estimated model parameters in the form of probability distributions. The output demonstrated that the algorithm converges closely to the true model.

DEDICATIONS

I would like to dedicate this dissertation to my husband, Hadi, my parents, Jalal and Mehri, my brother, Shayan, and also my lovely aunt, Sedigh, with all my love and affection.

ACKNOWLEDEMENTS

I'd like to extend my sincerest gratitude to all those who have made this dissertation possible. I appreciate my adviser, Dr. Chester J. Weiss, who guided me into this interesting research area. The support I received from him throughout these years helped me to publish the outcomes of my work in prestigious journals. Furthermore, I'd like to extend my appreciation to my committee members, Dr. John A. Hole, Dr. Martin C. Chapman, and Dr. Robert Weiss. I am also grateful for all guidance I received from them throughout my study at Virginia Tech. Furthermore, I would like to thank my friend and colleague, Jacob Beale, for constructive discussions we had on seismic signal processing.

I am also grateful to Dr. Roel Snieder from the Colorado school of mines, Dr. Kees Wapenaar from Delft University, and Dr. Yuanzhong Fan from the Shell Company for giving me directions and guidance that assisted me in sorting out the technical details of my work on interferometry. I'd also like to acknowledge Dr. Burke J. Minsley from the U.S. Geological Survey for the consultation on the Bayesian inversion method.

I believe that I have been fortunate in having received ongoing departmental support. My sincerest appreciation is extended to the Geoscience department at Virginia Tech for the financial and academic support during the course of my study. I would also like to thank Connie Lowe for her continuous help and support. Scholarship support during this period of time was kindly provided by J. K. Costain, Aubrey E. Orange, the Society of Petrophysicist and Well Log Analyst, the Society of Exploration Geophysicist, the College of Science, and the BP Company.

Special thanks to my parents for their love, understanding, and encouragement throughout my education path. Last, but not least, many thanks to my husband, Hadi Nazem-Bokaee, who was always there in difficult times. I am blessed to have his support and company throughout these years.

TABLE OF CONTENTS

LIST OF FIGURES

Chapter 1:

Chapter 2:

Chapter 3:

Chapter 4:

Appendices:

LIST OF TABLES

Chapter 1: Literature Review

1.1 Green's Function and Its Importance in Geophysics

Green's function in geophysics is the solution of partial differential equations due to impulsive sources. For a known source, $f(\mathbf{r})$, and the Earth model, $\mathbf{m}$, one can predict the observed field, $u(\mathbf{r})$, by solving the corresponding partial differential equation

$$L(\mathbf{m})u(\mathbf{r}) = f(\mathbf{r}) \tag{1.1}$$

in which L is a differential operator. Nonetheless, the problem is that the model is in general unobtainable. Assuming the source term, $f(\mathbf{r})$, is equal to the Dirac delta function, $\delta(\mathbf{r})$, the unknown function $u(\mathbf{r})$ is replaced by the Green's function, $G(\mathbf{r})$:

$$L(\mathbf{m})G(\mathbf{r}) = \delta(\mathbf{r}). \tag{1.2}$$

Then, the observed fields for different angular frequencies, ω, are simply derived using

$$u(\mathbf{r},\omega) = \int G(\mathbf{r},\omega) f(\mathbf{r},\omega) d\omega. \tag{1.3}$$

in the frequency domain. Interferometry, or virtual source method, is a new tool for geophysicists that benefits from this concept to find the impulse response of the Earth. Through interferometry we can compute the Green's function with complete ignorance of the model. In this method, cross-correlation of wavefields recorded at two different locations yields the

Green's function evaluated at one location *as if* there were an actual source at the other location. Hence, it recovers the response of physically absent sources.

1.2 Interferometry

The fluctuation-dissipation theorem in physics describes the derivation of the Green's function or the impulse response of a system excited by noises or disturbances (Nyquist, 1928; Callen & Welton, 1951). This theory states that it is possible to derive the impulse response of a thermodynamically equilibrium Hamiltonian system through correlation of field fluctuations inside the system (Nyquist, 1928; Callen & Welton, 1951). The Hamiltonian (energy) and Lagrangian principles both have applications for Green's function retrieval which is called interferometry. The term interferometry arises from radio astronomy in which the radio signals received from far away objects are cross-correlated. Radio interferometry was developed in 1946 for the purpose of increasing resolution of the recorded radio signals.

Interferometry is also called the virtual source method since it constructs the effect of a virtual source at the location of an observation point. Cross-correlation based interferometry – with a long history in geophysics – was introduced by Claerbout (1968), who considered a horizontally lossless and layered acoustic medium in 1-D with a point source in the lower homogenous half-space. The author showed that autocorrelation of the response recorded at a receiver on the surface due to a source in a half-space is proportional to the reflection response of a surface source recorded by the same receiver. Therefore, by measuring the response of a source in the subsurface, one could measure the effect of a virtual source positioned on the surface. Claerbout's work was later extended into 3-D inhomogeneous media (Rickett & Claerbout, 1999). It was shown that by cross-correlating the response to a source recorded at two locations

on the surface, one can reconstruct the response of a virtual source positioned at the location of one of the receivers and measured at the location of the other receiver. The research embarked by Claerbout (1968) could be applied in finding reflection seismograms from background noise sources. Recent examples on diffuse seismic fields (Lobkis & Weaver, 2001; Wapenaar et al., 2008; Snieder, 2004), ground penetrating radar (Slob & Wapenaar, 2007), synthetic aperture controlled source electromagnetics (Fan et al., 2010), seismic coda waves (Lobkis & Weaver, 2001; Sato, 2009, 2009a), seismic bias correction (Curtis & Halliday, 2010), surface waves (Li et al., 2010) and electrokinetic self potential (Slob et al., 2010) demonstrate the impact that interferometric theory continues to have on geophysical exploration.

The concept of interferometric imaging was first used by Schuster (2001) who applied the method on both noise and man-made seismic sources (Schuster, 2001; Schuster et al., 2004). Schuster & Zhou (2006) used the method to simulate the effect of sources that were spatially displaced to some other locations. The purpose of their study was to apply the findings to eliminate elevation statics at source or receiver locations. Bakulin & Calvert (2006) applied controlled source interferometry in seismology to image through a problematic overburden. In all cases of controlled source and ambient source interferometry, cross-correlation results of two receiver recordings due to the sources were considered to be the response of a source that would be measured at one of the receiver locations assuming there was a source at the location of the other receiver.

Curtis et al. (2006) described the method in a horizontally double half-space acoustic medium in 1-D assuming planar acoustic waves are emitted by two impulsive sources where one source is located above the interface and the other is positioned below. The responses of sources are recorded by two receivers located arbitrarily between sources (Figure 1.1, left). It is shown in

this figure that each receiver records both direct and reflected waves emitted by source 1, and one transmitted wave from source 2. Recordings due to different sources are cross-correlated and then summed over sources to get the interferogram. The interferogram shows the response of a virtual source assuming that it was located at the position of receiver *A* and recorded by receiver *B* or the other way around. Figure (1.1) demonstrates that those forward and reversed times are both recovered in the interferogram. It was shown by the authors that this example could be generalized to reconstruct a trace from an infinite number of arbitrarily located sources where those sources surround the pair of receivers (Curtis et al., 2006).

1.2.1 Interferometry in Lossless Media

Fink (1992, 1999) used an array of source-receiver transducers to show that acoustic waves for lossless medium are invariant under time reversal. He also designed an experiment using ultrasonic wavefields where a piezoelectric source emits a pulse in a heterogeneous medium with thousands of scatterers; then, an array of receivers records the scattered wavefields (Fink, 2006). In the next part of his experiment, the traces were time-reversed and those seen were focused on the location of the source; and hence, the source-receiver reciprocity was proved through his experiment. Snieder & Scale (1998) analyzed this experiment to show that waves remain stable after multiple scattering. They compared wave scattering with particle scattering. The experiment showed that waves remain stable after multiple scattering by a heterogeneous medium while it is not true for particles. They were reasoning that waves travel in all directions and are in contact with all scatteres; however, particles move only through one path. Therefore, wave propagation in a heterogeneous medium is invariant under time reversal. Thus, the wavefield can be reconstructed after back-propagation through a highly heterogeneous medium (Snieder & Scale,

1998). Derode et al. (2003) analyzed the effect of multiple scattering in an ultrasonic experiment using the concept of time-reversal symmetry. The cross-correlated impulse responses were recorded by two receivers to show that this result is equal to the pulse that is emitted by one of the receivers and its time-reversed pulse (Derode et al., 2003). The authors showed that if sources surround the medium of the study, then it is possible to retrieve the Green's function by summing the cross-correlation responses observed at two receiver positions inside that medium. Both Fink (2006) and Derode et al. (2003) discussed the definition of time-reversal in acoustic and its relationship with seismic interferometry.

Wapenaar & Fokkema (2006) derived representation of the Green's function formulae in the inhomogeneous medium, assuming that it is invariant under time reversal using acoustic and also elastic wavefields. For the case of acoustic wavefields, Wapenaar & Fokemma (2006) considered an open domain of Γ where boundary $\partial\Gamma$ is a subdomain of this configuration. It was assumed that two receivers positioned at the states of *A* and *B* are encompassed by this boundary. The authors started with the motion equation

$$j\omega\rho v_i + \partial_i p = f_i \tag{1.4}$$

and stress-strain relation

$$j\omega\kappa p + \partial_i v_i = q \tag{1.5}$$

to derive representation of acoustic Green's function in the lossless medium. In these equations, the acoustic wavefield and the particle velocity are shown by p and v_i – both are functions of time and position – and the lower-case subscripts indicate the Cartesian coordinate vector. Moreover, j is the imaginary unit, ω the angular frequency, ∂_i the partial derivative in the $\mathbf{r}_i$-direction, ρ the

mass density of the medium, and κ its compressibility where the last two are position dependent. Two terms f_i and q_i denote the external volume force density and volume injection rate density, respectively. It was assumed that there is no external force and the volume injection rate is equal to the delta function. Therefore, the acoustic pressure at the locations of *A* and *B* are equal to the Green's function in the frequency domain. The authors considered a closed surface as $\partial\Gamma=\partial\Gamma_0 U\partial\Gamma_1$ where $\partial\Gamma_0$ is a part of free surface and $\partial\Gamma_1$ is a surface with an arbitrary shape which is not coinciding with a physical boundary, Figure (1.2). Because Green's function vanishes on the free surface, sources only need to be on the $\partial\Gamma_1$. In addition, $\partial\Gamma_1$ boundary is a spherical surface with a very large radius to satisfy radiation conditions of the Green's function at infinity. Using above mentioned criteria and combining the relations with the wave equation resulted in

$$G(\mathbf{r}_B, \mathbf{r}_A, \omega) = G(\mathbf{r}_A, \mathbf{r}_B, \omega) \tag{1.6}$$

and

$$G^*(\mathbf{r}_B, \mathbf{r}_A, \omega) + G(\mathbf{r}_A, \mathbf{r}_B, \omega) = \oint_{\partial\Gamma} \frac{-1}{j\omega\rho(\mathbf{r})} (G^*(\mathbf{r}, \mathbf{r}_A, \omega)\partial_i G(\mathbf{r}, \mathbf{r}_B, \omega) - \partial_i G^*(\mathbf{r}, \mathbf{r}_A, \omega) G(\mathbf{r}, \mathbf{r}_B, \omega)) n_i d^2\mathbf{r}, \tag{1.7}$$

wherein, $G^*(\mathbf{r}, \mathbf{r}_A, \omega)$ is the Fourier transform of the causal time domain Green's function $G(\mathbf{r}, \mathbf{r}_A, -t)$ which represents an impulse response observed at $\mathbf{r}$, due to a source at $\mathbf{r}_A$ ($\mathbf{r}_A$ and $\mathbf{r}_B$ are receiver locations), Wapenaar & Fokemma (2006). To make their findings applicable to the field of seismic interferometry and also remove the 'ghost' effect, Wapenaar & Fokkema (2006) considered a homogenous medium outside the boundary with propagation velocity *c* and mass density ρ. The 'ghost' effect is a product of waves that propagate from outside of the previously

described boundary toward the medium in one state, and then propagate outward from this boundary through another state. The authors further assumed that the medium in a small region around $\partial\Gamma_1$ boundary does not vary; hence, the normal derivatives of the Green's functions in high frequencies and large spherical radius were approximated to be $(-j\omega/c(\mathbf{r}))\ G|\alpha(\mathbf{r})|$, where α indicates the angle between the ray and the normal on the boundary. Under the above mentioned criteria, Wapenaar & Fokemma (2006) derived representation of the acoustic Green's function

$$2\Re\{G(\mathbf{r}_A,\mathbf{r}_B,\omega)\} \approx \frac{2}{\rho c}\oint_{\partial\Gamma} G^*(\mathbf{r}_A,\mathbf{r},\omega)G(\mathbf{r}_B,\mathbf{r},\omega)d^2\mathbf{r}. \tag{1.8}$$

The approximation in Equation (1.8) holds for the situation when $\partial\Gamma$ is a sphere with a very large radius, since in this case all rays are perpendicular to the boundary. In order to derive the imaginary component of the Green's function instead of the real part, the authors suggested to transform the Green's function to $g=(1/j\omega)G$.

Replacing impulsive sources on the boundary by transient sources with the frequency spectrum of $s(\mathbf{r}, \omega)$, the observed fields and also equivalent of Equation (1.8) could be computed using

$$p^{obs}(\mathbf{r}_A,\mathbf{r},\omega) = G(\mathbf{r}_A,\mathbf{r},\omega)s(\mathbf{r},\omega), \tag{1.9}$$

$$p^{obs}(\mathbf{r}_B,\mathbf{r},\omega) = G(\mathbf{r}_B,\mathbf{r},\omega)s(\mathbf{r},\omega), \tag{1.10}$$

and

$$2\Re\{G(\mathbf{r}_A,\mathbf{r}_B,\omega)\}S_0(\omega) \approx \frac{2}{\rho c}\oint_{\partial\Gamma} F(\mathbf{r},\omega)p^{obs^*}(\mathbf{r}_A,\mathbf{r},\omega)\,p^{obs}(\mathbf{r}_B,\mathbf{r},\omega)d^2\mathbf{r} \tag{1.11}$$

,where $S_0(\omega)$ is some average power spectrum and $F(\mathbf{r}, \omega)$ is a shaping filter defined as $F(\mathbf{r}, \omega)=S_0(\omega)/S(\mathbf{r},\omega)$, Wapenaar & Fokemma (2006).

For the case that sources are mutually uncorrelated and act at the same time, the three upper equations are rewritten by Wapenaar & Fokemma (2006) as the followings:

$$p^{obs}(\mathbf{r}_A,\omega) = \oint_{\partial\Gamma} G(\mathbf{r}_A,\mathbf{r},\omega)N(\mathbf{r},\omega)d^2\mathbf{r}, \tag{1.12}$$

$$p^{obs}(\mathbf{r}_B,\omega) = \oint_{\partial\Gamma} G(\mathbf{r}_B,\mathbf{r}',\omega)N(\mathbf{r}',\omega)d^2\mathbf{r}', \tag{1.13}$$

and

$$2\Re\{G(\mathbf{r}_A,\mathbf{r}_B,\omega)\}S(\omega) \approx \frac{2}{\rho c}\left\langle p^{obs*}(\mathbf{r}_A,\omega)\, p^{obs}(\mathbf{r}_B,\omega)\right\rangle, \tag{1.14}$$

where $N(\mathbf{r}, \omega)$, $N(\mathbf{r}', \omega)$ denote uncorrelated sources at $\mathbf{r}$, $\mathbf{r}'$. Comparing these two sets of equations for transient and uncorrelated sources, we observe that for transient sources, the response of each source should be measured separately while this is not required for the uncorrelated sources. However, the power spectrum of all sources needs to be the same to be able to use Equation (1.14), and no correction should be made on differences of the spectra for different sources (Wapenaar & Fokemma 2006).

One of the commonly used applications of the interferometry is retrieving seismic waves between seismometers. Seismic interferometry has been applied on both surface waves and body waves using both engineered and natural sources by several authors (Campillo & Paul, 2003;

Roux et al., 2004; Shapiro et al., 2005; Sabra, 2005; Draganov et al., 2006; Ramirez & Weglein, 2007). Campillo & Paul (2003) applied interferometry technique using surface waves to produce interferometric impulse responses using correlation of surface waves from distant earthquakes. It was shown that it is possible to derive a direct wave between two receivers by cross-correlation of wavefields that are diffused due to the multiple scattering of coda waves. The authors demonstrated the possibility of deriving Green's function and it's time-reversed for randomly distributed noise sources. Roux et al. (2004) developed a theoretical approach to obtain wavefront through correlation of the observed wavefields in the time domain. The authors applied their findings to recover acoustic waves related to the structure of the time domain Green's function using measurements of ocean ambient noise. In their experiment ocean noises were distributed throughout the water column. They recovered Green's function in their correlation due to both ocean and shipping noises (Roux et al., 2004). Sabra (2005) cross-correlated the responses of wavetrains in the low frequency band by recording noises received by 150 seismic stations in Southern California. It was shown that the output is a coherent broadband wavetrains traveling across frequency band of 0.1–2 Hz (Sabra, 2005). Another example where seismic interferometry was applied is in the construction of tomographic images of the geological units of California through cross-correlation of recorded ambient noises (Shapiro et al., 2005). The authors demonstrated that using interferometry in their experiment has improved the resolution of crustal images taken from surface waves. Picozzi et al. (2009) applied the method to high-frequency seismic noise recordings for investigating a shallow structure at the Nauen test site in Germany through the retrieval of Rayleigh wave Green's functions. Then travel times estimated from Green's function were inverted to model a 3-D surface wave velocity structure at the engineering scale.

On the other hand, seismic interferometry was applied to the passively acquired seismic background noise data to reconstruct reflection events in a desert area (Draganov et al., 2006). An active reflection survey was also conducted by the authors to compare the output with the findings derived from interferometry due to background noises. The cross-correlation results of the recordings produced coherent events in the reconstructed shot gathers for a long recording time. The cross-correlation results were band-pass filtered between 2 and 10 Hz and then stacked to suppress events such as surface waves and also to improve the signal-to-noise ratio (Draganov et al., 2006).

1.2.2 Interferometry in Attenuative Media

The Green's function estimation method only appeared applicable to the systems whose governing differential equations were invariant under time reversal, (that is, for nonattenuating systems) until Roux et al. (2004) and Sneider (2007) developed the theory for lossy systems. Snieder (2007) proved that the interferometry method is also applicable to the media with losses where time-reversal invariant assumption is not fulfilled. In lossless media the compressibility term has only real part which is included in the propagation velocity term '*c*' (Equation 1.8) while in the existence of loss, compressibility has both real and imaginary components. For the first, Wapenaar & Fokemma (2006) showed the surface integral should be sufficient for Green's function retrieval using the criteria mentioned in the previous section. Snieder (2007) demonstrated that for the latter, however, a volume integral needs to be added to the surface integral to include imaginary component of the compressibility, which was ignored for lossless systems (Snieder, 2007). This means that in addition to having sources at the boundary, those sources are required throughout the volume as well. However, the surface integral vanishes,

assuming the volume is infinite, since for attenuative media the wavefield vanishes exponentially at infinity. The Green's function representation in a medium with loss is shown by

$$G^*(\mathbf{r}_B, \mathbf{r}_A, \omega) + G(\mathbf{r}_B, \mathbf{r}_A, \omega) = 2\omega \int_{\Gamma} \kappa_i(\mathbf{r}, \omega) G(\mathbf{r}_B, \mathbf{r}, \omega) G^*(\mathbf{r}_A, \mathbf{r}, \omega) d^3\mathbf{r}, \qquad (1.15)$$

where κ_i denotes the imaginary part of the compressibility in an infinite medium (Snieder, 2007). Equivalent of seismic interferometry in lossy systems was adopted into electromagnetics by Slob & Wapenaar in 2007. In their derivation Maxwell's equations were used to extract the representation of correlation and also convolution type. For the first derivation, two receivers *A* and *B* are required to be surrounded by sources on a closed boundary $\partial\Gamma$, while receiver *B* should be outside the boundary for the latter in order to derive Green's function using the convolution method (Slob & Wapenaar, 2007). Slob & Wapenaar (2007) showed that Green's function for electromagnetic waves after applying far-field approximation could be extracted using a similar equation as of Equation (1.8) in which ρ and *c* are replaced by the magnetic permeability and velocity respectively. It was assumed that the medium outside the boundary with uncorrelated electric current sources is isotropic and the medium outside the boundary varies smoothly. These considerations were mainly made in order to approximate magnetic sources in terms of electric current sources.

The authors discussed the possibility of using controlled sources or noise sources with high frequencies in the air using above mentioned formulae. The advantage of using interferometric method in GPR (ground-penetrating radar) application is that background ambient noises could be utilized to derive the impulse response of the Earth.

Slob & Wapenaar (2007a) derived interferometry representation to be applied in GPR problems using both natural and controlled noise sources. They derived Green's function representations for electromagnetic waves in dissipative media in high frequencies. It was assumed the time-reversal invariance is not required and the medium in the neighborhood of the boundary does not vary. In their study, contributions of all sources were added to reconstruct a wave that could be emitted from one of the receivers, due to a virtual source at the location of the other receiver. In addition, scattering in a heterogeneous medium decreases the amplitude error in data reconstruction. When the medium is highly scattered, the spurious events due to incomplete cancellation of waves emitted by different sources are more suppressed. If noise sources are coherent, this noise can cause amplitude errors. The electromagnetic sources could be either noise or transient sources. When these are uncorrelated noise sources, they act simultaneously and hence can be measured simultaneously; however, when those are transient sources, their signals should be measured separately. The authors also demonstrated that in the case where transient sources are used, the cross-convolution method is the preferred method for Green's function retrieval in lossy media rather than other techniques (Slob & Wapenaar, 2007a).

Slob et al. (2007b) showed that by using electromagnetic waves, Green's function could be extracted correctly where the loss factor is not high around the boundary sources. They analyzed the case when one receiver is inside the source boundary and the other is located outside, using cross-convolution instead of cross-correlation representation. To simplify the relation and make it applicable to the real experiment, Slob et al. (2007b) considered sources which were located on two horizontal planes which straddle the interface between the semi-infinite half-spaces. These surfaces were assumed to be parts of a cylinder in which the closing boundaries at infinity do not

contribute to the result. Although numerical experiments resulted in impulse response retrieval with a high accuracy, some types of errors occurred during their experiments. One type of error was due to incomplete cancellation of amplitudes when cross-correlations for different source-receiver configuration were summed. The second source of error was due to the loss mechanisms of wave energy in cross-correlation methods. This also caused amplitude errors that resulted in artificial events (Slob et al., 2007b).

Fan et al. (2010) applied the concept of virtual source method to synthetic aperture controlled source electromagnetics. Synthetic aperture (SA) imaging is the practice of using a single source antenna, moved over a target of interest, to generate a sequence of transient responses which are stored and later summed with predetermined phase shifts to reconstruct the transient that would have been measured if the source locations were instead occupied by a spatially distributed phase array. The choice of which phase shifts to apply is done to optimize the beam shape of the equivalent phase array, typically to minimize scattering from targets of disinterest or to focus the radiation pattern of the array on the target of interest. Synthetic aperture uses the interference of fields generated by different sources for the purpose of constructing a virtual source with a desired radiation pattern.

Direct waves and air waves are challenges in CSEM technique. These types of waves are weakening the field refracted from the target and hence mask a part of the energy coming from the reservoir. Using synthetic aperture technique, one can design sources with different radiation patterns; hence, it is possible to concentrate the energy towards the target. Therefore, direct and air waves are reduced and also the depth of the investigation can be increased using this method. Moreover, the source can be towed at shallower depth to simplify the acquisition and also reduce the costs (Fan et al., 2010).

1.2.3 Virtual Source Method in Diffusive Systems

Diffusion mechanism is described through the Fick's law, which states that flux moves from regions of high concentration to regions of low concentration where the amplitude is proportional to the concentration gradient (Fick, 1855). Diffusion in hydrology and petrophysics is related to diffusive flux of fluids such as water or oil under a concentration gradient of that fluid. Low-frequency electromagnetic wavefields is another example when diffusion mechanism plays a role in the wave propagation. Diffusive wavefields are the ones that are equipartitioned, a mixture of uncorrelated plane waves propagating in all directions (Weaver & Lobkis, 2004). Weaver & Lobkis (2001) derived Green's function formulae for acoustic thermal fluctuation. They examined the accuracy of their theory through conducting ultrasonic experiments using diffusive wavefields. They proved that Green's function can be retrieved from cross-correlation of the wavefields exited by randomly distributed sources throughout a volume. They showed that by correlating noises at two independent locations one can obtain Green's function at one location due to a source at the other location. Weaver & Lobkis (2006) examined Green's function retrieval using different experimental scenarios for ultrasonic wavefields to derive impulse response of systems.

Snieder (2006) used diffusion equation to derive impulse response of pressure fluctuation in attenuative media. Using diffusion equation, wavefield is not invariant under time-reversal but source-receiver reciprocity holds. Sneider (2006) showed that the Green's function could be extracted from the correlation of time-series as long as sources of random noises are volumetrically distributed throughout an infinite volume. Considering reciprocity relation, Green's function for uncorrelated noises was estimated in the frequency domain

$$G(\mathbf{r}_A,\mathbf{r}_B,\omega)-G^*(\mathbf{r}_A,\mathbf{r}_B,\omega)=2j\omega\int_\Gamma G(\mathbf{r}_B,\mathbf{r},\omega)G^*(\mathbf{r}_A,\mathbf{r},\omega)d^3\mathbf{r}, \tag{1.16}$$

(Snieder, 2006). In Equation (1.16), G is the Green's function caused by a point source at $\mathbf{r}$ measured at two receiver locations $\mathbf{r}_A$ and $\mathbf{r}_B$ and the asterisk denotes complex conjugation. Snieder (2006) considered spatially uncorrelated pressure fluctuations with power spectrum $|q(\omega)|^2$:

$$\left\langle q(\mathbf{r}_1,\omega)q^*(\mathbf{r}_2,\omega)\right\rangle=\delta(\mathbf{r}_1-\mathbf{r}_2)\left|q(\omega)\right|^2. \tag{1.17}$$

In this equation, q denotes the source term which depends on both frequency and space, and angular brackets show the expectation value. By considering spatially uncorrelated sources, equation

$$(G(\mathbf{r}_A,\mathbf{r}_B,\omega)-G^*(\mathbf{r}_A,\mathbf{r}_B,\omega))\left|q(\omega)\right|^2=2j\omega\left\langle p(\mathbf{r}_A,\omega)p^*(\mathbf{r}_B,\omega)\right\rangle \tag{1.18}$$

in the frequency domain was derived by the author, where $p(\mathbf{r}, \omega)$ is the pressure at location $\mathbf{r}$ due to random forcing. Equation

$$(G(\mathbf{r}_B,\mathbf{r}_A,t)-G^*(\mathbf{r}_B,\mathbf{r}_A,-t))*C_q(t)=-2\frac{d}{dt}\left\langle p(\mathbf{r}_A,t)\otimes p(\mathbf{r}_B,t),\right\rangle \tag{1.19}$$

which is the equivalent of Equation (1.18) in the time domain, states that the subtraction of the Green's function and its time-reversed, after multiplication with the power spectrum of the fluctuation, is equal to the correlation of the random fields at locations $\mathbf{r}_A$ and $\mathbf{r}_B$ (Snieder, 2006). In this equation, the asterisk denotes convolution, $\otimes$ denotes correlation, and $Cq(t)$ is the autocorrelation of $q(t)$.

1.2.4 General Form of the Green's Function Extraction

As it was shown, the theory of the Green's function extraction from field fluctuations was based on using $G(t) + G(-t)$ or $G(t) - G(-t)$ depending on the type of problem ($G(\omega) + G^*(\omega)$ or $G(\omega) - G^*(\omega)$ in the frequency domain). Snieder et al. (2010) showed that the theory for Green's function extraction in the Lagrangian form can be extended to a variety of problems using acoustic, electrostatic and or diffusion equations. They showed that both subtraction and summation of $G(t)$ and $G(-t)$ could be used depending on the nature of sources and their distributions. The authors considered fields that satisfy the following scalar relation:

$$\left(a_n(\mathbf{r},t) * \frac{\partial^n}{\partial t^n} + \cdots + a_1(\mathbf{r},t) * \frac{\partial}{\partial t} \right) * u(\mathbf{r},t) = H(\mathbf{r},\nabla,t) * u(\mathbf{r},t) + q(\mathbf{r},t), \qquad (1.20)$$

where the asterisk denotes temporal convolution and $u(\mathbf{r}, t)$ is the field, $H(\mathbf{r}, \nabla, t)$ is a spatial differential operator, and $q(\mathbf{r}, t)$ is the source. Table (1.1) shows how using Equation (1.20) and changing parameters of a_n and H would modify this equation to be suited for solving a particular problem. The table demonstrates the type of source and its relevant relation required for Green's function extraction. It was shown that using this formulation assuming that attenuation is constant; the Green's function of acoustic waves can be retrieved. In this formulation; however, body forces instead of injections are the source of fluctuations in the system. For diffusive fields, the authors' derivation of

$$G(\mathbf{r}_A,\mathbf{r}_B,\omega) - G^*(\mathbf{r}_A,\mathbf{r}_B,\omega) = 2j\omega \int_\Gamma G(\mathbf{r},\mathbf{r}_A,\omega) G^*(\mathbf{r},\mathbf{r}_B,\omega) d^3\mathbf{r}, \qquad (1.21)$$

$$G(\mathbf{r}_A,\mathbf{r}_B,\omega)+G^*(\mathbf{r}_A,\mathbf{r}_B,\omega)=2\int_{\Gamma} D(r)(\nabla G(\mathbf{r},\mathbf{r}_A,\omega)\cdot\nabla G^*(\mathbf{r},\mathbf{r}_B,\omega)d^3\mathbf{r} \qquad (1.22)$$

made it possible to extract the Green's function from either injection sources or current sources where D denotes the diffusion coefficient.

Expressions (1.21, 22) show that both $G - G^*$ and $G + G^*$ can be extracted from field fluctuations. The difference between these equations is the source of excitation, where for the first (Equation 1.21) these fluctuations must be excited by monopole sources and for the latter (Equation 1.22) the fluctuations must be due to current or dipole sources.

Alternatives to the volume-distributed source formulation for electromagnetics have been investigated (Slob & Wapenaar, 2007, 2007a; slob et al., 2007b) which in case the sources are taken to lie on some bounding surface encapsulating the region of study. Unified theories of EGF (Empirical Green's Function) estimation have also been proposed (Wapenaar et al., 2008) in which electric and magnetic fields are coupled. However, the work (Shamsalsadati & Weiss, 2010) which will be presented in the next chapter is the first demonstration of EGF estimation for decoupled magnetic fields and heterogeneous media assuming the area of study is full of random point sources of current or time varying magnetization.

1.3 Required Distribution of Sources

Wavefields in lossless media and diffusive media have different criteria on requisite areas of sources. Surface source should be enough to apply interferometry in the first case. For the second case, volumetrically distributed sources are required in order to reconstruct the EGF

accurately. Wapenaar & Fokkema (2006) showed that for the case of acoustic and elastic wavefields where the outside boundary is homogeneous, sources in the Fresnel zones around the stationary points of the cross-correlation kernel for a given receiver pair contribute the most to the EGF estimate. For the case of acoustic wavefields, the authors considered a closed domain in the shape of a semicircle (Figure 1.3) assuming a part of this surface is the Earth's free surface ($\partial\Gamma_0$) and sources are uniformly distributed on the other surface ($\partial\Gamma_1$). In the numerical example conducted by Wapenaar & Fokkema (2006), it was further assumed that the medium outside this boundary is homogenous and also a single diffractor (C) exists inside the medium along with two receivers (*A*, *B*). Figure (1.4a) shows the cross-correlation results of the waves recorded by two receivers *A* and *B* (convolved with a wavelet) for different source positions in the time domain. The resulted traces in Figure (1.4a) are then summed to get the interferogram (Figure 1.4b). This figure demonstrates that the important areas of sources are the ones in the Fresnel zones around the stationary points of the integrand ($0^\circ < \phi < 45^\circ$ and $135^\circ < \phi < 180^\circ$), Wapenaar & Fokkema (2006).

Fan & Snieder (2009) analyzed a similar experiment for a homogenous medium when the boundary of sources is a full circle. It was assumed that sources are uniformly distributed around a circle with the radius of 40 km when the receivers are 6 km far apart. Fan & Snieder (2009) demonstrated that at least 50 sources are needed to reconstruct the EGF precisely (Figure 1.5). This figure also demonstrates that as number of sources is increasing, the oscillation between reconstructed signals is decreasing. It was also shown that sources in the stationary phase zone contribute the most to the EGF retrieval (Figure 1.6). These authors analyzed the source distribution problem in a heterogeneous medium. They considered 200 isotropic point scatterers in an 80×80 m^2 square around two receivers where the receivers are separated by 20 m with the

source radius is 90 m. Figure (1.7) demonstrate the reconstructed Green's function between two receivers for 300 uniformly distributed sources. Their experiment showed that more sources are needed for a heterogeneous medium in comparison to the homogenous medium in order to reconstruct the Green's function, accurately. They also compared their findings with the case when a single source is used. The correlation coefficient between the exact and the causal part of the reconstructed signal was shown to be around 0.97 for the 300 uniformly distributed sources while it was -0.03 for the single source. Therefore, Fan & Snieder (2009) proved inaccuracy of the beliefs about sufficiency of a single source in highly heterogeneous systems in order to apply interferometry therein. The authors showed that source density for a homogenous medium is proportional to the wave number, receivers distance and also the number of sources within the period of the most rapid oscillation. For a heterogonous medium; however, they found that the source density depends on the wavelength and also phase shifts along the paths from source to the receivers,

$$d\mathbf{r} \leq \frac{\lambda}{\sin\alpha_A + \sin\alpha_B}, \tag{1.23}$$

wherein $d\mathbf{r}$ is the source separation, λ is the wavelength, and $\alpha_{A,B}$ are phase shifts.

Slob et al. (2007b) applied electromagnetic interferometry using a similar approach. They considered a pair of receivers encompassed by sources in a circle (Figure 1.8). Figures (1.9a, b) demonstrate the correlation gathers and also the sum of traces. It was shown that sources close to the stationary point at 90° are important to find casual part of the Green's function while the ones in the opposite stationary point (270°) contribute to the reconstruction of the anticausal part. For the situation that one receiver (*B*) is outside the source domain (Figure 1.10), the authors showed that sources around 270° gives the most contribution for full Green's function retrieval (Figure

1.11) while the sources around 90° have vanishing contribution. Therefore, Slob et al. (2007b) concluded that only waves that are traveling inward contribute to the result.

Slob & Wapenaar (2007a) applied the theory developed for Green's function estimation using electromagnetic field for the GPR application. These authors started by conducting numerical experiments to quantify requisite areas where sources need to be positioned. For this purpose, they considered line sources of electromagnetic fields in the air where those are separated by 10 cm. In this numerical experiment, two homogenous layers exist below the surface with one receiver above the surface and the other one in the air above the top boundary. It was demonstrated that direct wave is reconstructed from contribution of sources in the lower boundary while the refracted event is built from contribution of all sources. The effect of far-field approximation and the 'ghost' event was leaded to spurious events as it was discussed by Slob & Wapenaar (2007a). The authors discussed that these spurious events are created through the sources exist on the upper boundary since they come from correlation of the waves that travel from the boundary outward to $\mathbf{r}_B$ and inward from the boundary to $\mathbf{r}_A$. In this case, travel time for the latter is larger than the travel time to $\mathbf{r}_B$ from which is subtracted. It was further concluded that the effect of far-field approximation is minimal and resulted in decrease in the amplitude of the direct arrival (Slob &Wapenaar, 2007a).

The required source distribution problem was mostly focused in elastic systems until Fan & Snieder (2009) analyzed the problem for pressure fields in diffusive systems. For a homogeneous, diffusive system with identical, closely spaced receiver points, Fan & Snieder (2009) simulated time-series where the source was imperfect – both through sparse sampling and spatial bias. In the third chapter we aim to extend the research embarked by Fan & Snieder (2009) on the required distribution of sources in diffusive systems through investigating the

effects of material heterogeneity and receiver separation on the cross-correlation kernel in 1-D and 2-D. The time-series of data will also be analyzed in the fourth chapter through conducting numerical experiments in order to demonstrate those effects on the requisite source

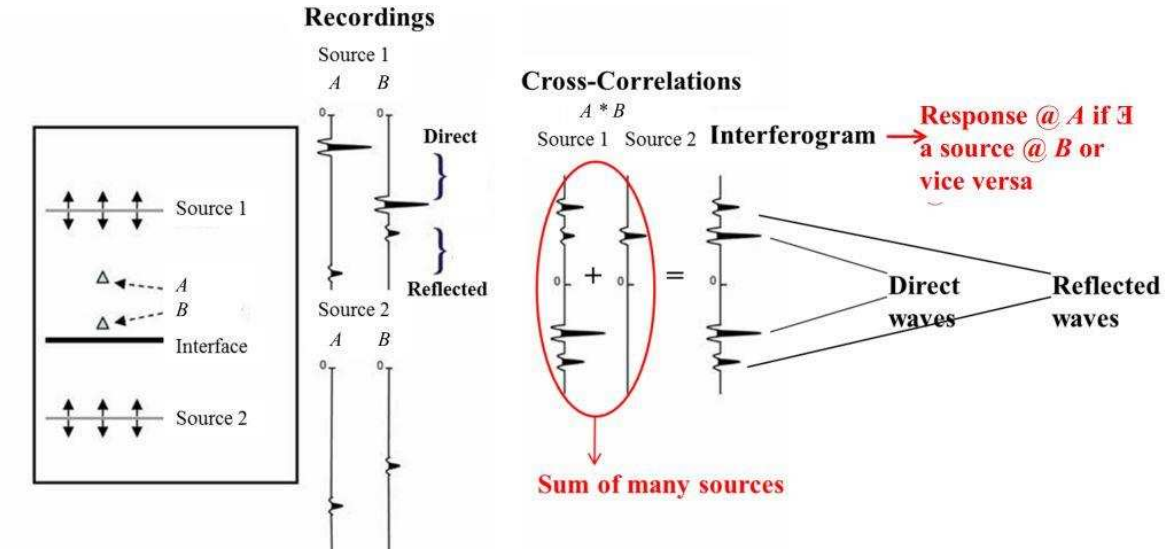

Figure 1.1: Seismic interferometry. One dimension acoustic double half-space medium with two sources, one on the top of the interface and the other one below that with two receivers above the interface between two sources (left). Traces are recorded for each receiver (*A* and *B*) due to source 1 and source 2 which recovers direct, reflected, and transmitted responses (recordings; center). Pair of traces for source 1 and for source 2 are cross-correlated (cross-correlations; center). Summations of the cross-correlations result in an interferogram including both causal and anticausal parts (bottom). At positive times, this trace shows response of a virtual source assuming that it was located at the position of receiver *A* and recorded by receiver *B* or vice versa. Figure modified from Curtis et al. (2006), used under fair use (2013).

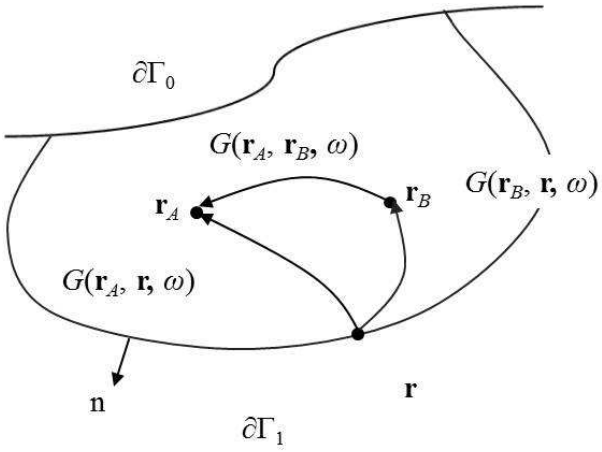

Figure 1.2: 1st Configuration for Green's function retrieval using acoustic waves. The boundary $\partial\Gamma$ encompasses two receivers of *A* and *B* in an acoustic medium. This boundary is including two surfaces of $\partial\Gamma_0$ and $\partial\Gamma_1$ which the first shows the free surface and the second is the surface where sources with **r** coordinates are positioned along it. Figure modified from Wapenaar and Fokemma (2006).

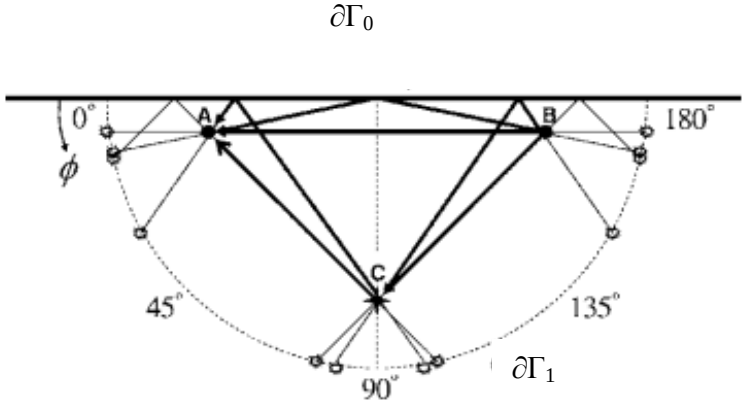

Figure 1.3: 2nd Configuration for Green's function retrieval using acoustic waves. *A* and *B* denote the receiver positions and C shows a diffractor in a homogeneous medium below a free surface. Sources are located on the surface $\partial\Gamma_1$.The causal contributions come from stationary points between 0°, 45° while the anticausal ones come from sources located between 135° and 180°. SEG allows reprint of figure without permission, Wapenaar, K. & Fokkema, J., 2006. Green's function representations for seismic interferometry: Geophysics, 71, SI 33–46.

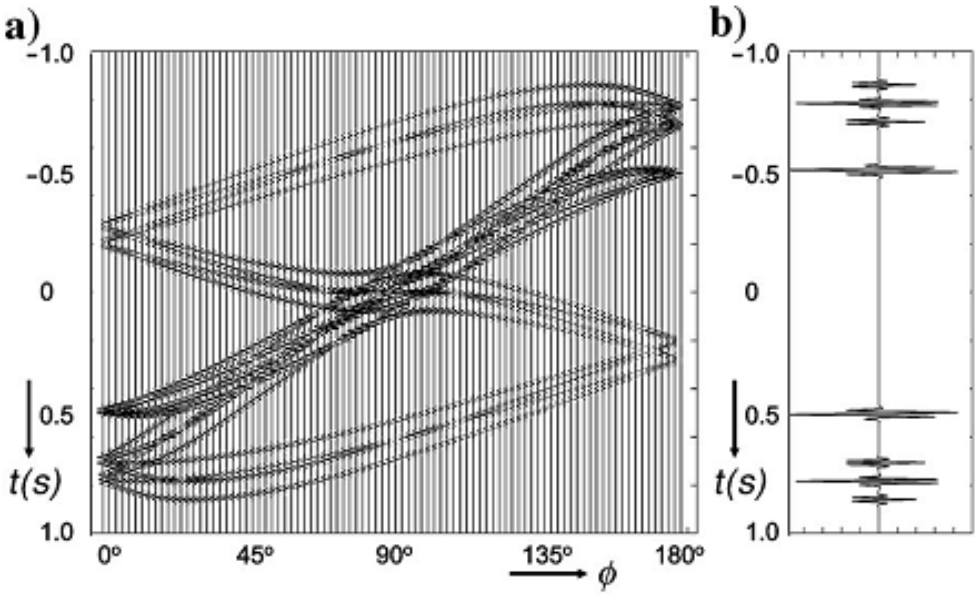

Figure 1.4: Cross-correlation result of the time domain interferometry using acoustic waves. (a) Time domain representation of the correlation kernel. (b) Sum of the traces in (a). SEG allows reprint of figure without permission, Wapenaar, K. & Fokkema, J., 2006. Green's function representations for seismic interferometry: Geophysics, 71, SI 33–46.

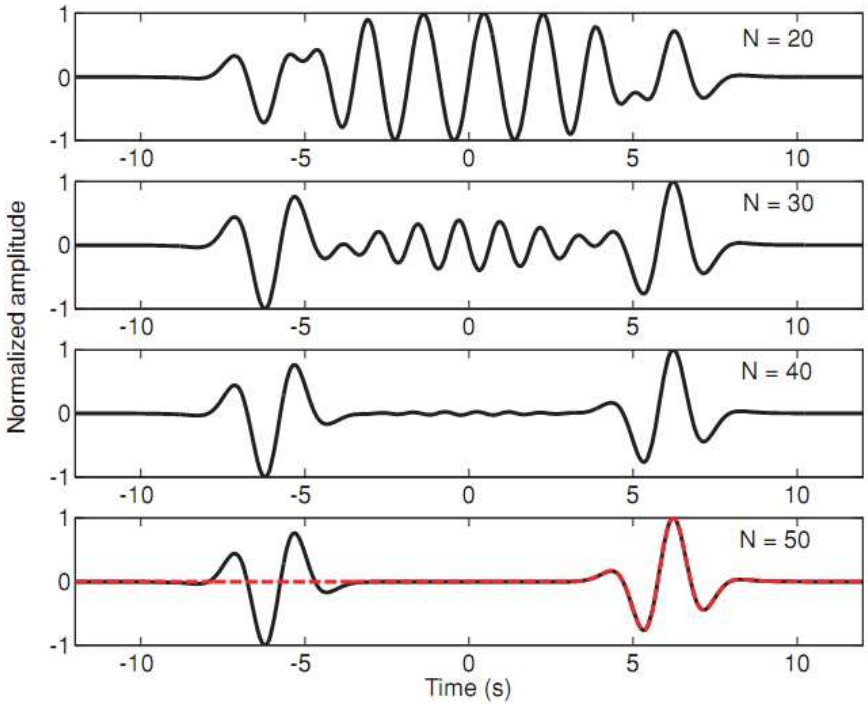

Figure 1.5: EGF reconstruction for a lossless homogenous medium with sources positioned around a circle. Reconstructed responses (solid lines) using interferometry for homogenous medium with different number of sources. Actual (direct) measurement between two receivers for N=50 (red dashed line). Oxford allows reprint of figure without permission, Fan, Y. & Snieder, R., 2009. Required source distribution for interferometry of waves and diffusive fields: Geophysical Journal International, 179, 1232–1244.

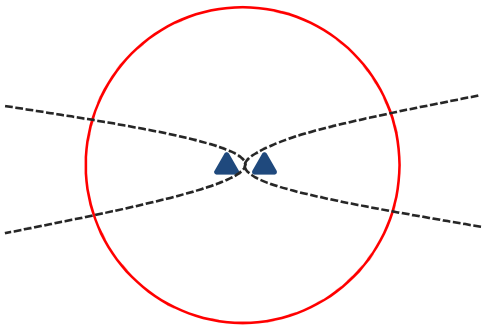

Figure 1.6: Stationary phase zone in a homogenous medium. The stationary phase zone for sources located on the circle is shown by dashed curves. It was shown that, using interferometry, sources in the stationary regions are more important than other sources. Figure modified from Fan and Snieder (2009).

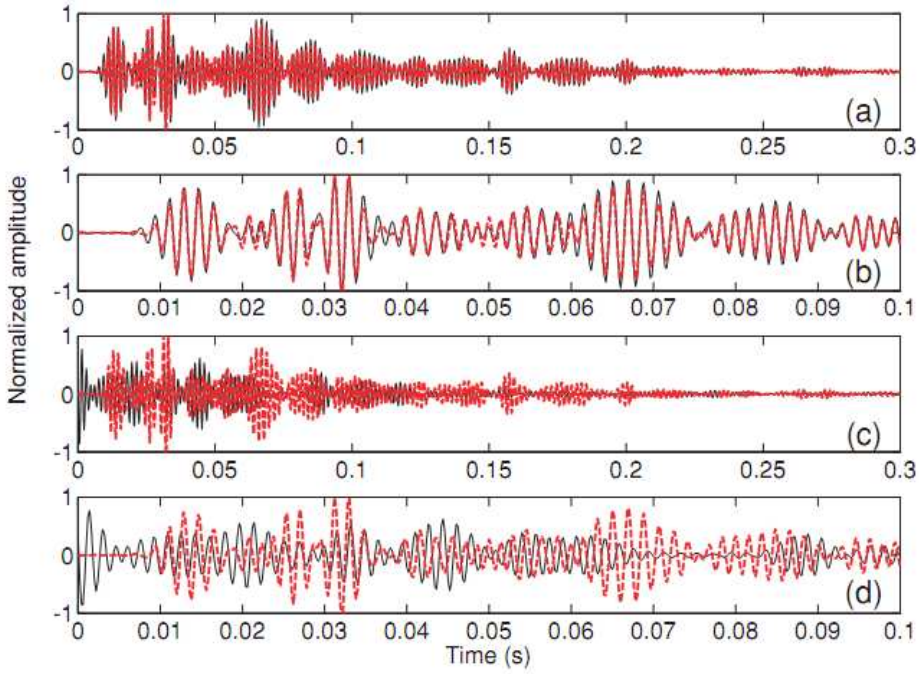

Figure 1.7: EGF reconstruction in a highly scattering medium. Reconstructed response is shown by the black curve and the actual measurement is demonstrated by the red curve. (a) Shows the reconstruction using 300 uniformly distributed sources while the (c) shows it when a single source is used. (b) and (d) are enlarged versions of (a) and (b), respectively. Oxford allows reprint of figure without permission, Fan, Y. & Snieder, R., 2009. Required source distribution for interferometry of waves and diffusive fields: Geophysical Journal International, 179, 1232–1244.

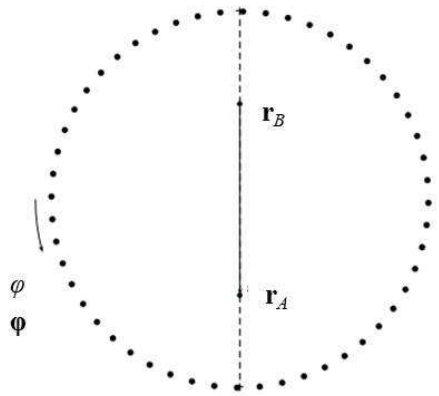

Figure 1.8: Interferometry using electromagnetic wavefields (1st configuration). Receivers *A* and *B* in a homogenous medium encompassed by sources located on a circle. Figure modified from Slob, et al. (2007b).

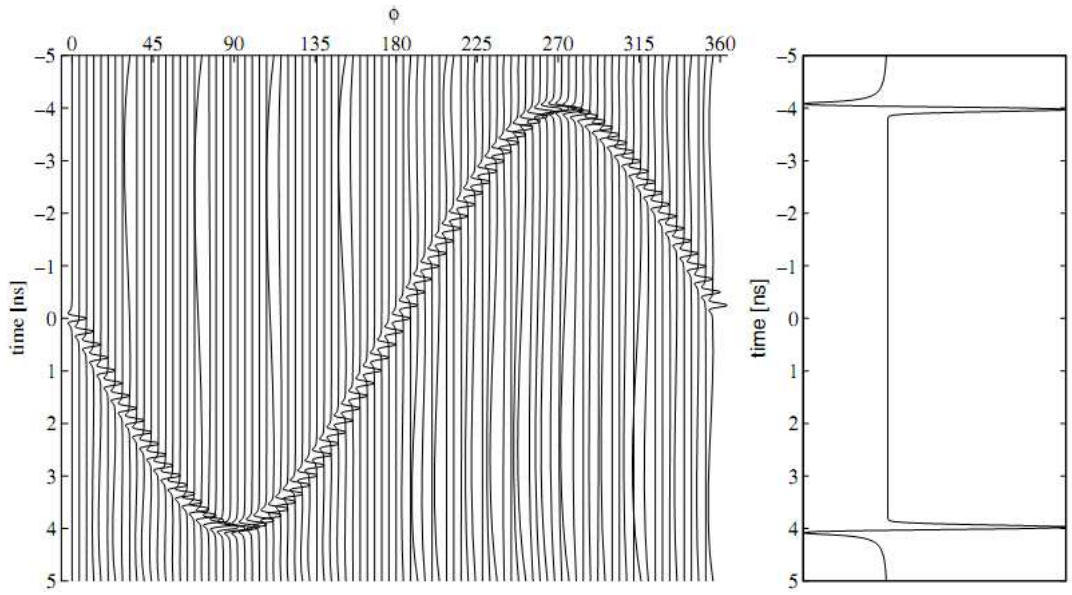

Figure 1.9: EGF reconstruction using electromagnetic wavefields for the 1st configuration. (a) Correlation gathers and also (b) the sum of traces in Figure (1.8). Oxford allows reprint of figure without permission, Slob, E., Wapenaar, K. and Snieder, R., 2007b. Interferometric electromagnetic Green's functions representations using propagations invariants: Geophysical Journal International, 169, 60-80.

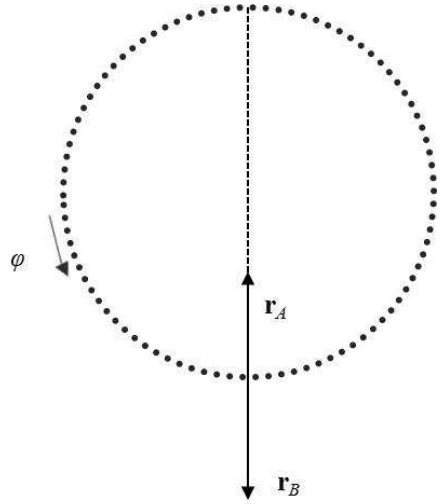

Figure 1.10: Interferometry using electromagnetic wavefields (2nd configuration). Receiver *A* is located inside a homogenous medium while receiver *B* is outside of this domain for sources positioned in a circle. Figure modified from Slob et al. (2007b).

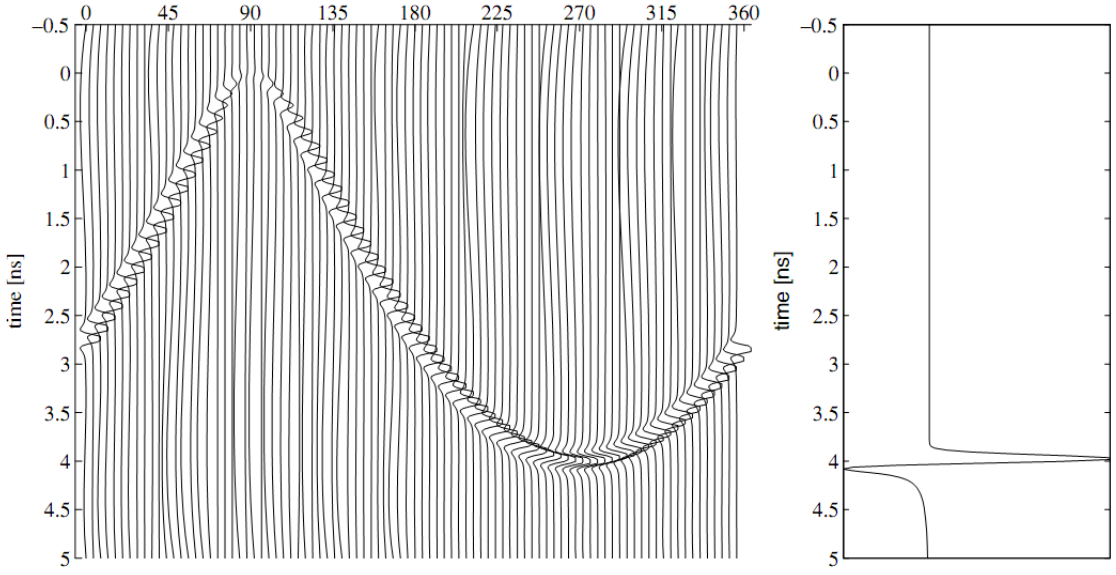

Figure 1.11: EGF reconstruction using electromagnetic wavefields for the 2nd configuration. (a) correlation gathers and also (b) the sum of traces of Figure (1.10). Oxford allows reprint of figure without permission, Slob, E., Wapenaar, K. and Snieder, R., 2007b. Interferometric electromagnetic Green's functions representations using propagations invariants: Geophysical Journal International, 169, 60-80.

Equation	a_n	H	G-G^*	G+G*
Diffusion	a_1=1	$\nabla\cdot(D(\mathbf{r})\nabla)$	Injection sources in volume	Current sources in volume
Acoustic waves (no attenuation)	$a_2=\kappa(\mathbf{r},\omega)$ (Im (κ)=0)	$\nabla\cdot(\rho^{-1}(\mathbf{r})\nabla)$	Injection sources on boundary	Difference of correlations
Acoustic waves (with attenuation)	$a_2=\kappa(\mathbf{r},\omega)$ (Im (κ)≠0)	$\nabla\cdot(\rho^{-1}(\mathbf{r})\nabla)$	Injection sources in volume	Volume forces ($\nabla\gamma$=0)
Electrostatics	all a_n=0	$\nabla\cdot(\varepsilon(\mathbf{r})\nabla)$	Not possible	Dipole sources
Systems invariant under time reversal	Re (a_n)=0 for n odd Im (a_n)=0 for n even	H=H*	sources on boundary	Sources in volume

Table 1.1: Green's function retrieval for different systems and source types. The symbols used represent: κ = compressibility, D = diffusion parameter, ρ = mass density, ε = electric permittivity and γ = inverse of quality factor. New Journal of Physics allows reprint of table without permission, Snieder, R., Slob, E. and Wapenaar, K., 2010. Lagrangian Green's function extraction, with applications to potential fields, diffusion and acoustic waves: New Journal of Physics, 12.

References

Bakulin, A. and Calvert, R., 2006. The virtual source method: Theory and case study*: Geophysics*, **71**(4), SI139-SI150.

Callen, H. B. and Welton T. A., 1951. Irreversibility and generalized noise: *Physical Review* **83**, 34–40.

Campillo, M. & Paul, A., 2003. Long-range correlations in the diffuse seismic coda: *Science*, **299**, 547–549.

Claerbout, J.F., 1968. Synthesis of a layered medium: *Geophysics*, **33**, 264–269.

Curtis, A., Gerstoft, P., Sato, H., Snieder, R., and Wapenaar, K., 2006. Seismic interferometry: turning noise into signal: *The Leading Edge*, **25**, 1082-1092.

Curtis, A. & Halliday, D., 2010. Directional balancing for seismic and general wavefield interferometry: *Geophysics*, **75**, SA1–SA14.

Derode, A., Larose, E., Campillo, M., Fink, M., 2003. How to estimate the Green's function of a heterogeneous medium between two passive sensors? Application to acoustic waves: *Applied Physics Letters*, **83**(15).

Draganov, D. Wapenaar, K., Mulder, W., Singer, J., 2006. Seismic Interferometry on background-noise field data: *SEG/New Orleans 2006 Annual Meeting*, 590-594.

Fan, Y. & Snieder, R., 2009. Required source distribution for interferometry of waves and diffusive fields: *Geophysical Journal International*, **179**, 1232–1244.

Fan, Y., Snieder, R., Slob, E., Hunziker, J., Singer, J., Sheiman, J. & Rosenquist, M., 2010. Synthetic aperture controlled source electromagnetics: *Geophysical Research Letters*, **37**, L13305, doi:10.1029/2010GL043981.

Fick, A., 1855. On liquid diffusion, *Philosophical Magazine and Journal of Science*., **10**, 31–39.

Fink, M., 1992. Time-reversal of ultrasonic fields: Basic principles: *IEEE Transactions on Ultrasonics, Ferroelectrics, and Frequency Control*, **39**, 555- 566.

Fink, M., 1999. Time-reversed acoustics: *Scientific American*, 91-97.

Fink, M., 2006. Time-reversal acoustics in complex environments: *Geophysics*, **71**, SI151-SI164.

Green, G., 1828. An essay on the application of mathematical analysis to the theories of electricity and magnetism: *Printed for the Author by T. Wheelhouse*, Nottingham.

Li, H., Bernardi, F. & Michelini, A., 2010. Surface wave dispersion measurements from ambient seismic noise analysis in Italy: *Geophysical Journal International*, **180**, 1242–1252.

Lobkis, O. I. & Weaver, R. L., 2001.On the emergence of the Green's function in the correlations of a diffuse field: *Journal of the Acoustical Society of America*., **110**, 3011–3017.

Nyquist, H., 1928. Certain topics in telegraph transmission theory: *Trans. AIEE*, **47**, 617–644.

Picozzi, M., S. Parolai, D. Bindi, and A. Strollo, 2009. Characterization of shallow geology by high-frequency seismic noise tomography: *Geophysical Journal International*, **176**, 164-174.

Ramirez, A.C. and Weglein A. B., 2007. The role of the direct wave and Green's Theorem in seismic interferometry and spurious multiples: *SEG Expanded Abstracts*, **26**, 2471.

Rickett, J. and Calerbout, J., 1997. Passive seismic imaging applied to synthetic data: *Stanford Exploration Project.*

Roux P., Kuperman W. A., and the NPAL Group, 2004. Extracting coherent wave fronts from acoustic ambient noise: *Journal of the Acoustical Society of America*., **116**(4).

Sabra, K.G., 2005. Extracting time-domain Green's function estimates from ambient seismic noise: *Geophysical Research Letters*, **32**(3).

Sato, H., 2009. Green's function retrieval from the CCF of coda waves in a scattering medium: *Geophysical Journal International*, **179**, 1580–1583.

Sato, H., 2009a. Retrieval of Green's function having coda from the cross-correlation function in a scattering medium illuminated by surrounding noise sources on the basis of the first order Born approximation: *Geophysical Journal International*, **179**, 408–412.

Schuster, G. T., 2001. Theory of daylight/interferometric imaging: tutorial: *63rd Meeting, European Association of Geoscientists and Engineers, Extended Abstracts*, SessionA32.

Schuster, G. T., Yu, J., Sheng, J. and Rickett, J. 2004. Interferometric/daylight seismic imaging: *Geophysical Journal International*, **157**,838–852.

Schuster, G. T. and M. Zhou, 2006. A theoretical overview of model-based and correlation-based redatuming methods: *Geophysics*, **71**, SI103-SI110.

Shamsalsadati, S. & Weiss, C.J., 2010. Retrieving the impulse response of the Earth due to random electromagnetic forcing: *Physical Review E*, **81**, 036603.

Shapiro, N. M., Campillo, M., Stehly, L. and Ritzwoller, M. H., 2005. High-resolution surface-wave tomography from ambient seismic noise: *Science*, **307**, 1615–1618.

Slob, E. and Wapenaar, K., 2007. Electromagnetic Green's functions retrieval by cross-correlation and cross-convolution in media with losses: *Geophysical Research Letters*, **34**(5).

Slob, E. & Wapenaar, K., 2007a. GPR without a source: cross-correlation and cross-convolution methods: *IEEE Geoscience and Remote Sensing Society*, **45**, 2501–2510.

Slob, E., Wapenaar, K. and Snieder, R., 2007b. Interferometric electromagnetic Green's functions representations using propagations invariants: *Geophysical Journal International*, **169**, 60-80.

Slob, E., Snieder, R. and Revil, A. 2010. Retrieving electric resistivity data from self potential measurements by cross-correlation: *Geophysical Research Letters*, **37**(4).

Snieder, R. K. and Scales, J. A., 1998. Time-reversed imaging as a diagnostic of wave and particle chaos: *Physical Review E*, 58, 5668-5675.

Snieder, R., 2004. Extracting the Green's function from the correlation of coda waves: a derivation based on stationary phase: *Phys. Rev .E*, **69**, 046610.

Snieder, R., 2006. Retrieving the Green's function of the diffusion equation from the response to a random forcing: *Physical Review E*, **74**, 046620.

Snieder, R., 2007. Extracting the Green's function of attenuating heterogeneous acoustic media from uncorrelated waves: *Journal of the Acoustical Society of America.*, **121**, 2637–2643.

Snieder, R., Slob, E. and Wapenaar, K., 2010. Lagrangian Green's function extraction, with applications to potential fields, diffusion and acoustic waves: *New Journal of Physics*, **12**.

Wapenaar, K. & Fokkema, J., 2006. Green's function representations for seismic interferometry: *Geophysics*, **71**, SI 33–46.

Wapenaar, K., Slob, E. & Snieder, R., 2008. Seismic and electromagnetic controlled source interferometry in dissipative media: *Geophysical Prospecting*, **56**, 419–434.

Weaver, R.L. and Lobkis, O.I., 2001. Ultrasonics without a source: Thermal fluctuation correlations at MHz frequencies: *Physical Review Letters*, **87** (13).

Weaver, R.L. and Lobkis, O.I., 2004. Diffuse fields in open systems and the emergence of the Green's function (L*): Journal of the Acoustical Society of America*, **116**(5), 2731-2734.

Weaver, R.L. and Lobkis, O. I, 2006. Diffuse fields in ultrasonics and seismology: *invited for special issue of Geophysics* **71** (4), SI5-SI9.

Chapter 2:

PHYSICAL REVIEW E **81**, 036603 (2010)

Retrieving the impulse response of the Earth due to random electromagnetic forcing

Sharmin Shamsalsadati and Chester J. Weiss*
Department of Geosciences, Virginia Polytechnic Institute and State University, 4044 Derring Hall (0420), Blacksburg, Virginia 24061, USA

(Received 4 March 2009; revised manuscript received 31 December 2009; published 12 March 2010)

A derivation is presented of Green's function in an arbitrary, heterogeneous conductive medium subject to random, ambient, uncorrelated noise sources. The approach for extracting Green's function is based on the correlation of time series of magnetic field components at two independent locations. As in the related case for the electric field, where the volume distribution of noise sources must be spatially correlated with the heterogeneous conductivity distribution, Green's function for magnetic field requires noise sources to be spatially correlated with the volume distribution of magnetic permeability. For applications of electromagnetic imaging of Earth's deep subsurface, the effect of magnetic permeability variations in the subsurface is often assumed to be negligible when compared to the effect of conductivity variations. Hence, the expressions derived here may be useful for passive electromagnetic subsurface imaging, in apparent contrast to their electric field counterparts. Numerical validation exercises are described which validate this theory for Green's function estimation in the low-frequency limit.

DOI: 10.1103/PhysRevE.81.036603 PACS number(s): 41.90.+e, 91.25.Qi, 05.40.Ca, 82.56.Lz

I. INTRODUCTION

The idea of empirical Green's function (EGF) estimation from correlation of time series in response external random forcing has a long history in seismology and acoustics [1] and has recently gained traction toward becoming a mainstream Earth exploration method to image, for example, deep crustal structure [2], hydrocarbon reservoirs [3], and earthquake dynamics [4]. The attraction of such an approach is clear: sources of noise, whose effects previously required heuristic filtering to isolate the primary signal from a known seismic source, could now be embraced in their full complexity, and furthermore, exploited for improved subsurface seismic resolution.

Until recently, EGF theory only appeared applicable to systems whose governing differential equations were invariant under time reversal [5], that is, for nonattenuating systems. However, it has since been shown [6] that for the case of pressure diffusion the EGF could be extracted from correlation of time series as long as the sources of random noise were assumed to be volumetrically distributed throughout the system. Applying this same approach to the quasistatic electromagnetic induction in a heterogeneous electrically conductive material would further require the power spectrum of the noise sources to be spatially correlated with the conductivity variations in the medium if the EGF for electric field is sought [6], but not, as will be shown below, for the case of magnetic field EGF.

Alternatives to the volume-distributed source formulation for electromagnetics have been investigated, e.g., [7–9], in which case the sources are taken to lie on some bounding surface encapsulating the region of study. Unified theories of EGF estimation have also been proposed [10] in which the electric and magnetic fields are inherently coupled. However, to our knowledge, the present work is the first explicit demonstration of EGF estimation for decoupled magnetic fields and heterogeneous media assuming the area of study is fully impregnated with random point sources of current or time varying magnetization.

Take Faraday's law of induction,

$$\nabla \times \mathbf{E} = -\partial_t \mu(\mathbf{H} + \mathbf{M_s}) \tag{1}$$

and Ampere's current law

$$\nabla \times \mathbf{H} = \sigma \mathbf{E} + \partial_t \varepsilon \mathbf{E} + \mathbf{J_s} \tag{2}$$

as the starting point for the discussion that follows, where the electric field $\mathbf{E}$, magnetic field $\mathbf{H}$ are functions of both time t and position $\mathbf{r}$ throughout a stationary medium of heterogeneous electrical conductivity $\sigma(\mathbf{r})$, dielectric permittivity $\varepsilon(\mathbf{r})$, and magnetic permeability $\mu(\mathbf{r})$, and subject to both electric $\mathbf{J_s}$ and magnetic $\mathbf{M_s}$ sources. Assuming the Fourier Transform with respect to time of Eqs. (1) and (2) exists such that $\partial_t \rightarrow \mathrm{i}\omega$, that is

$$\mathfrak{F}\{\mathbf{F}(\mathbf{r},t)\} = \mathbf{f}(\mathbf{r},\omega) = \int_{-\infty}^{\infty} \mathbf{F}(\mathbf{r},t)\exp(-\mathrm{i}\omega t)dt$$

with $\mathrm{i} = \sqrt{-1}$, the electric and magnetic fields are mapped into the complex frequency domain as $(\mathbf{E},\mathbf{H}) \rightarrow (\mathbf{e},\mathbf{h})$. Provided the electrical conductivity and magnetic permeability are time-invariant, the frequency-domain equivalents of Eqs. (1) and (2) become

$$\nabla \times \mathbf{e} = -\mathrm{i}\omega\mu(\mathbf{h} + \mathfrak{F}\{\mathbf{M_s}\}) \tag{3}$$

and

$$\nabla \times \mathbf{h} = \hat{\sigma}\mathbf{e} + \mathfrak{F}\{\mathbf{J_s}\} \tag{4}$$

with complex conductivity $\hat{\sigma}(\mathbf{r}) = \sigma(\mathbf{r}) + \mathrm{i}\omega\varepsilon(\mathbf{r})$. Substituting Eq. (3) into Eq. (4) results in the fundamental partial differential equation from which Green's function will ultimately be derived

*cjweiss@vt.edu

$$\nabla \times \frac{1}{\hat{\sigma}} \nabla \times \mathbf{h} + i\omega\mu\mathbf{h} = \mathbf{f}, \tag{5}$$

where

$$\mathbf{f}(\mathbf{r},\omega) = \Im\left\{ - i\omega\mu\mathbf{M}_s(\mathbf{r},t) + \nabla \times \frac{1}{\hat{\sigma}}\mathbf{J}_s(\mathbf{r},t) \right\}. \tag{6}$$

Observe that Eq. (5) is a "full physics" solution to the Maxwell equations where the spatially variable complex conductivity $\hat{\sigma}$ permits both diffusive and wavelike energy transport by its real and imaginary components, respectively. In regions such as the air, where the electrical conductivity is effectively zero, the value of $\hat{\sigma}$ is dominated by its nonzero imaginary component, and hence, the quotient in curl-curl term of Eq. (5) remains well-defined. Denoting complex conjugation by the superscript *, the time-reversed equivalent of Eq. (5) is

$$\nabla \times \frac{\hat{\sigma}}{|\hat{\sigma}|^2} \nabla \times \mathbf{h}^* - i\omega\mu\mathbf{h}^* = \mathbf{f}^*. \tag{7}$$

In Eq. (3)–(5) and (7) note that the material properties σ, ε, and μ remain space-dependent (scalar) quantities, representing an arbitrary (isotropic) heterogeneous medium, with an implicit dependence on the position vector $\mathbf{r}$ unless stated otherwise. This more compact notation will be continued throughout the remainder of the manuscript without any loss of generality.

II. REPRESENTATION THEOREMS OF THE CORRELATION AND CONVOLUTION TYPE

Following the development in Snieder [6], which itself is based on Fokkema and van den Berg and co-workers [11,12], representation theorems of the correlation and convolution type are derived specifically for the time-forward and time-reverse expressions in Eq. (5) and (7). For each of the representation theorems, the magnetic field resulting from an arbitrary source $\mathbf{f}_A$ is denoted with a subscript as $\mathbf{h}_A$, and similarly for a source B.

Considering first the time-forward expression in Eq. (5), the fields $\mathbf{h}_A$ and $\mathbf{h}_B$ are related by

$$\mathbf{h}_B \cdot \nabla \times \frac{1}{\hat{\sigma}} \nabla \times \mathbf{h}_A + i\omega\mu(\mathbf{h}_B \cdot \mathbf{h}_A) = \mathbf{h}_B \cdot \mathbf{f}_A \tag{8}$$

and

$$\mathbf{h}_A \cdot \nabla \times \frac{1}{\hat{\sigma}} \nabla \times \mathbf{h}_B + i\omega\mu(\mathbf{h}_A \cdot \mathbf{h}_B) = \mathbf{h}_A \cdot \mathbf{f}_B \tag{9}$$

for arbitrary sources A and B, where $\cdot$ denotes the dot product. Subtraction of Eq. (9) from Eq. (8) and subsequent volume integration over the domain Ω results in

$$\int_\Omega \left(\mathbf{h}_B \cdot \nabla \times \frac{1}{\hat{\sigma}} \nabla \times \mathbf{h}_A - \mathbf{h}_A \cdot \nabla \times \frac{1}{\hat{\sigma}} \nabla \times \mathbf{h}_B \right) d\Omega = \int_\Omega (\mathbf{h}_B \cdot \mathbf{f}_A - \mathbf{h}_A \cdot \mathbf{f}_B) d\Omega, \tag{10}$$

the left-hand side of which is equivalent to a surface integral over the domain Γ bounding Ω with outward-pointing normal $\mathbf{n}$ as

$$\int_\Gamma \frac{\hat{\sigma}^*}{|\hat{\sigma}|^2} [(\nabla \times \mathbf{h}_A) \times \mathbf{h}_B - (\nabla \times \mathbf{h}_B) \times \mathbf{h}_A] \cdot \mathbf{n} \, d\Gamma. \tag{11}$$

For any compact sources A and B, this integral vanishes as $\Omega = (-\infty, +\infty)^3$ due to exponentially vanishing fields $\mathbf{h}_A$ and $\mathbf{h}_B$ on Γ, and hence, the *representation theorem of convolution type* is given by

$$\int_\Omega (\mathbf{h}_B \cdot \mathbf{f}_A - \mathbf{h}_A \cdot \mathbf{f}_B) d\Omega = 0. \tag{12}$$

Note, however, that the assumption of an infinite domain Ω is not a prerequisite for Eq. (12) to hold. All domains Ω and source pairs (A,B) where Eq. (11) is equal to zero are equally valid and yield an equivalent representation theorem Eq. (12). However, for simplicity, only the infinite domain will be considered further here.

Following in a similar fashion to the preceding development of Eq. (8) through Eq. (12), consideration of the time-reversed expression Eq. (7) for source B yields the following pair of coupled equations:

$$\mathbf{h}_B^* \cdot \nabla \times \frac{\hat{\sigma}^*}{|\hat{\sigma}|^2} \nabla \times \mathbf{h}_A + i\omega\mu(\mathbf{h}_B^* \cdot \mathbf{h}_A) = \mathbf{h}_B^* \cdot \mathbf{f}_A \tag{13}$$

and

$$\mathbf{h}_A \cdot \nabla \times \frac{\hat{\sigma}}{|\hat{\sigma}|^2} \nabla \times \mathbf{h}_B^* - i\omega\mu(\mathbf{h}_A \cdot \mathbf{h}_B^*) = \mathbf{h}_A \cdot \mathbf{f}_B^*. \tag{14}$$

Subtraction of Eq. (14) from Eq. (13) and subsequent volume integration over the domain Ω yields the *representation theorem of the correlation type*,

$$-2\int_\Omega \frac{\mathrm{Im}[\hat{\sigma}]}{|\hat{\sigma}|^2} (\nabla \times \mathbf{h}_A) \cdot (\nabla \times \mathbf{h}_B^*) d\Omega + 2i\omega \int_\Omega \mu \mathbf{h}_B^* \cdot \mathbf{h}_A d\Omega = \int_\Omega (\mathbf{h}_B^* \cdot \mathbf{f}_A - \mathbf{h}_A \cdot \mathbf{f}_B^*) d\Omega, \tag{15}$$

provided the following boundary integral is zero:

$$\int_\Gamma \left[\frac{\hat{\sigma}^*}{|\hat{\sigma}|^2} (\nabla \times \mathbf{h}_A) \times \mathbf{h}_B^* - \frac{\hat{\sigma}}{|\hat{\sigma}|^2} (\nabla \times \mathbf{h}_B^*) \times \mathbf{h}_A \right] \cdot \mathbf{n} \, d\Gamma. \tag{16}$$

As was noted for Eq. (11), there may be several $(A,B)-\Omega$ configurations that result in Eq. (16) equaling zero. For now, the simple requirement that (A,B) are compact sources within the infinite domain Ω simultaneously sets to zero the value of the integrals in Eq. (11) and Eq. (16).

Furthermore, we observe that in the quasistatic limit $(\omega\varepsilon/\sigma \ll 1)$ used for low-frequency electromagnetic induction studies of the deep Earth, with the additional assumption that the spatial variability in the magnetic permeability of the rocks in question is minimal and therefore assumed to take the value of free space $\mu_0 = 4\pi \times 10^{-7}$ H/m, the representation theorem of correlation type simplifies considerably,

$$2i\omega\mu_0 \int_\Omega \mathbf{h}_B^* \cdot \mathbf{h}_A d\Omega \approx \int_\Omega (\mathbf{h}_B^* \cdot \mathbf{f}_A - \mathbf{h}_A \cdot \mathbf{f}_B^*)\ d\Omega \quad (17)$$

and is reminiscent of the functional form for the scalar pressure diffusion equation [6].

III. REPRESENTATION THEOREMS AND GREEN'S FUNCTIONS

We denote by $\bar{\mathbf{h}}_A$ and $\bar{\mathbf{h}}_B$, respectively, Green's functions for magnetic field due to the impulsive sources $\mathbf{f}_A = \mathbf{s}_A \delta(\mathbf{r}-\mathbf{r}_A)$ and $\mathbf{f}_B = \mathbf{s}_B \delta(\mathbf{r}-\mathbf{r}_B)$ where $\delta(\cdot)$ is Dirac's delta function and $\mathbf{s}$ is a unit vector. Hence, the representation theorem of convolution type in Eq. (12) reduces to a reciprocity relation

$$\mathbf{s}_A \cdot \bar{\mathbf{h}}_B(\mathbf{r}_A) - \mathbf{s}_B \cdot \bar{\mathbf{h}}_A(\mathbf{r}_B) = 0 \quad (18)$$

with the usual caveat that the integral Eq. (11) vanishes. Moreover, these specific definition for the source terms $\mathbf{f}_A$ and $\mathbf{f}_B$ simplify Eq. (17) to,

$$\mathbf{s}_A \cdot \bar{\mathbf{h}}_B^*(\mathbf{r}_A) - \mathbf{s}_B \cdot \bar{\mathbf{h}}_A(\mathbf{r}_B) = 2i\omega\mu_0 \int_\Omega \bar{\mathbf{h}}_B^* \cdot \bar{\mathbf{h}}_A d\Omega, \quad (19)$$

while the additional constraints of the quasistatic limit, constant magnetic permeability, and vanishing boundary integral Eq. (16) remain. Using the reciprocity expression Eq. (18), the left-hand side of Eq. (19) can now be written entirely in terms of Green's function observed at B for a source at A

$$\mathbf{s}_A \cdot [\bar{\mathbf{h}}_B^*(\mathbf{r}_A) - \bar{\mathbf{h}}_B(\mathbf{r}_A)] = 2i\omega\mu_0 \int_\Omega \bar{\mathbf{h}}_B^* \cdot \bar{\mathbf{h}}_A d\Omega \quad (20)$$

and vice versa

$$\mathbf{s}_B \cdot [\bar{\mathbf{h}}_A^*(\mathbf{r}_B) - \bar{\mathbf{h}}_A(\mathbf{r}_B)] = 2i\omega\mu_0 \int_\Omega \bar{\mathbf{h}}_B^* \cdot \bar{\mathbf{h}}_A d\Omega. \quad (21)$$

To understand the role of random noise in the evaluation of the volume integrals on the right side of Eq. (20) and (21), let's start by examining this term in its discrete form where the domain Ω is discretized into a set of infinitesimal differential elements $d\Omega_j$ such that

$$\int_\Omega \bar{\mathbf{h}}_B^* \cdot \bar{\mathbf{h}}_A d\Omega \approx \sum_j \bar{\mathbf{h}}_B^*(\mathbf{r}_j) \cdot \bar{\mathbf{h}}_A(\mathbf{r}_j) d\Omega_j. \quad (22)$$

Letting $\mathbf{s}_A = \mathbf{s}_B = \mathbf{s}$, substitution of the reciprocity relation Eq. (18) into Eq. (22) yields

$$\bar{\mathbf{h}}_B^*(\mathbf{r}_j) \cdot \bar{\mathbf{h}}_A(\mathbf{r}_j) = (\mathbf{s} \cdot \bar{\mathbf{h}}_j^*(\mathbf{r}_B))(\mathbf{s} \cdot \bar{\mathbf{h}}_j(\mathbf{r}_A)), \quad (23)$$

where the sources at point $\mathbf{r}_j$ are also taken in to lie in the $\mathbf{s}$ direction. It is now clear that Green's functions in Eq. (20) and (21), or more specifically, the $\mathbf{s}$ component of which, arise from an the summation of an infinite number of $\mathbf{s}$-directed impulsive sources j throughout the volume Ω, whose effects need only be known at two locations: $\mathbf{r}_B$ and $\mathbf{r}_A$.

To account for the variable spectral content $f(\omega)$ of a naturally occurring random noise source, the product of the squared power spectrum amplitude $|f(\omega)|^2$ with the j-summation terms on the right-hand side of Eq. (23) is $|f(\omega)|^2(\mathbf{s} \cdot \bar{\mathbf{h}}_j^*(\mathbf{r}_B))(\mathbf{s} \cdot \bar{\mathbf{h}}_j(\mathbf{r}_A))$, which, in turn, can be written as

$$\left(\int \mathbf{s} \cdot \bar{\mathbf{h}}_j(\mathbf{r}) f(\omega) \delta(\mathbf{r} - \mathbf{r}_B) d\Omega \right)^* \times \left(\int \mathbf{s} \cdot \bar{\mathbf{h}}_j(\mathbf{r}) f(\omega) \delta(\mathbf{r} - \mathbf{r}_A) d\Omega \right). \quad (24)$$

As a consequence of the representation theorem of convolution type, Eq. (12), the expression in Eq. (24) simplifies to $(\mathbf{s} \cdot \mathbf{h}_j(\mathbf{r}_B))^* (\mathbf{s} \cdot \mathbf{h}_j(\mathbf{r}_A))$, whereupon substitution into Eq. (20) and (21), our final expression for Green's function in the Fourier domain emerges

$$\mathbf{s} \cdot [\bar{\mathbf{h}}_B^*(\mathbf{r}_A) - \bar{\mathbf{h}}_B(\mathbf{r}_A)] |f(\omega)|^2 = \mathbf{s} \cdot [\bar{\mathbf{h}}_A^*(\mathbf{r}_B) - \bar{\mathbf{h}}_A(\mathbf{r}_B)] |f(\omega)|^2 = 2i\omega\mu_0 \langle (\mathbf{s} \cdot \mathbf{h}(\mathbf{r}_B))^* (\mathbf{s} \cdot \mathbf{h}(\mathbf{r}_A)) \rangle, \quad (25)$$

where $\langle \cdot \rangle$ denotes expectation value.

Inspection of Eq. (25) reveals that the difference between Green's function for magnetic field and its complex conjugate projected in the $\mathbf{s}$ direction and scaled by the power spectrum of the uncorrelated and volume-distributed random noise sources, is given simply by the correlation of the $\mathbf{s}$ components of the field measured at two distinct points. Transforming this expression into the time domain, the product between spectral power density and Green's function becomes a convolution operation, whereas the prefactor $i\omega$ maps into a time-derivative. Hence, in the time domain, Green's function for magnetic field $\bar{\mathbf{H}}(\mathbf{r},t)$ becomes

$$\begin{aligned} &\mathbf{s} \cdot [\bar{\mathbf{H}}_B(\mathbf{r}_A, -t) - \bar{\mathbf{H}}_B(\mathbf{r}_A, t)] * F(t) \\ &= \mathbf{s} \cdot [\bar{\mathbf{H}}_A(\mathbf{r}_B, -t) - \bar{\mathbf{H}}_A(\mathbf{r}_B, t)] * F(t) \\ &= 2\mu_0 \frac{\partial}{\partial t} \langle [\mathbf{s} \cdot \mathbf{H}(\mathbf{r}_B, t)] \otimes [\mathbf{s} \cdot \mathbf{H}(\mathbf{r}_A, t)] \rangle, \end{aligned} \quad (26)$$

in which $F(t)$ is the autocorrelation of the noise. The symbols $\otimes$ and $*$ denote correlation and convolution, respectively.

IV. VALIDATION EXAMPLE

To determine whether the aforementioned theory holds promise for eventual interpretation of observational data, a simple numerical experiment was conducted to validate the accuracy of Eq. (25) in the low frequency limit upon which the theory is based. The calculation is as follows: Assuming a double-half space model with conductivity $\sigma = 1.0$ S/m in the $z > 0$ region and $\sigma = 0.1$ S/m elsewhere, we compute the EGF at two points A and B due to a volume distribution of 100 Hz "noise" sources whose response is recorded at these two points. For simplicity, we choose $\mathbf{s} = \hat{z}$, and further distribute the noise sources equidistant over a $\Delta = 25$ m grid in the x, y, and z directions. With this model configuration the corresponding skin depth is 160 m in the resistive half space and 50 m in the conductive one. Hence, with points A and B at coordinates $(x,y,z)_A = (206.25, 206.25, -6.25)$ m and $(x,y,z)_B = (-206.25, -206.25, -6.25)$ m, respectively, a

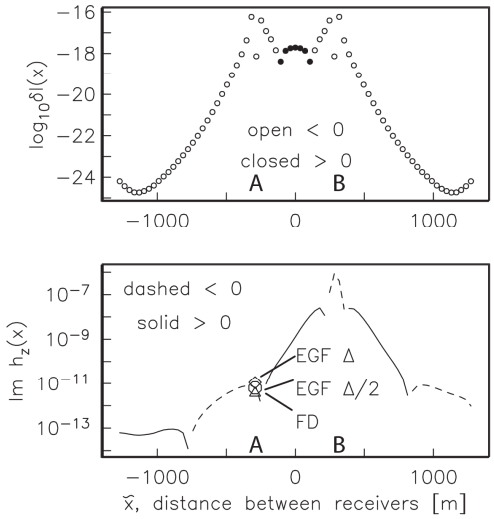

FIG. 1. (top) Relative contribution of noise sources δI to EGF estimation as a function of position $\tilde{x}$ along a line passing through two passive receiver locations A and B at $\tilde{x}=\pm 291$ m. (bottom) In symbols, finite difference (FD) and EGF calculated values of the vertical magnetic field at A due to a source $\mathbf{M}_s=\hat{z}\delta(\mathbf{r}-\mathbf{r}_B)$. Lines indicate FD-computed h_z at $z=0$.

noise source volume extending from $|x|,|y|,|z|\leq 900$ m encompasses several skin depths of distance between observation points A and B and the noise sources.

Choosing $\Delta=25$ m results in 389 017 independent noise-source forward calculations. Halving Δ increases this number to over three million. Hence, even though quasianalytic solutions for induction in layered media have been known and revisited for over a century [13–17], the Hankel transforms at the core of such calculations amount to a significant computational cost when the number of forward calculations is large, as in the present case. Various quadrature and digital filter techniques have been developed to minimize this cost [18–20], but even at 10–100 calculations per second, the wall clock time required for the proposed noise volume quickly escalates to several hours for a desktop computer.

To make this straightforward problem tractable in a reasonable amount of time, we turn instead to the staggered grid finite difference (FD) method [21,22], which by virtue of the reciprocity relation in Eq. (18), allows for the calculation of millions of noise sources with only two forward solves: One with a source at A, the other with a source at B. For the calculations shown here, the finite difference grid is partitioned over a modest $81\times 81\times 81$ nodes on a $1\times 1\times 1$ km volume.

The numerical results (Fig. 1, bottom) are in general agreement with the direct-calculated FD field value at point A and the EGF-estimated ones (symbols), with increasing accuracy realized by the dense $\Delta/2$ distribution of noise sources. FD-computed field values $h_z(\tilde{x})$ along the $z=0$ elevation (lines) illustrate the exponential decay and oscillatory nature of the magnetic field as a function of distance. Notice that the point A lies near a rapid sign-inflexion in the field and therefore represents a particularly challenging place to recover the EGF. To assess which of noise sources contribute most to the EGF estimation (Fig. 1, top) we plot the integrand in the left-hand side of Eq. (17) along the same $z=0$ elevation. The exponential decay and oscillatory behavior of the integrand along this profile reinforce our appreciation for the numerical difficulty of accurately evaluating this multidimensional integral.

V. DISCUSSION

The magnetotelluric (MT) method is a classic geophysical method for inferring the spatial distribution of electrical conductivity of Earth's interior which relies on ambient electromagnetic disturbances of magneto- and ionosphere origin for the source of electromagnetic forcing [23,24]. Inaccuracies in the resulting inferences on the physiochemical state of Earth's interior can be amplified by nonplane wave sources such as power lines, electric fences, trains and the like. Contrary to the MT method, the EGF procedure outlined above *relies* on random uncorrelated noise sources and, hence, has the potential for improved subsurface mapping in areas where the MT method fails due to excessive cultural interference.

Previous work on dissipative, scalar fields (e.g., pressure diffusion) has demonstrated that time-reversal invariance of the governing differential equation is not a prerequisite for EGF estimation [6]. The work presented here parallels the development of the pressure diffusion problem and applies the analysis to low-frequency electromagnetism, treating the fields in their full vector form. Like the pressure diffusion case, the low-frequency magnetic field EGF can be recovered by cross-correlation of time series measured at two discrete locations and time-reversal invariance is not a prerequisite.

The assumption of low-frequencies—that is, the quasistatic limit—is only a simplifying component of the preceding development and does not affect the implications of the final result in Eq. (25). To see what effect incorporation of "full physics" would have, observe that the first integral in Eq. (15), when retained to account for the wave propagation terms, can be rewritten as $i\omega\int_\Omega \varepsilon \mathbf{e}_A\cdot\mathbf{e}_B^* d\Omega$. Assuming that electric permittivity is sufficiently uniform throughout the volume Ω, this added term would ultimately result in the additional requirement of correlating electric fields, too. Regardless of whether the electric field terms are kept or discarded, the magnetic field EGF is a direct reflection of the conductivity distribution throughout the system. Our work shows that *a priori* knowledge of this distribution is not required for EGF estimation.

It has been previously pointed out that when considering the electromagnetic problem, the noise sources must be spatially correlated with the conductivity variations in the medium [6]. For the case of magnetic fields, we have shown that this restriction is no longer necessary. However, when considering electric field Green's functions, its necessity is clear: The conductivity term in the electric field "curl-curl" equation plays the same functional role as the permeability does in Eq. (5). And while it's reasonable in many geophys-

ical exploration scenarios to neglect permeability variations in the rocks, a corresponding dismissal of the conductivity variations would be defensible only in exceptional circumstances [25].

Examination of the final expression in Eqs. (25) and (26) for the superposition of the magnetic field EGF and its time-reversed form reveals that parallel components (**s**-directed) of the ambient magnetic field are required at the two locations A and B, *and* that the noise sources are all taken to be polarized in the same **s** direction. While the former is unremarkable from an implementation perspective, the latter appears absurd in light of the random nature of the noise. To reconcile this apparent problem, we observe that a random spatial distribution of point noise sources might also be randomly distributed in its polarization, and hence, within this latter distribution there will be a component parallel to **s** for each of the sources.

The preceding development also does not place any restrictions on the type of noise, other than is must be "infinitesimal" in some spatial sense. Both magnetic and electric current sources are admissible, including idealized dipole sources. Hence, electromagnetically cluttered environments such as urban areas, oilfields and industrial facilities may provide a rich spectrum of noise from which to draw upon for Green's function estimation and are attractive sites for future potential validation exercises with observed time series of magnetic field. The effect of *correlated*, heterogeneous, and anisotropic noise sources on the recovered EGF is an interesting question, but lies beyond the scope of the present study and will be addressed in future publications.

ACKNOWLEDGMENT

Special thanks are extended to Roel Snieder for helpful comments and clarifying our thinking on the ideas presented here.

[1] J. Claerbout, Geophysics **33**, 264 (1968).
[2] G. D. Bensen, M. H. Ritzwoller, and N. M. Shapiro, J. Geophys. Res. **113**, B05306 (2008).
[3] A. Bakulin and R. Calvert, Geophysics **71**, SI139 (2006).
[4] S. de Lorenzo, M. Filippucci, and E. Boschi, J. Geophys. Res. **113**, B10314 (2008).
[5] A. Curtis, P. Gerstoft, H. Sato, R. Snieder, and K. Wapenaar, The Leading Edge **25**, 1082 (2006).
[6] R. Snieder, Phys. Rev. E **74**, 046620 (2006).
[7] E. Slob and K. Wapenaar, Geophys. Res. Lett. **34**, L05307 (2007).
[8] E. Slob and K. Wapenaar, IEEE Trans. Geosci. Remote Sens. **45**, 2501 (2007).
[9] K. Wapenaar, E. Slob, and R. Snieder, Geophys. Prospect. **56**, 419 (2008).
[10] K. Wapenaar, E. Slob, and R. Snieder, Phys. Rev. Lett. **97**, 234301 (2006).
[11] J. T. Fokkema and P. M. van den Berg, *Seismic Applications of Acoustic Reciprocity* (Elsevier, Amsterdam, 1993).
[12] J. T. Fokkema and P. M. van den Berg, in *Wavefields and Reciprocity*, edited by P. M. van den Berg, H. Blok, and J. T. Fokkema (Delft University Press, Delft, 1996), pp. 99–108.
[13] H. Weyl, Ann. Phys. **60**, 481 (1919).
[14] A. Sommerfeld, Ann. Phys. **28**, 665 (1909).
[15] A. D. Chave and C. S. Cox, J. Geophys. Res. **87**, 5327 (1982).
[16] J. R. Wait, Can. J. Phys. **39**, 1017 (1961).
[17] A. Baños, *Dipole Radiation in the Presence of a Conducting Halfspace* (Pergamon Press, New York, 1966).
[18] A. D. Chave, Geophysics **48**, 1671 (1983).
[19] D. Guptasarma and B. Singh, Geophys. Prospect. **45**, 745 (1997).
[20] F. N. Kong, Geophys. Prospect. **55**, 83 (2007).
[21] C. J. Weiss and S. Constable, Geophysics **71**, G321 (2006).
[22] K. Yee, IEEE Trans. Antennas Propag. **14**, 302 (1966).
[23] A. N. Tikhonov, Dokl. Akad. Nauk **73**, 295 (1950).
[24] L. Cagniard, Geophysics **18**, 605 (1953).
[25] T. Meglish, Y. Li, L. Pasion, D. Oldenburg, R. L. van Dam, and S. Billings, *SEG Technical Program Expanded Abstracts* (Society for Exploration Geophysics, Tulsa, OK, 2008), Vol. 27, pp. 1248–1251.

Chapter 3:

Geophysical Journal International

Geophys. J. Int. (2012) **190,** 1526–1532 doi: 10.1111/j.1365-246X.2012.05567.x

Empirical Green's function estimation for lossy systems: analysis of the volume of relevance for the origin of ambient fluctuations

Sharmin Shamsalsadati and Chester J. Weiss

Department of Geosciences, Virginia Tech, Blacksburg, VA 24061, *USA. E-mail: cjweiss@vt.edu*

Accepted 2012 June 7. Received 2012 June 5; in original form 2011 June 2

SUMMARY

From a theoretical perspective, perfect Green's function recovery in diffusive systems is based on cross-correlation of time-series measured at distinct locations arising from background fluctuations from an infinite set of uncorrelated sources, either naturally occurring or engineered. Clearly such a situation is impossible in practice, and a relevant question to ask, then, is how does an imperfect set of noise sources affect the quality of the resulting empirical Green's function (EGF)? We narrow down this broad question by exploring the effect of source location and make no distinction between whether the noise sources are natural or man made. Following the theory of EGF recovery, the only requirement is that the sources are uncorrelated and endowed with the same (or nearly so) frequency spectrum and amplitude. As such, our intuition suggests that noise sources proximal to the observation points are likely to contribute more to the Green's function estimate than distal ones. However, in what manner and over what spatial extent our intuition is less clear. Thus, in this short note we specifically ask the question, 'Where are the noise sources that contribute most to the Green's function estimate in heterogeneous, lossy systems?' We call such a region the volume of relevance (VoR). Our analysis builds upon recent work on 1-D homogeneous systems by examining the effect of heterogeneity, dimensionality and receiver location in both one and two dimensions. Following the strategy of previous work in the field, the analysis is conducted out of mathematical convenience in the frequency domain although we stress that the sources need not be monochromatic. We find that for receivers located symmetrically across an interface between regions of contrasting diffusivity, the VoR rapidly shifts from one side of the interface to the other, and back again, as receiver separation increases. For the case where the receiver pair is located on the interface itself, the shifting is less rapid, and for moderate-to-high diffusivity contrasts, the VoR remains entirely on the more diffusive side over receiver separations up to two to three skin depths based on the high-diffusivity value. Finally, because diffusivity plays a role analogous to resistivity in electromagnetic induction problems, our results suggest that the VoR for the latter is dominated by the air region when the receivers are located on the Earth's surface—a finding that demonstrates the minimal impact of subsurface noise sources for EGF estimation from surface-based electromagnetic geophysical experiments.

Key words: Spatial analysis; Interferometry; Electromagnetic theory; Hydrogeophysics.

INTRODUCTION

Interferometry, or equivalently, cross-correlation, of wavefields recorded at two receiver positions to obtain the impulse response of the Earth has a long history in geophysics. The idea was introduced by Claerbout (1968) who showed that cross-correlating time-series of ambient fluctuations recorded at two separate locations yields the wavefield response that would be recorded at one receiver as if there was an actual source at the other. Recent examples on diffuse seismic fields (Lobkis & Weaver 2001; Snieder 2004; Wapenaar *et al.* 2008), ground-penetrating radar (Slob & Wapenaar 2007), synthetic aperture controlled-source electromagnetics (Fan *et al.* 2010), seismic coda waves (Lobkis & Weaver 2001; Campillo & Paul 2003; Sato 2009a,b), seismic bias correction (Curtis & Halliday 2010), surface waves (Li *et al.* 2010) and electrokinetic self potential (Slob *et al.* 2010) demonstrate the breadth of impact that interferometric theory continues to have on geophysical exploration. However, it is impossible to find an area fully impregnated with random, uncorrelated noise sources as required by the interferometry theory (see Snieder 2007, for example). Wapenaar & Fokkema (2006) showed that for the case of acoustic and elastic wavefields, noise sources in the Fresnel zones around the stationary points of the cross-correlation

kernel for a given receiver pair contribute the most to the empirical Green's function (EGF) estimate. Although there has been much research on EGF retrieval using the physics of wave propagation, the development of interferometry for the case of diffusive fields is less mature.

Recently, Snieder (2006) demonstrated that for lossy systems where diffusion, rather than wave propagation prevails, Green's function can be estimated also by the cross-correlation method, provided that the sources of ambient signals fully permeate the medium surrounding the two observation points (see, e.g. Shamsalsadati & Weiss 2010; Slob & Weiss 2011, and references therein for application to simple electromagnetic systems). In areas free of naturally occurring noise sources, one could engineer an experiment whereby sources are known *a priori* as in the case of controlled source CSEM (Fan & Snieder 2009). Nonetheless, such a distinction is lost in the application of interferometry theory because of the requirement that the source power spectrum is known *a priori*. However in either case, whether the sources are naturally occurring or engineered, the relationship between source location density and proximity to the observation points is the key unknown we investigate. In other words, for the controlled-source experimenter, our results point out where the sources should be placed; for the natural-source experimenter, our results point out where those natural sources need to be.

For a homogeneous, diffusive system with identical, closely spaced receiver points, Fan & Snieder (2009) simulated time-series under compromised conditions where the source was imperfect—both through sparse sampling and spatial bias. They showed that the early-time EGF response is most affected by changes in the source density. A short spread of closely spaced sources centred about the receiver pair do a better job of early-time EGF recovery than fewer, widely spaced ones over the same region. This dense cluster of sources over a small region was insufficient, however, to recover the late time response. To remedy this deficiency, the dense source spread was expanded by roughly a factor of 3 in spatial extent. Decimating the source distribution had little effect on the late time response, thus leading the authors to conclude that a wide distribution (roughly 34 times the receiver separation for their 1 km^2 s^{-1} medium) of densely spaced sources was necessary for accurate EGF estimation.

In this study we extend their work through investigating the effects of material heterogeneity and receiver separation on the cross-correlation kernel in one and two dimensions. In our numerical experiments, double half-space models are examined with one receiver located on either side of the contact. For the 2-D case, the receiver pair is rotated 90° degrees with respect to the contact. The rotation simulates a pair of receivers located along a line oblique to an idealized geological contact, with the end-member case consisting of both receivers lying on the contact where we are then free to loosen our definition of the contact to include the air/Earth interface. Such a suite of calculations is designed to accommodate a plurality of geophysical exploration scenarios, including single borehole, cross-borehole and surface-based experiment designs. Recent efforts in the study of electromagnetic self potential (a Poisson process) at the laboratory scale (Slob *et al.* 2010) show that thermally induced noise sources (the diffusion process to which this discussion applies) are one possible mechanism by which the EGF can be estimated by cross-correlation theory, and hence, our modelling results may be relevant to the interpretation of such data. However, at the field scale, thermal fluctuations alone may be swamped by the noise due to anthropogenic sources and/or macroscopically averaged fluxes in pressure (due to tidal or atmospheric loading, stress field relaxation, etc.) and surface chemical potential resulting from, for example, pore-scale rock/fluid interactions.

METHOD

Because we are interested in extracting Green's function from observations in lossy, dissipative systems, we base our analysis on Fickian diffusion in a heterogeneous medium with space-dependent diffusivity D, Fourier-transformed $\partial_t \rightarrow \mathrm{i}\omega$ into the frequency domain:

$$-\nabla \cdot D(\mathbf{r},\omega)\nabla u(\mathbf{r},\omega) + \mathrm{i}\omega u(\mathbf{r},\omega) = s(\mathbf{r},\omega), \tag{1}$$

where ω represents angular frequency and, $\mathrm{i} = \sqrt{-1}$ and s is, in general, a frequency-dependent source term with power spectrum $f(\omega)$. For a point source $f(\omega)\delta(\mathbf{r}-\mathbf{r}_A)$, we write Green's function for eq. (1) as $G_A(\mathbf{r})$, which is simply $u_A(\mathbf{r})$ scaled by $f^{-1}(\omega)$. Following Snieder (2006) and Fan & Snieder (2009), we can then write

$$\left[G_A(\mathbf{r}_B) - G_A^*(\mathbf{r}_B)\right]|f(\omega)|^2 \;=\; 2\mathrm{i}\omega \int u_s(\mathbf{r}_A)u_s^*(\mathbf{r}_B)\,\mathrm{d}V \tag{2}$$

with the integration taken over the volume containing the sources s, and * denoting complex conjugation. In the time-domain, eq. (2) is a cross-correlation and thereby the fundamental relation for extracting the superposition of the Green's function and its time-reversed equivalent based on observations at two locations A and B. By inspection of eq. (2), the 'Volume of Relevance' is defined as that region which contributes the most to Green's function. Plotting the integrand of eq. (2), the EGF kernel, gives a visual sense of how this volume is distributed in space. Note that the spatial character of the VoR is independent of the choice of scaling function $f(\omega)$, which out of simplicity is taken here as unity.

Starting simply, we examine a double half-space model in one dimension, with diffusivity D_1 in the region $x < 0$ and diffusivity D_2 in the region $x > 0$. As such, for an impulsive source located at $x_s > 0$, eq. (1) simplifies to

$$-\frac{\mathrm{d}^2u(x)}{\mathrm{d}x^2} + \frac{\mathrm{i}\omega}{D_1}u(x) = 0 \qquad x < 0, \tag{3a}$$

$$-\frac{\mathrm{d}^2u(x)}{\mathrm{d}x^2} + \frac{\mathrm{i}\omega}{D_2}u(x) = K_2\delta(x-x_s) \qquad x > 0, \tag{3b}$$

where $\delta(\cdot)$ denotes Dirac's delta function and $K_2 = 1/D_2$. Enforcing the homogeneous Dirichlet boundary condition as $x \rightarrow \pm\infty$ along with continuity of density u and flux $D\partial_x u$ at $x = 0$ yields a solution of the form:

$$u(x<0) \;=\; A_1\mathrm{e}^{\gamma_1 x}, \tag{4a}$$

$$u(x>0) \;=\; A_2\mathrm{e}^{\gamma_2 x} + B_2\mathrm{e}^{-\gamma_2 x} + \frac{1}{2\gamma_2 D_2} \times \left(\mathrm{e}^{-\gamma_2(x-x_s)} - \mathrm{e}^{\gamma_2(x-x_s)}\right) H(x-x_s), \tag{4b}$$

where H is Heaviside's function and $\gamma_\xi = (1+\mathrm{i})\sqrt{\frac{\omega}{2D_\xi}}$ for $\xi = 1, 2$. Values of the constant coefficients A_1, A_2 and B_2 in eqs (4a and b) are given by

$$A_2 = \frac{K_2}{2\gamma_2}\mathrm{e}^{-\gamma_2 x_s}, \quad B_2 = \left(\frac{D_2\gamma_2 - D_1\gamma_1}{D_2\gamma_2 + D_1\gamma_1}\right)A_2 \quad \text{and}$$

$$A_1 = \left(\frac{2D_2\gamma_2}{D_2\gamma_2 + D_1\gamma_1}\right)A_2.$$

Similarly, we wish also to consider the case where the source is located on the negative x-axis, in which case the governing equations are

$$-\frac{\mathrm{d}^2u(x)}{\mathrm{d}x^2}+\frac{\mathrm{i}\omega}{D_1}u(x)=K_1\delta(x-x_s)\qquad x<0, \tag{5a}$$

$$-\frac{\mathrm{d}^2u(x)}{\mathrm{d}x^2}+\frac{\mathrm{i}\omega}{D_2}u(x)=0\qquad x>0, \tag{5b}$$

with general solutions of the form

$$u(x<0)\;=\;A_1\mathrm{e}^{\gamma_1 x}+\frac{1}{2\gamma_1 D_1}\left(\mathrm{e}^{-\gamma_1(x-x_s)}-\mathrm{e}^{\gamma_1(x-x_s)}\right)H(x-x_s) \tag{6a}$$

and

$$u(x>0)\;=\;B_2\mathrm{e}^{-\gamma_2 x}. \tag{6b}$$

Values of A_1 and B_2 in eqs (6a and b) are

$$B_2=\frac{D_1K_1\mathrm{e}^{\gamma_1 x_s}}{D_1\gamma_1+D_2\gamma_2}\quad\text{and}\quad A_1=B_2-\frac{K_1}{2\gamma_1}\left(\mathrm{e}^{\gamma_1 x_s}-\mathrm{e}^{-\gamma_1 x_s}\right).$$

For a pair of receivers A and B located on the positive and negative sides, respectively, of the origin, we substitute the u from eqs (4) and (6) into the integrand of eq. (2) to quantify the VoR for the 1-D case.

For the 2-D case, we take the diffusivity as invariant in the y-direction same as the 1-D case and Fourier transform eq. (1) into the mixed (x, k) domain. Such a system is sometimes referred to as a '1.5-D problem' because the material interface is invariant in one coordinate direction whereas the source is not. For clarity, however, we will retain the '2-D' nomenclature to distinguish this problem from the previous one and to emphasize the 2-D nature of its solution. General forms of the solution in two dimensions are identical to eqs (4) and (6) upon the substitutions $\gamma_\xi^2=k^2+\frac{\mathrm{i}\omega}{D_\xi}$ and $K_\xi=\frac{1}{D_\xi}\mathrm{e}^{-\mathrm{i}ky_s}$ for $\xi=1,2$. Fourier transform over k back to the (x, y) domain were computed numerically using an adaptive quadrature scheme with a continued fraction expansion (Chave 1983).

Using the results of Fan & Snieder (2009, fig. 23) as a starting point for our analysis, we interrogate a series of models in one and two dimensions using the aforementioned formulae and constrain our investigation to a frequency of 0.02 Hz so that we may directly compare our results with theirs. Our models are double half-space models with diffusivity contrasts of 1:1, 1:3, 1:10 and 1:100 $\mathrm{m^2\,s^{-1}}$. Pairs of receivers are located symmetrically about the origin and with variable separation from 2 to 20 m.

Assuming that noise sources throughout the volume are similar in amplitude, those sources proximal to the receiver pair will surely contribute more the EGF than distal ones. Complications such as location-dependent source strength are beyond the scope of this study. As such, we restrict our analysis to a finite region around the origin containing the largest amplitude extrema of the EGF kernel—much like that done for the uniform model analysed in Fan & Snieder (2009). Furthermore, we exploit reciprocity along with eqs (4a and b) and (6a and b) to evaluate the EGF kernel (the integrand of eq. 2) on a discrete grid of sufficient density to visually reveal its structure, but not optimized for accurate evaluation of the integral in eq. (2). In other words, the nodes of the discrete grid are the locations of the sources. While a very dense grid is certainly important for accurate EGF estimates, simply plotting the kernel on a coarse grid is sufficient for revealing the VoR.

RESULTS

For the degenerate case of a homogeneous medium $D_1=D_2=1\ \mathrm{m^2\,s^{-1}}$ with receivers A and B separated by 2 m about the origin, we verify the results in Fan & Snieder (2009, fig. 23) and then extend their analysis to include separations up to 20 m over a range of diffusivity contrasts up to 1:10 (Fig. 1). Examination of these EGF kernels illustrates that as the receiver separation is increased, the VoR—that region with the greatest area under the curve—is generally constrained to lie between the receivers. However, we observe that as the receiver separation increases, the EGF kernel changes from being a function with only one extremum at the origin, to a function containing multiple extrema. In fact, in the region between the receivers, the EGF is the cosine function when D is uniform for all x. We can generalize this result for all offsets $0<x_A<\infty$ in the following way. Substituting the results of eqs (4a and b) and (6a and b) into the expression $G_A(x)G_B^*(x)$ from eq. (2), which is the EGF kernel with reciprocity applied, we find that the real part is given by

$$\mathrm{Re}\{G_A(x)G_B^*(x)\}=\frac{1}{4D\omega}\exp\left(-a\sqrt{\frac{2\omega}{D}}\right)\cos\left(x\sqrt{\frac{2\omega}{D}}\right), \tag{7}$$

for the case where the receiver locations are given by $\pm a$ and $|x|\le a$. In the remainder of the x domain, where $|x|>a$, the EGF kernel

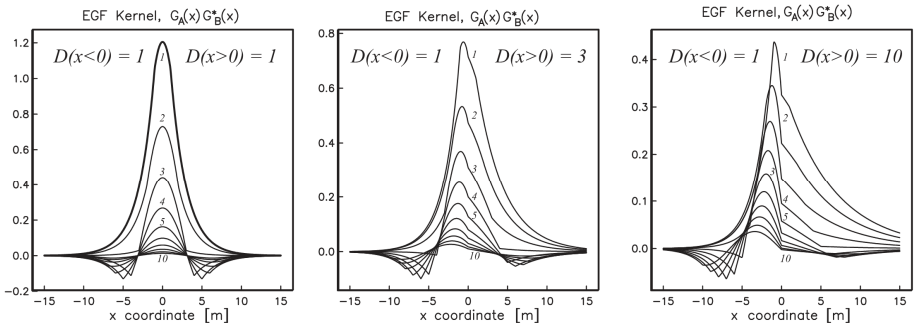

Figure 1. Integrand of eq. (2) for three different diffusion models: $D=1\ \mathrm{m^2\,s^{-1}}$ whole-space (left panel); double half-space with $D=1\ \mathrm{m^2\,s^{-1}}$ for $x<0$ and $D=3\ \mathrm{m^2\,s^{-1}}$ for $x>0$ (middle panel); and, double half-space with $D=1\ \mathrm{m^2\,s^{-1}}$ for $x<0$ and $D=10\ \mathrm{m^2\,s^{-1}}$ for $x>0$ (right panel). For each diffusion model, 10 different receiver pairs A and B are considered, located at x_A and $x_B=-x_A$, respectively, where the value of x_A annotates the resulting kernel functions.

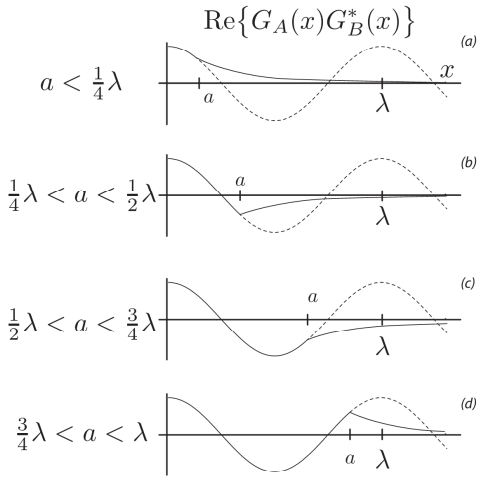

Figure 2. Sketch of the EGF kernel (solid line) for increasing receiver separation in a homogeneous 1-D whole-space. Receivers located at $x = \pm a$, see text for definition of λ.

is a simple exponential decay:

$$\mathrm{Re}\{G_A(x)G_B^*(x)\} = \frac{1}{4D\omega}\cos\left(a\sqrt{\frac{2\omega}{D}}\right)\exp\left(-|x|\sqrt{\frac{2\omega}{D}}\right). \quad (8)$$

In the segment (region) between receiver locations, the amplitude of the EGF extrema is bounded by the constant in eq. (7) preceding the cosine term, while the location of the zeros in the EGF kernel are driven by the 'wavelength' $\lambda = \pi\sqrt{2D/\omega}$ of the cosine term as $\cos(2\pi x/\lambda)$. Note that as a increases, more oscillations of the cosine term are revealed (Fig. 2) along with, in cases where $\frac{1}{4}\lambda < |a| (\mathrm{mod}\,\pi) < \frac{1}{2}\lambda$, cusps located directly at receiver locations. Therefore, for the 1-D homogeneous system, the relevance to EGF recovery of sources outside the region between any two receivers is inescapable. What matters in this region is that noise sources are located close enough to the receivers such that the envelope of the exponentially decaying EGF kernel is sufficiently large. The relevance of the region between the receivers, however, is separation dependent. For the special case where the receivers are separated by an integer product of the wavelength λ, the EGF kernel is identically zero and those noise sources do not contribute to the EGF.

However, when the medium is heterogeneous this specific conclusion is no longer valid. Most notable is the fact that the peak in the EGF kernel is skewed towards the domain with smaller diffusivity D, independent of receiver separation. While tempting to conclude at this point that the VoR lies mainly on the low-D side, observe also that the high-D side has a heavy tail with slow decay whereas the low-D side has comparatively large negative excursions of the EGF kernel.

Numerical integration of the EGF kernel over the semi-infinite domains $-\infty < x < 0$ and $0 < x < \infty$ quantifies the amount by which sources in these two domains each contribute to the total EGF estimate (Fig. 3). That is, it is a direct measure of whether the VoR lies in the more diffusive half-space or the less diffusive one or both. Because of the trade-off between negative and positive excursions of the EGF kernel, as receiver separation increases symmetrically about the origin, VoR shifts back and forth from the more diffusive domain to the less diffusive one and back again. Moreover, there exist critical receiver separations where the contribution from one side of the domain is identically zero (see Fig. 3), indicating that the entire EGF estimate is coming from sources in the other.

When examining the 2-D EGF kernel, we see that heterogeneity has a similar effect to the skew as it does in 1-D (Fig. 4), and that in general, the VoR for homogeneous media is again constrained to that region nearest and between the receivers. Numerical integration of the EGF kernel with Gaussian quadrature reveals that, as in the 1-D case, the VoR shifts between the positive and negative half-spaces as receiver separation increases (Fig. 5). We also observe in both one and two dimensions that the frequency over which these shifts occur decreases as the diffusivity contrast increases. Thus, for high diffusivity contrasts, the low-D side remains the VoR for separations up to a few tens of metres.

Finally, we observe that moderate rotations of the symmetric receiver pair about the origin (Fig. 6) do not change the overall conclusions stated earlier, which were based on receivers located along a line orthogonal to the diffusivity interface. However, as the receiver pair is rotated 90° (Fig. 7), with each receiver on the interface itself, the VoR flips to the high-D side for short offsets—the reverse of that seen for receivers oriented orthogonal to the interface. For large diffusivity contrasts, the VoR remains on the high-D side for larger receiver separations than seen earlier, extending upwards towards several tens of metres (Fig. 8).

DISCUSSION

Although the analysis presented earlier is not aimed directly at a particular experiment design or exploration scenario, it is worth pointing out the EGF estimation in dissipative systems (the details of which are examined here) is potentially relevant to

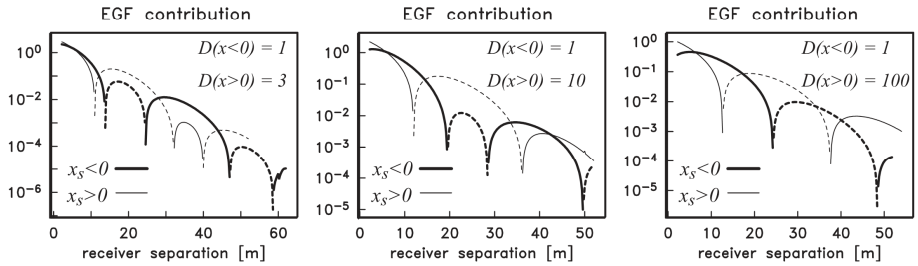

Figure 3. Evaluation of the 1-D EGF kernel over the semi-infinite domains $-\infty < x < 0$ (heavy line) and $0 < x < \infty$ (light line) for last two diffusion models described in Fig. 1 (left-hand side, centre) and a high-contrast 1:100 model (right-hand side). As before, the receiver separation is symmetric about the origin and given by $x_A - x_B = 2x_A$. Negative values of the integral are indicated by the dashed line.

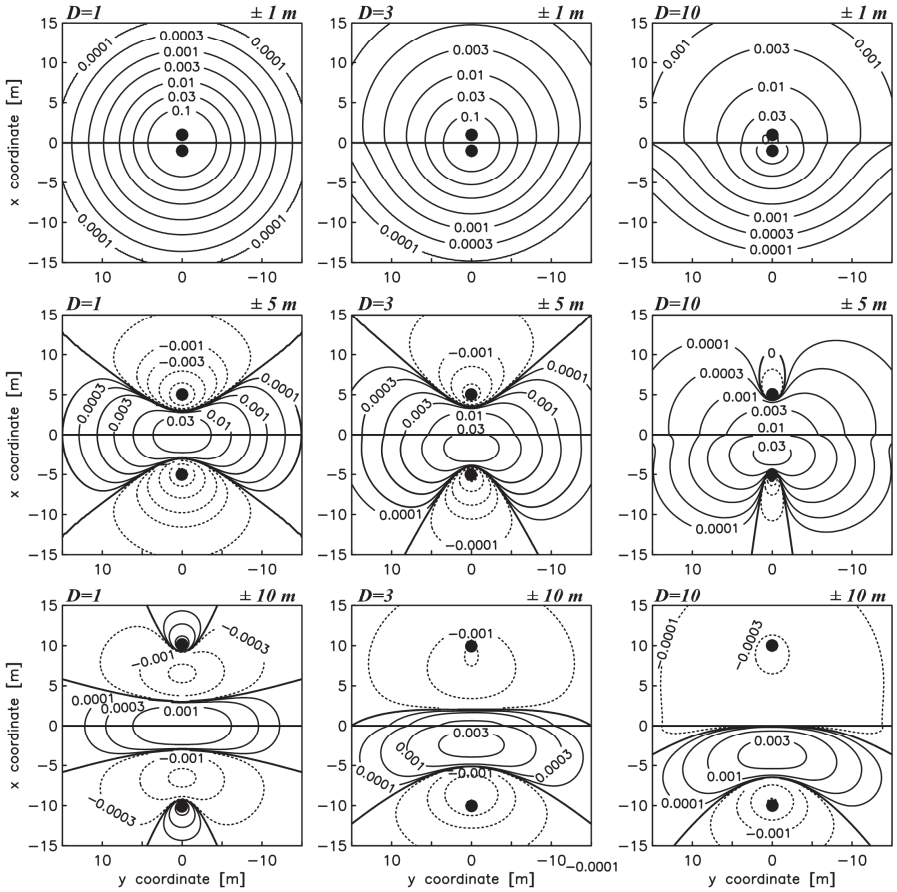

Figure 4. 2-D equivalent of the 1-D results shown in Fig. 1, but for a limited selection of receiver offsets: ±1 m (top panels); ±5 m (middle panels); and, ±10 m (bottom panels). Receiver locations are indicated by the heavy dots. As before, the value of D for the $x > 0$ upper half-space varies from 1 (left-hand side) to 3 (centre) to 10 m^2 s^{-1} (right-hand side) whereas $D = 1$ m^2 s^{-1} for the $x < 0$ lower half-space.

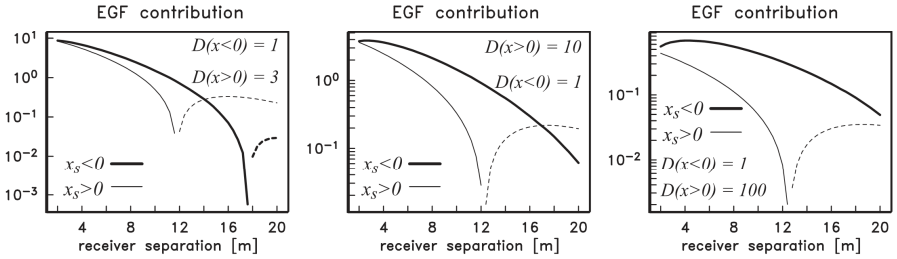

Figure 5. Evaluation of the 2-D EGF kernel in Fig. (3) over the semi-infinite domains $-\infty < x < 0$, $-\infty < y < \infty$ (heavy line) and $0 < x < \infty$, $-\infty < y < \infty$ (light line) for the 1:3 (left-hand side), 1:10 (centre) and 1:100 (right-hand side) diffusion models. Receivers A and B are located at $\mathbf{x}_A = (x_A, 0)$ and $\mathbf{x}_B = (x_B = -x_A, 0)$, respectively, along a line orthogonal to the interface separating the two half-spaces. As before, negative values of the integral are indicated by the dashed line.

common problems in exploration geophysics. It is already well known that the diffusion equation is a reasonable model for understanding the late-time intensity of multiply scattered acoustic waves (e.g. Lobkis & Weaver 2001). As in Snieder (2006) our use of the term 'pressure' may also follow from the concept of 'pore pressure' in the modelling of fluid flow in porous media whose theory is built upon the diffusion equation. When considering how might our theoretical results apply to exploration problems, the easiest leap

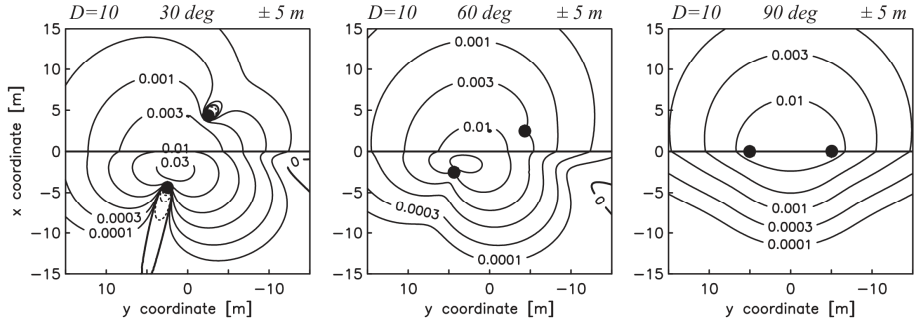

Figure 6. Distortion of EGF kernel for the 1:10 model as a pair of receivers separated by 10 m is rotated about the origin by 30° (left-hand side), 60° (centre) and 90° (right-hand side).

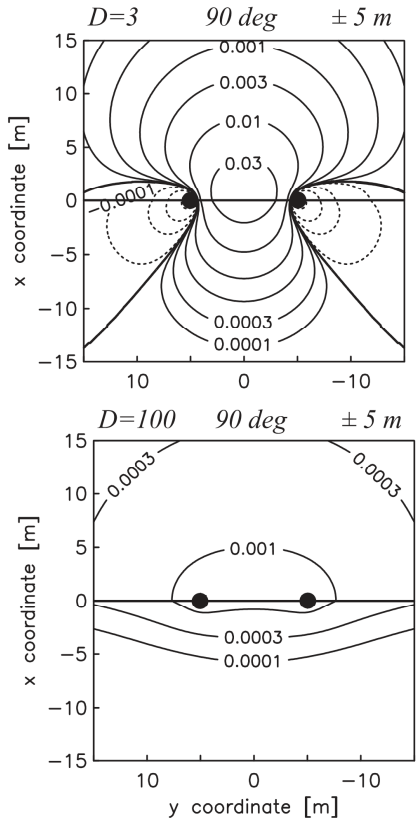

Figure 7. Distortion of the EGF kernel for a pair of receivers on the $x = 0$ interface, separated by 10 m like in Fig. 4, as D in the upper half-space is varied from 3 (top panel) to 100 m^2 s^{-1} (bottom panel).

to make is towards problems involving estimation of subsurface hydrological and/or reservoir parameters. Measurement of concentrations of aqueous contaminants may also lead to Green's function retrieval, provided that the pore-scale interstitial/surface chemistry is properly modelled. Such details, however, are beyond the scope of this study.

Instead, while the question, 'Which part of the system contributes most to EGF estimation?' can be recast entirely in terms of analytic formulae (indeed, integrals of the EGF kernels are straightforward to evaluate), the richness of the EGF kernel's complexity is easily observed through simple graphical representation. The region which contributes most—the VoR—is a complicated function of the observation points from which the cross-correlated time-series is drawn. However, for short offsets we can draw some general conclusions. In the case where receivers are located opposite an interface in diffusivity, the VoR in the limit of decreasing receiver separation is the low-diffusivity region. Such a scenario might occur in a borehole environment with a pair of downhole receivers straddling a lithological contact. In contrast, when the receivers are both located on the interface itself, the VoR for short separations is the 'more' diffusive side. In the limit of extreme contrasts in diffusivity, say 1:10 or 1:100, this observation remains true for separations up to several tens of metres. Downhole receivers on a given lithological contact in neighbouring boreholes would be one exploration scenario where such a generalization might apply.

Low-frequency electromagnetic induction also obeys a diffusion equation similar to eq. (1) depending on the electromagnetic source and underlying geology. In such cases the electrical resistivity plays the role of diffusivity D and our results suggest that EGF estimation from surface-based measurements are more strongly influenced by sources located in the resistive air region than those located in the relatively conductive Earth region. This should not be too surprising, given the contrast in electrical conductivity between the air and Earth regions by several orders of magnitude. Nonetheless, such conclusion is simply and end-member case of the more general behaviour such solutions exhibit, behaviour that is laid out here for range of contrasts extending beyond the simple air/Earth interface problem.

Note that the application of our results to surface-based geophysical measurements rests on the assumption that the 'air' region be described by a very large, but still finite, diffusivity. Although such an approximation is common in computational electromagnetics, it is important to note that in the special case where this region is assigned an infinite diffusivity value, the volume integrals in our eq. (2) are no longer appropriate and instead are replaced by a surface integral along the air/Earth interface. Fan *et al.* (2010) exploit this fact in their application of EGF concepts to marine electromagnetic exploration scenarios.

Note that the choice of length scales, diffusion coefficients and frequencies used in this paper were chosen for direct comparison

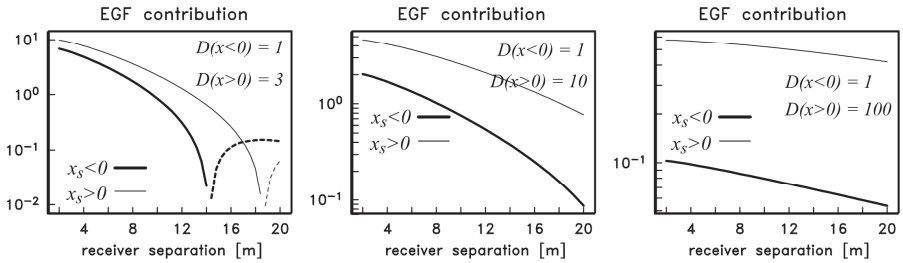

Figure 8. Evaluation of the 2-D EGF kernel over the semi-infinite domains $-\infty < x < 0$, $-\infty < y < \infty$ (heavy line) and $0 < x < \infty$, $-\infty < y < \infty$ (light line) for the 1:3 (left-hand side), 1:10 (centre) and 1:100 (right-hand side) diffusion models. Receivers A and B are located at $\mathbf{x}_A = (0, y_A)$ and $\mathbf{x}_B = (0, y_B = -y_A)$, respectively, lying directly on the interface separating the two half-spaces. As before, negative values of the integral are indicated by the dashed line.

with the results in Fan & Snieder (2009). However, in applying these results to the electromagnetic problem—as suggested earlier—the choice of diffusivity values in the range 1–100 $m^2\,s^{-1}$ corresponds to electrical resistivities on the order of 1–100 $\mu\Omega$m, values uncommon in general geological settings. Simply scaling the diffusivity and units of $km^2\,s^{-1}$ and length to km instead of m puts the resistivity values back in the geologically sensible range and emphasizes that the fact that terms like 'short' as used earlier are relative, depending on the value of the material properties.

ACKNOWLEDGMENTS

The authors are grateful for the many helpful comments provided by Mark Everett, Evert Slob and one anonymous reviewer and for their assistance in improving both the readability and rigour of the original manuscript. Scholarship support for SS was kindly provided by the Society of Petrophysicists and Well Log Analysts (SPWLA).

REFERENCES

Campillo, M. & Paul, A., 2003. Long-range correlations in the diffuse seismic coda, *Science,* **299,** 547–549.

Chave, A.D., 1983. Numerical-integration of related Hankel-transforms by quadrature and continued-fraction expansion, *Geophysics,* **48,** 1671–1686.

Claerbout, J.F., 1968. Synthesis of a layered medium, *Geophysics,* **33,** 264–269.

Curtis, A. & Halliday, D., 2010. Directional balancing for seismic and general wavefield interferometry, *Geophysics,* **75,** SA1–SA14.

Fan, Y. & Snieder, R., 2009. Required source distribution for interferometry of waves and diffusive fields, *Geophys. J. Int.,* **179,** 1232–1244.

Fan, Y., Snieder, R., Slob, E., Hunziker, J., Singer, J., Sheiman, J. & Rosenquist, M., 2010. Synthetic aperture controlled source electromagnetics, *Geophys. Res. Lett.,* **37,** L13305, doi:10.1029/2010GL043981.

Li, H., Bernardi, F. & Michelini, A., 2010. Surface wave dispersion measurements from ambient seismic noise analysis in Italy, *Geophys. J. Int.,* **180,** 1242–1252.

Lobkis, O.I. & Weaver, R.L., 2001. On the emergence of the Green's function in the correlations of a diffuse field, *J. acoust. Soc. Am.,* **110,** 3011–3017.

Sato, H., 2009a. Green's function retrieval from the CCF of coda waves in a scattering medium, *Geophys. J. Int.,* **179,** 1580–1583.

Sato, H., 2009b. Retrieval of Green's function having coda from the cross-correlation function in a scattering medium illuminated by surrounding noise sources on the basis of the first order Born approximation, *Geophys. J. Int.,* **179,** 408–412.

Shamsalsadati, S. & Weiss, C.J., 2010. Retrieving the impulse response of the Earth due to random electromagnetic forcing, *Phys. Rev. E,* **81,** 036603, doi:10.1103/PhysRevE.81.036603.

Slob, E., Snieder, R. & Revil, A., 2010. Retrieving electric resistivity data from self-potential measurements by cross-correlation, *Geophys. Res. Lett.,* **37,** L04308, doi:10.1029/2009G.

Slob, E. & Wapenaar, K., 2007. GPR Without a source: cross-correlation and cross-convolution methods, *IEEE Trans. Geosci. Remote Sens.,* **45,** 2501–2510.

Slob, E. & Weiss, C.J., 2011. Lagrangian energy norms for retrieving the impulse response of the Earth due to random electromagnetic forcing, *Phys. Rev. E,* **84,** doi:10.1103/PhysRevE.84.027601.

Snieder, R., 2004. Extracting the Green's function from the correlation of coda waves: a derivation based on stationary phase, *Phys. Rev. E,* **69,** 046610, doi:10.1103/PhysRevE.69.046610L042247.

Snieder, R., 2006. Retrieving the Green's function of the diffusion equation from the response to a random forcing, *Phys. Rev. E,* **74,** 046620, doi:10.1103/PhysRevE.74.046620.

Snieder, R., 2007. Extracting the Green's function of attenuating heterogeneous acoustic media from uncorrelated waves, *J. acoust. Soc. Am.,* **121,** 2637–2643.

Wapenaar, K. & Fokkema, J., 2006. Green's function representations for seismic interferometry, *Geophysics,* **71,** SI 33–46.

Wapenaar, K., Slob, E. & Snieder, R., 2008. Seismic and electromagnetic controlled-source interferometry in dissipative media, *Geophys. Prospect.,* **56,** 419–434.

SUPPORTING INFORMATION

Additional Supporting Information may be found in the online version of this article:

Scripts. The MATLAB scripts used for the calculations in this paper.

Please note: Wiley-Blackwell are not responsible for the content or functionality of any supporting materials supplied by the authors. Any queries (other than missing material) should be directed to the corresponding author for the article.

Chapter 4: Time-Series Analysis of Lossy Interferometry Data and Its Application to Bayesian Inversion of Synthetic Borehole Pressure Data

4.1 Abstract

Applying cross-correlation based interferometry in diffusive systems requires volumetrically distributed sources in an infinite domain. However, having such a source distribution in the real world practice is not possible. In this study, the number and distribution of sources required to reconstruct EGF (Empirical Green's Function) to a given error tolerance is investigated through numerical modeling. Time-series analysis of the interferometry data confirmed the previous findings in homogenous media where the width of source distribution needed to reconstruct EGF up to a desired time depends on the receiver separation and diffusivity of the medium. Here, a suite of 1-D double half-space models is examined in which receivers are located on either side of the interface. Results show that sources need to be further into the region with higher diffusivity than into the low diffusivity region. In the limiting case of a closely spaced receiver pair far from the bed contact, sources are required only in the region where the receivers reside, as expected. However, in the intermediate case where the receivers are sufficiently close to the bed contact such that the wholespace response extends a distance z across the contact, the requisite region across the contact expands by the factor of square root of D_2/D_1. Analysis of a three-layered system simulating a reservoir layer between two impermeable layers revealed that the EGF could be reconstructed due to sources mainly in the middle reservoir layer. The 1-D Bayesian inversion of the interferometry data demonstrated that the true

model and its uncertainty could be recovered using the noisy data. For large 3-D problems where the number of models is greater than the number of data, calculation of the Jacobian matrix is computationally prohibitive. As a preliminary step towards this ultimate goal, an adjoint-based sensitivity calculation for diffusive system is presented (Appendix B).

4.2 Introduction

The Empirical Green's Function (EGF) estimation from cross-correlation of time-series measured at two receiver locations, called interferometry or virtual source method enables the characterization of the subsurface properties without the need for engineered sources. In experiment scenarios where deployment of an engineered source is not possible, the EGF method provides previously unobtainable data (Schuster and Zhou, 2006).

Wavefields in lossless media and diffusive fields have different criteria on the requisite areas and the distribution of – random, naturally occurring or engineered – sources for EGF recovery. Far-field sources on an arbitrarily shaped surface bounding the receiver pair are enough to apply interferometry in the first case (Wapenaar & Fokkemma, 2006). For the second case; however, volumetrically distributed sources are required in order to reconstruct the EGF with a high accuracy (Snieder, 2006). Although there has been much study on EGF estimation using the physics of wave propagation, the virtual source method for the case of attenuative and diffusive systems is comparatively less developed. The impossibility of an infinite number of volumetrically distributed sources – required by the theory of interferometry in lossy and diffusive systems – challenges the application of this method in practice. The theory of the Green's function was developed for both pressure diffusive fields (Snieder, 2006) and also low-frequency inductive electromagnetics (Slob et al., 2007; Wapenaar et al., 2008; Shamsalsadati &

Weiss, 2010; Slob & Weiss, 2011); however, it is impossible to find an area fully impregnated with random, uncorrelated noises or engineered sources as required by these theories. Fan & Snieder (2009) studied a homogenous medium to quantify the number and distribution of sources that enables one to reconstruct EGF within an acceptable error. This work was then extended through investigating the effect of material heterogeneity and receiver separation in the frequency domain (Shamsalsadati & Weiss, 2012a). The purpose of the current study is to analyze the time-series of data through numerical experiments to demonstrate the effect of inhomogeneity and receiver location on the requisite source distribution.

The recovered EGF is then inverted using a Bayesian statistical approach to recover the material properties, namely – diffusivity. Bayesian methodology has a long history in the Earth sciences and continues to receive renewed attention (Jeffreys, 1924, 1939; Grandis et al., 1999; Malinverno, 2002; Chen et al., 2007; Ray & Key, 2012). There are practical advantages to the Bayesian approach, like its ability to quantify ambiguities of the solution by incorporating, in a statistical sense, the prior knowledge on the model parameters and their uncertainties. The Bayesian inversion results in a final solution called the posterior distribution that provides information on the uncertainties of the model parameters. Inspection of the posterior model distribution quantifies the non-uniqueness part of the inverse problem (Tarantola & Valette, 1982; Malinverno, 2002).

The content of this section runs as follows. I describe the methodology for the reconstruction of the time-series interferometry, followed by numerical experiments in double half-space and three-layered examples. In the first experiment the width and density of sources for different scenarios with variety of source-receiver configuration and diffusivity contrast between the layers is examined. For the three-layered medium interferometry data is

reconstructed in 1-D and 2-D; sources in the middle layer have a high diffusivity while the top and bottom layers are impermeable. The result of this last part is used to invert data for modeling fluid diffusivity (and corresponding permeability) using a Bayesian inversion approach in 1-D. A methodology is also introduced to speed up the inversion procedure by reducing the number of forward modeling needed in order to calculate the Jacobian matrix in the inversion for the cases of model overparametrization (Appendix B).

4.3 Reconstruction of Interferometry Data in the Time Domain

To investigate the requisite source distribution in lossy and diffusive media, it is important to understand first how the wavefield behaves in these systems. The analysis is based on the equation of Fickian diffusion in a generalized medium with space-dependent diffusivity *D*. Diffusion equation in time domain is given by Equation (4.1),

$$\frac{du(\mathbf{r},t)}{dt} - \nabla \cdot (D(\mathbf{r})\nabla u(\mathbf{r},t)) = s(\mathbf{r},t) \tag{4.1}$$

where u (wavefield) and s (source) are functions of both t (time) and $\mathbf{r}$ (position). For simplicity, we work with Equation (4.1) in the frequency domain, noting that a spatio-temporal impulse yields the Gaussian function G for u

$$-\nabla \cdot (D(\mathbf{r})\nabla G(\mathbf{r},\omega)) + i\omega G(\mathbf{r},\omega) = \delta(\mathbf{r}). \tag{4.2}$$

Equation (4.2) is solved analytically for double half-space model in both one and two dimensions (Shamsalsadati & Weiss, 2012a). In 1-D, the case of a double half-space model was examined, with diffusivity D_1 in the region $x < 0$ and diffusivity D_2 in the region $x > 0$. Enforcing the radiation condition as $x \to \pm\infty$ along with continuity of Green's function G and flux $D\partial_x G$ at $x =$

0 for an impulsive source located at $x_s < 0$, yields the Green's function solution in the following form

$$G(x<0)=\left\{\begin{array}{l}\left(\frac{1}{D_1\alpha_1+D_2\alpha_2}-\frac{1}{2D_1\alpha_1}\right)e^{\alpha_1(x+x_s)}+\left(\frac{1}{2D_1\alpha_1}\right)e^{\alpha_1(x-x_s)}\\ +\frac{1}{2D_1\alpha_1}\left(e^{-\alpha_1(x-x_s)}-e^{\alpha_1(x-x_s)}\right)H(x-x_s)\end{array}\right\} \quad (4.3a)$$

and

$$G(x>0)=\left(\frac{1}{D_1\alpha_1+D_2\alpha_2}-\frac{1}{2D_1\alpha_1}\right)e^{\alpha_1 x_s-\alpha_2 x} \quad (4.3b)$$

where H is Heaviside's function and $\alpha_n=(1+j)\sqrt{\omega/2D_n}$ for n= 1, 2 (Shamsalsadati & Weiss, 2012a). For the case of 2-D, the diffusion equation in the frequency domain for a double half-space model was solved by Fourier transforming space coordinate y into the wave number domain, k. Using this transformation, the 2-D solutions take the same form as Equations (4.3a-b) with the substitution $\alpha_n=\sqrt{k^2+(j\omega/D_n)}$. Extension to multi-layered systems is straightforward, resulting in recursion formulae for finding the unknown coefficients of the $e^{\pm kz}$ terms in each of the layers formulae based on continuity of flux and the wavefield at layer boundaries.

Following the theory of interferometry developed in diffusive systems (Snieder, 2006) we can simulate the effect of a virtual source at the location of one of the receivers by cross-correlating results of the Green's functions due to random excitations. We can derive the response of a virtual source by cross-correlation of the wavefields measured at two locations, A and B, due to the volumetrically distributed sources s with the power spectrum $|f(\omega)|^2$,

$$\left[G_A(\mathbf{r}_B)\text{-}G_A^*(\mathbf{r}_B)\right]\left|f(\omega)\right|^2 = 2i\omega\int_s u_s(\mathbf{r}_A)u_s^*(\mathbf{r}_B)d\mathbf{r}. \tag{4.4}$$

In this equation, $u_s(\mathbf{r}_A)$ and $u_s(\mathbf{r}_B)$ denote observed fields measured at the location of receivers A and B and integrated over the area contain sources, and * indicates the complex conjugate. For impulsive sources, the scalar field $u_s(\mathbf{r}_A)$ in the Equation (4.4) is replaced by the Green's function $G_s(\mathbf{r}_A)$, which is equivalent to $u_s(\mathbf{r}_A)$ scaled by $f^{-1}(\omega)$. The left hand side of this equation, $G_A(\mathbf{r}_B)\text{-}G^*_A(\mathbf{r}_B)$, represents the measured field at the location of one of the receivers (B) due to an impulsive source positioned at the location of the other receiver (A). Our purpose here is to reconstruct the response of the virtual source due to impulsive sources in the time domain using the aforementioned formulas. Note, however, that the diffusion equation solved in the frequency domain using Equation (4.4) gives the imaginary component of the Green's function only. To derive the full signal in the time domain both real and imaginary components are needed. For this purpose, the real part of the signal is reconstructed using the Kramers-Kronig relations. These equations are mathematical tools that relate real and imaginary components of response functions in physical systems (Toll, 1956; Kronig, 1926; Kramers, 1927) and are common in optical materials research for full signal reconstruction (Lucarini et al., 2005). For a known imaginary component $F_2(\omega)$ of a causal signal $F(\omega)$, Kramers-Kronig relations require the real component of $F(\omega)$ to be

$$F_1(\omega) = \frac{2}{\pi}P\int_0^\infty \frac{\omega' F_2(\omega')}{\omega'^2 - \omega^2}\, d\omega' \tag{4.5}$$

wherein P indicates the Cauchy principal value. Once both real and imaginary components of the EGF were recovered, we Fourier transform the full signal into the time domain.

4.3.1 Numerical Analysis for Double Half-Space Models in 1-D

Using the results of Fan & Snieder (2009; Figure 1a, top) as a starting point for our analysis, a series of models are cross-examined in 1-D using the aforementioned formulae. The first models (Figure 4.1a-c) are simple double half-space models with diffusivity, *D*, contrasts of 1:1, 1:10 and 1:100 m^2s^{-1}. Receivers are located symmetrically about the origin with separation of 2 m. The source distribution width ranges between -17 m and 17 m for homogenous medium with the source density of 1.147 m^{-1} (Fan & Snieder, 2009). Extending the work of Fan and Snieder to include inhomogeneous models (Figure 4.1a, middle and bottom), reveals that sources must be distributed asymmetrically in the system, and extend a distance into the high-*D* (D_2) side. For small receiver separations, this distance would be approximately proportional to $\sqrt{D_2/D_1}$ times the distance into the low-*D* (D_1) side. For full construction of the EGF time-series, it is found that sources must extend far into the high-*D* side of the model, whereas the locations of the requisite sources in the low-*D* side appears to be not affected by the presence of discontinuity at the interface (Shamsalsadati & Weiss, 2012b). Figure (4.1b) compares reconstructed EGF and the actual measurement between the virtual source and receiver for the three models shown in Figure (4.1a).

Using similar reasoning discussed by other authors for homogenous media (Mehrer, 2007; Fan & Snieder, 2009) and definition of the skin depth, sources within one skin depth, defined as the sources with the largest contribution. Let's assume that $D_2=X^2D_1$ and Δ indicates the distance between maximum width of the source distribution in the first medium where receiver A resides and this receiver (see Figure 4.2). Adding this information to the derivations in Equation (4.3), the maximum width of the source distribution in the second medium can be derived as

$$w_{S2} = \left(\Delta + |x_A|\right)X. \tag{4.6}$$

This relation could be developed for the other medium using the same reasoning discussed above. Then, Δ' which is equivalent of Δ in the high-*D* would be proportional to ($\sqrt{D_2/D_1}$) Δ. Consequently, one can find the width of distribution as

$$w = \Delta + r_{AB} + \Delta\sqrt{D_2/D_1} \tag{4.7}$$

where r_{AB} indicates the separation between two receivers *A* and *B* or the virtual source-receiver distance (Figure 4.2). Figure (4.3) demonstrates that increasing receiver separation in the first example (Figure 4.1) to 6 m about the origin increases the required width of sources in comparison to the first experiment. Based on the results of this experiment the density of sources is changed so that two to three sources remain between the receivers. This new result confirms previous findings that sources between the receivers are more important than the distal ones (Fan & Snieder, 2009; Shamsalsadati & Weiss, 2012a).

The third numerical experiment is conducted using diffusivity contrast of 1:10 m^2s^{-1} where the receiver pair separated by 2 m is located in the medium with lower diffusivity. It is shown that when receivers are far from the interface (centered at -16 m), the majority of sources need to be in the low-*D* side. However, as the receiver pair gets closer to the interface, this important region of sources shifts towards the other medium, high-*D* side (Figure 4.4). It can be concluded from this experiment that in the case where the receivers are sufficiently close to the bed contact such that the wholespace response extends a distance *z* across the contact, *z* is scaled by the factor of $\sqrt{D_2/D_1}$.

Figure (4.5) demonstrates the outputs of the numerical experiments where the sensor pairs located in the first and second medium are symmetric about the interface (separated by 2 m and centered at ± 18 m). The results indicate that for receivers located in the low diffusive side, EGF could be reconstructed without any source being in the second medium. However, this is not true for the latter where sensors are in the opposite side of the interface. In this case, it seems that not only more sources are needed in the domain with higher diffusivity where receivers are positioned but also some are still needed to be in the other side of the interface (Figure 4.5). Therefore, for a close-spaced receiver pair far from the interface, sources are desired only in the region where the sensors exist since it simulates the wholespace response. However, in the case where the sensors are close enough to the interface such that the wholespace response extends a distance *z* across the interface, the essential region across the contact expands by the factor of $\sqrt{D_2/D_1}$ (Shamsalsadati & Weiss, 2012b).

4.3.2 Numerical Analysis of a Three- Layered Medium in 1 and 2D

In this section, a numerical study is conducted to analyze the problem for a three-layered medium, representing a homogenous reservoir with a hydraulic diffusivity of 100 m^2/hour located between two impermeable layers with hydraulic diffusivities of 1 m^2/hour, Figure (4.6). In this figure, the triangles indicate pressure transducers which are cemented behind casing (Babour et al., 1995). The possibility of using the pressure transducers in the borehole was examined in the past (van Kleef et al., 2001; Bryant et al., 2002; Alpak et al., 2004). For 1-D case, sources separated by a meter reside in a line that connect receivers and exist in the middle layer only, Figure (4.7, bottom). In this experiment, it is assumed that for 2-D problem a large but limited number of impulsive sources are located inside the reservoir layer and also are

extended about 160 m at each side of the wells. The assumption for sources being in the high diffusive layer has been made based on the previous findings (Shamsalsadati & Weiss, 2012a), but it is also more realistic to expect majority of pressure fluctuations to be inside the reservoir layer. In addition, to simplify this experiment, Green's function due to ambient and uncorrelated sources is used. Adjustment for natural transient sources (see Wapenaar & Fokkema, 2006) merits further investigation but is beyond the scope of the current study.

Figure (4.7, top) demonstrates how the results of the time-series for the actual and EGF calculations fit with each other in 1-D for receivers separated by 4 m in the middle of the second layer. In 2-D, the time-series of interferometry data is reconstructed for the receivers located in the first well (shown by A , B) and also where those are cemented at two different wells (A , B') opposite to each other. Figure (4.8, top) shows the results of the EGF for receivers A and B separated by 10 m (Figure 4.6) which fit with the actual measurements. Figure (4.8, bottom) demonstrates a similar plot of the time-series data in 2-D for receivers A, B'. The total error caused by using the interferometry and also applying Kramers-Kronig to reconstruct the EGF is less than 10% in average and increases to about 13% or more at a few points. Note also that the error increases at very late times. The time up to which EGF could be reconstructed with a high accuracy depends on the factors such as diffusivity, receiver separations, and also the width of the source distribution (Fan & Snieder, 2009).

4.4 Inversion of Data Derived from Interferometry in 1-D

4.4.1 Nonlinear Inversion

Broadly speaking, our goal in inversion is to recover estimates – and more importantly, uncertainties – of subsurface material properties. However, there is no single solution to the inverse problem; therefore, the most important task is quantification of non-uniqueness. In addition to finding the model that provides the best "fits" with the data, we aim to address the uncertainties of that model; thus, this approach is statistical in nature and probability theory can be used as a tool to describe the inverse problem. The conventional methods for nonlinear inversion such as the gradient based inversion approaches attempt to regularize the problem through penalizing the model roughness or derivative of the model. These methods result in a point estimate of the model parameter and do not address the nonsingular part of the inversion problem. Bayesian approach is another way of inverting different data sets which takes fuller account of uncertainties of the model parameters in comparison to the classical methods by quantifying ambiguities based on the conditional probabilities. These conditional probabilities indicate the degree to which one set of model parameters fit with the data better than the other set of model parameters. Probabilistic Bayesian inference updates prior beliefs on the model after observing data; therefore, one needs to define the probability in terms of degree of belief before starting the analysis. Bayesian combines the prior knowledge on the model with the information on how well this Earth model fits with the observed data. The new results are then used to update the prior knowledge on the model parameters. This information results in a solution called posterior distribution which is an indicator of the uncertainty of the proposed model. Examination of the posterior distribution quantifies non-uniqueness part of the inverse problem (Tarantola & Valette, 1982; Malinverno, 2002). Bayesian inversion is different than other inversion methods common in geoscience problems in that it considers a probability distribution which reflects *our* uncertainty in ambiguity in the true value of a given model parameter (Jaynes,

2003). Using Bayes, regularization in the gradient methods is replaced by prior probability through confining the space limit of the possible Earth models. The application of the Bayesian statistical methodology in Earth sciences has a long history (Jeffreys, 1924, 1939) and revitalized by Mosegaard & Tarantola (1995) and Tarantola (2005). It has gained recent popularity for solving inverse problems in DC resistivity (Malinverno, 2000, 2002), seismic tomography (Bauer et al., 2003), self potential (Woodruff et al., 2010), airborne electromagnetics (Minsley, 2011), Marine CSEM (Ray & Key, 2012), among other applications.

Given a PDF (Probability Distribution Function) $p(\mathbf{m})$ representing our prior and belief in the value and uncertainty of model parameters **m**, Bayes rule,

$$p(\mathbf{m} \mid \mathbf{d}) = \frac{p(\mathbf{d} \mid \mathbf{m})\, p(\mathbf{m})}{p(\mathbf{d})} \tag{4.8}$$

provides a mechanism for updating this belief based on $p(\mathbf{m}|\mathbf{d})$ in light of new evidence $p(\mathbf{d}|\mathbf{m})$. The sampling distribution $p(\mathbf{d}|\mathbf{m})$ reflects the likelihood of observing data under the specified prior model. The posterior distribution, $p(\mathbf{m}|\mathbf{d})$, represents the probability that the model is true, given the data and previous information about the model parameters (or in Bayes literature, the "hypothesis"). The denominator in Equation (4.8) is the marginal likelihood independent of **m**, and hence a simple scaling constant that can be safely ignored. One of the advantages of this approach in comparison to the classical regularization methods is that it is easier to analyze and defend the degree of regularization by showing the probability of various possible model parameters under the prior distribution.

Markov chain Monte Carlo (MCMC) algorithms are common algorithms to implement Bayesian approach (Robert & Casella, 2004). These algorithms consist of a random sampling

from the probability distribution where the choice of the next state depends on the current state. After an initial burn-in period in which random walkers move in the sampling region, the chain samples posterior PDF with higher probabilities (Robert & Casella, 2004). The burn-in period is a number of iterations at the early stage of the MCMC sampling before the chain converges to the high probability region. There are several MCMC algorithms that produce Markov chains in order to be implemented in the Bayesian inversion (Robert & Casella, 2004; Metropolis et al., 1953; Hasting, 1970; Green, 1995). The sampling scheme used in this study to invert the interferometry data is based on the Metropolis-Hasting algorithm (Metropolis et al., 1953; Hasting, 1970) which is a MCMC method aim to achieve random samples from a proposal probability distribution.

We can model diffusivity given the data derived from interferometry using the Bayesian inversion method. The inversion is applied on the data measured for the three-layered medium. There is a total number of 271 data measured by 9 pairs of receivers positioned in the second layer (Figure 4.7, bottom). Model parameters are defined as a vector of log-diffusivities in each layer $\mathbf{m} = (\log D_1, \log D_2, \log D_3)$ and interferometry data as $\mathbf{d} = (d_1, d_2, d_3, \ldots d_N)$. The Diffusion equation relates the scalar diffusive field u and also diffusion coefficient D (Equation 4.1, 2); and hence, one can model diffusivity having the pressure data. Note also that permeability (k) can be readily estimated having the fluid properties and the porosity

$$D = \frac{k}{\eta \phi \beta} \tag{4.9}$$

where η and β denote viscosity and compressibility of the fluid flowing through the pore spaces of the rocks. On the other hand, porosity shown by φ and also thickness of each layer are assumed to be available by well log information. It is further assumed that there is a single phase

fluid flowing through the pore spaces of the homogenous rock within each layer. These parameters are listed in Table (4.1).

Metropolis-Hasting algorithm, a commonly used MCMC algorithm, is used to invert the data sets. This algorithm uses a proposal distribution to sample a new model where the choice of this model depends on the current model. Then, the proposed model is accepted with an acceptance probability which depends on the prior, likelihood, and proposal PDFs for the current and also the proposed models. These PDF functions are all described by multivariate normal distributions assuming that the noise in the data is Gaussian (Malinverno, 2002; Ray & Key, 2012). The prior distribution depends on the current model **m**, its mean $\bar{\mathbf{m}}$, and the covariance matrix of $\mathbf{C_m}$

$$p(\mathbf{m}) = \frac{1}{[(2\pi)^M \det \mathbf{C_m}]^{1/2}} \exp\left[-\frac{1}{2}(\mathbf{m}-\bar{\mathbf{m}})^T \mathbf{C}_{\mathbf{m}}^{-1}(\mathbf{m}-\bar{\mathbf{m}})\right]. \tag{4.10}$$

In this equation, *M* denotes the number of layers and the covariance matrix indicates the uncertainty in the model parameters. Likelihood function which is the probability of data given the model can be found as

$$p(\mathbf{d}\,|\,\mathbf{m}) = \frac{1}{[(2\pi)^N \det \mathbf{C_d}]^{1/2}} \exp\left[-\frac{1}{2}(\mathbf{d}-f(\mathbf{m}))^T \mathbf{C}_{\mathbf{d}}^{-1}(\mathbf{d}-f(\mathbf{m})\right], \tag{4.11}$$

wherein *f(***m***)* is a forward modeling function that results in a vector of predicted data given the model. In this equation, the covariance matrix $\mathbf{C_d}$ indicates the error expected for each of the observed data and *N* represents the total number of data used. The best choice of the proposal distribution would be a function that approximates posterior PDF of the model (Malinverno,

2002). Hence the covariance of $\mathbf{C_{pos}}$ used for sampling is considered to be proportional to the posterior's covariance ($\mathbf{J}^T\,\mathbf{C_d}^{-1}\,\mathbf{J}+\mathbf{C_m}^{-1})^{-1}$ (Malinverno, 2002; Bard, 1974) where **J** is the Jacobian matrix or derivatives of the predicted data with respect to the model. The proposal distribution is given as the following

$$g(\mathbf{m'}\,|\,\mathbf{m}) = \frac{1}{[(2\pi)^M \det \mathbf{C_{pos}}]^{1/2}} \exp\left[-\frac{1}{2}(\mathbf{m'}-\mathbf{m})^T\,\mathbf{C}_{\mathbf{pos}}^{-1}(\mathbf{m'}-\mathbf{m})\right] \qquad (4.12)$$

where the proposed model is shown by **m'**. It needs to be mentioned that all of the above distributions are transformed in to the logarithmic scale to avoid numerical errors.

The Metropolis-Hasting algorithm starts by sampling a candidate model (**m′**) based on the current model (**m**). Then, the probability of acceptance α is calculated using

$$\alpha = \min\left[1, \frac{p(\mathbf{m'})}{p(\mathbf{m})}\cdot\frac{p(\mathbf{d}\,|\,\mathbf{m'})}{p(\mathbf{d}\,|\,\mathbf{m})}\cdot\frac{g(\mathbf{m}|\mathbf{m'})}{g(\mathbf{m'}|\mathbf{m})}\right] \qquad (4.13)$$

=min [1, (prior ratio)·(likelihood ratio)·(proposal ratio)].

The proposed model is accepted if the probability of acceptance α takes a value which is greater than a random number *r* sampled between 0 and 1. For $r < \alpha$, the current model is **m** replaced by the new model **m'** otherwise no change should be considered. The samples taken after the time when the burn-in period is reached represent the output. We stop the sampling when the samples are large enough to describe the posterior PDF (Malinverno, 2002). Note also that using the proposal distribution of Equation (4.12) makes the Bayesian inversion computationally expensive since the Jacobian matrix embedded in the posterior covariance needs to be evaluated at each iteration. To calculate the Jacobian, predicted data calculated by the forward model is

differentiated with respect to the model parameter; hence, the number of forward calculation depends on both the number of data (N) and the number of models (M).

McGillivray et al. (1994) discussed an alternative approach to reduce the cost of Jacobian calculation for inverse problems in electromagnetics using Maxwell equations. Their derivation was different than many others (Lanczos, 1961; Morse & Feschback, 1963; Oldenburg, 1990) in that the adjoint operator was not developed by the McGillivray et al., (1994), but they made it simpler to be applied on electromagnetic inverse problems in comparison to the previous works. The development of their work into the diffusion equation for scalar fields could be used in order to reduce the required number of forward calculations (Appendix B). Although applying this method reduces the cost of inversion, this would not make a significant change when using only a few models. Hence, the finding of (Equation B-5, see Appendix B) is not used in the current inversion example with three layers, but it is expected to be a helpful tool for future practices where the size of the model is large.

4.4.2 Inversion Results

Through using the Bayesian inversion method, I looked for the model that best describes the interferometry data. Data measured by the receivers positioned in the middle of the second layer are sampled up to 140 hours while this time is reduced as receivers get closer to the boundaries. This is due to the fact that the time up to which interferometry data can be reconstructed is higher where the pair of receivers is surrounded by a large number of sources (Fan & Snieder, 2009). For the receivers that reside in the neighborhood of the interfaces, this maximum time decreases noticeably as there is no source in the first and third layers.

To start the MCMC chain an initial Earth model was needed. It was assumed that enough information is not available on the model parameters and therefore the initial model was started to be homogenous everywhere about the most probable value of 25 m^2/hour. Then the model information and the errors were translated into the logarithmic scale. The code ran for 10,000 iterations where at each step the proposed model was evaluated for the acceptance which resulted in taking the total number of 4034 samples. Figure (4.9) shows how the misfit (the root mean square error) decreases as the number of samples increases until the burn-in period is reached. The burn-in period was reached after taking 95 samples when the misfit level in the order of 3×10^{-5} was achieved. The results of the Figure (4.10, right) demonstrate the posterior PDF for the three-layered model in the logarithmic space. The expected value of 1 m^2/hour for the impermeable layers on the top and bottom of the reservoir is within the 95% confidence interval of the posterior PDFs. The PDF of the sampled models for the reservoir layer also shows that the true diffusivity of 100 m^2/hour is sampled with a high probability. The diffusivity models could be replaced by the fluid permeability using the parameters of the reservoir and fluid parameters listed in Table (4.1), Figure (4.10, left).

4.5 Discussion

The two objectives of these experiments were first to analyze sensitivity on the required source distribution when using interferometry and second to model the data offered by this method using an effective tool such as a Bayesian inversion. EGF estimation in diffusive systems is related to the common exploration problems to find electromagnetic fields in low frequencies or pore pressure fields in fluid flowing media. Hence, an exploration scenario would be characterizing physical properties of fluids in hydrological or reservoir explorations.

Therefore, a synthetic reservoir experiment was designed to show the feasibility of using this method in practice. On the other hand, a perfect fit between the actual source and the receiver measurement with the EGF could not be retrieved by interferometry due to the assumed source requirements in addition to the Kramers-Kronig relation which was used for the full signal reconstruction. The majority of hydrological/ reservoir field measurements are completed in the time domain. Therefore, an alternative form of the EGF equation in the time domain (Snieder, 2006) can be used to avoid numerical error in the full signal reconstruction in the frequency domain. We may still expect the observation error caused by imperfect instrumentation, experiment designs, or other types of disturbances. The Bayesian inversion approach is a suitable approach for inverting data sets associated with large error since it gives a better understanding on the uncertainties of the model parameters. Although it is more expensive than other inversion methods, Bayes is an effective tool to invert geophysical or geological data in nonlinear problems. The derivation introduced in the appendix (Equation B.5) reduces the computational cost of the forward calculation in the Jacobian; and therefore, speeds up the MCMC convergence.

In the numerical experiments discussed a simplified version of the Earth model was used by making assumptions that could not exactly meet the requirements in a real world scenario. Note that physics and chemistry of the Earth in a real system is more complicated than what is outlined here and hence careful considerations should be made to treat the problem in practice. Considering the theory of EGF estimation in diffusive fields (Snieder, 2006; Shamsalsadati & Weiss, 2010; Slob & Weiss, 2011), and recent research developments to minimize the restrictions on the EGF method (Fan & Snieder, 2009; Shamsalsadati & Weiss, 2012a), the new

findings are useful to study the limitations on EGF estimation caused by imperfect sources or complexities of the subsurface.

4.6 Conclusion

Reconstruction of the time-series interferometry data for the proposed synthetic models revealed that sources must be expanded further into the high-*D* side in comparison to the low-*D* side of the model. A derivation for finding the required width of source distribution was also formulated which depends on the diffusivity in each medium, their contrast, and the receiver separation. It was further found that for a higher receiver separation, an essential density of sources is lower. It was concluded that the density of sources should be changed such that two to three sources remain between the receivers which verified prior studies that sources between the receivers are more important than the other sources. The numerical experiments pointed out that, in the case of a close-spaced receiver pair far from the interface, sources are required only in the region where the receivers exist.

The results of the numerical experiments showed that the fit between the actual source and the receiver measurement and the EGF is not exactly identical. This is due to the fact that the imperfect source distribution in addition to the Kramers-Kronig relation which was used for the full signal reconstruction introduces error. On the other hand, the Bayesian statistical inversion of the synthetic data calculated for a reservoir layer embedded in an impermeable region demonstrated that the algorithm converges toward the model that is close to the true model. Nonetheless, Bayesian inversion is computationally more expensive than other methods which make it difficult to apply especially where number of model is greater than the number of data. The Calculation of the Jacobian matrix for nonlinear inversion is one of the reasons the inversion

algorithm is slow. To overcome this problem, a formula was suggested to reduce the computational costs of the Jacobian matrix which an extension of the previous works into the generic form of scalar diffusive fields.

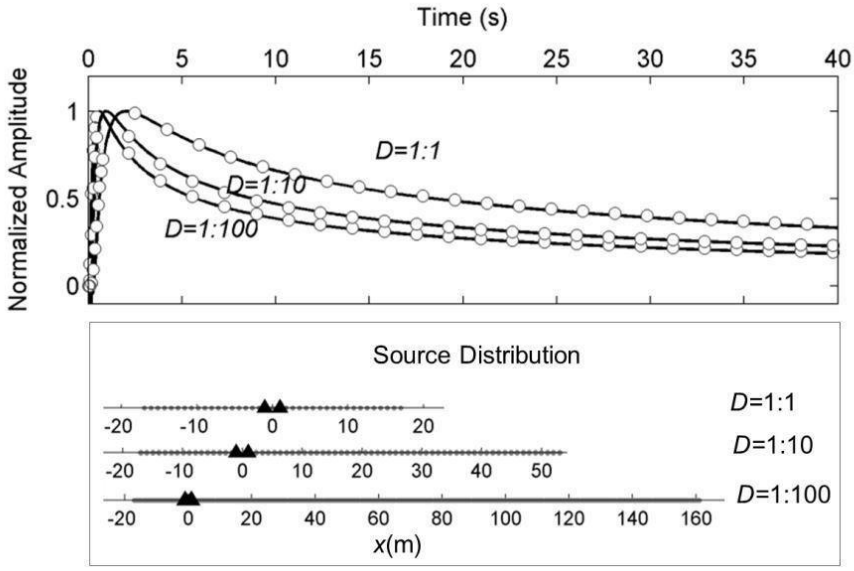

Figure 4.1: Time-domain analytic (solid black lines) and EGF (open circles) of the response of three diffusive systems: D=1 m^2/s wholespace (Fan & Snieder, 2009), 1:10 double half-space; and, 1:100 double half-space (top figure). Receivers are located at x = ±1 m (black triangles) with the interface at x = 0 and source locations are shown by the closed circles (bottom figure). Note that as diffusivity contrast increases, location of the requisite sources extends further into the high-D side of the model.

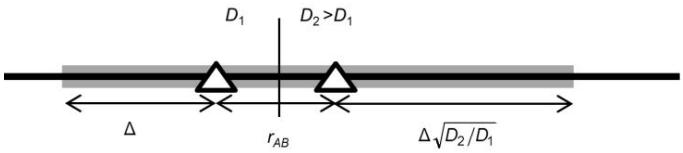

Figure 4.2: Sketch of receivers (circles) symmetric about the interface (vertical line) between the D_1 and D_2 half-spaces. The width of source distribution (thick gray line) depends on the diffusivity of each medium and also the receiver separation (r_{AB}).

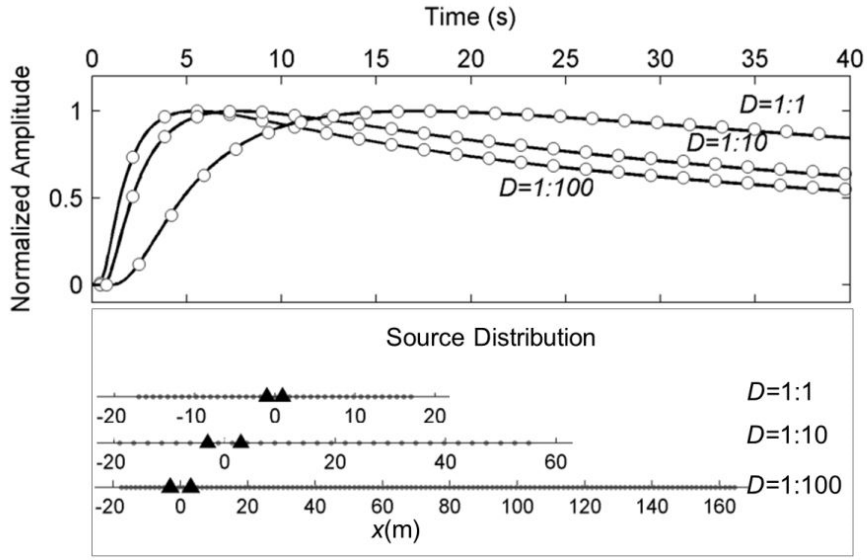

Figure 4.3: Time-series of analytic (solid black lines) and extracted EGF (open circles) for homogenous medium double half-spaces heterogeneous of 1:10, and 1:100 (top figure). Receivers are located at $x = \pm 3$ m (black triangles) with the interface at $x = 0$ and source locations are shown by the closed circles (bottom figure). Observe that location of the requisite noise sources extends further in both sides in comparison to the previous example, (Figure 4.1).

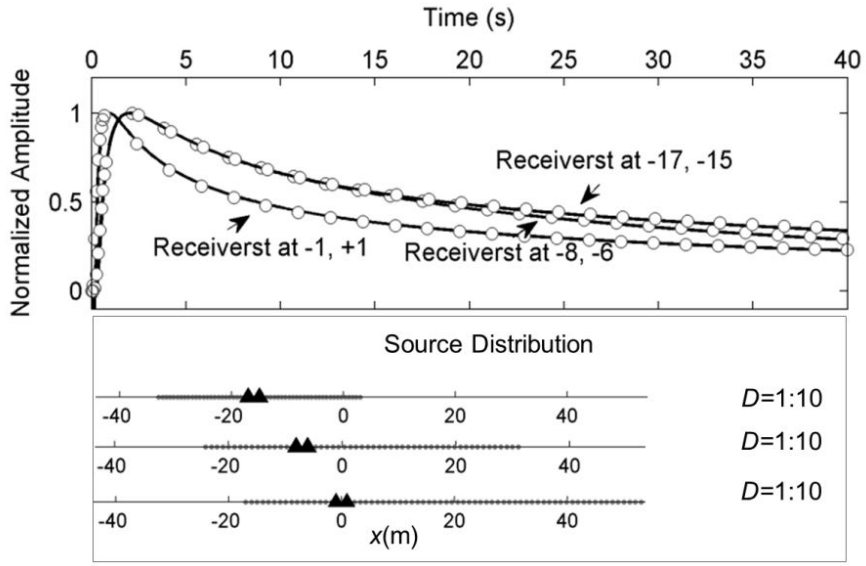

Figure 4.4: Time-domain analytic (solid black lines) and EGF (open circles) response of three systems with different receiver locations for fixed diffusivities of D_1=1 m^2/s and D_2= 10 m^2/s (top figure). Receivers are located at x = -17, -15 m, x = -8,-6 m; and, x = ±1 m with the interface at x = 0 and source locations are shown by closed circles. Notice that as the receiver pair gets closer to the interface, the important region of sources shifts towards the other medium (high-D side).

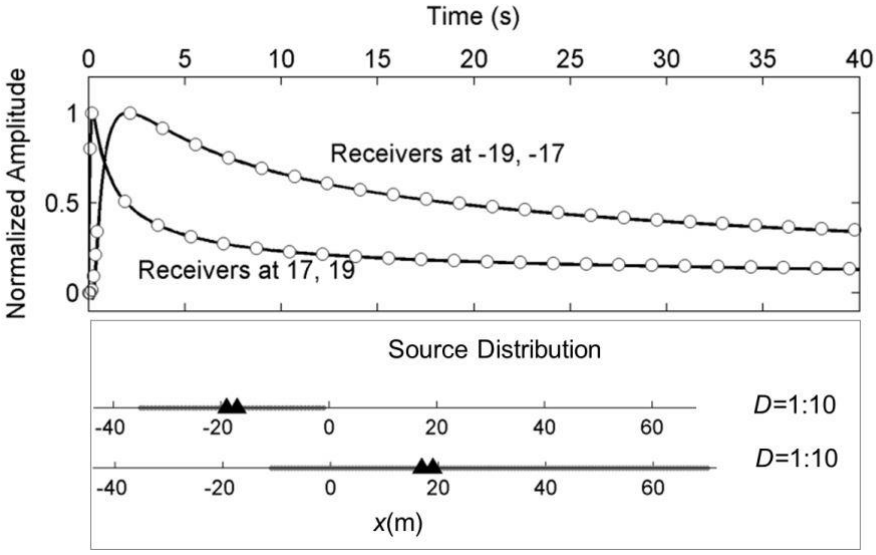

Figure 4.5: Analytic (solid black lines) and EGF (open circles) of response in the time domain of two systems for receiver pairs being symmetric about the origin and fixed diffusivities of D_1=1 m^2/s and D_2= 10 m^2/s (top figure). Receivers are located at x = -19,-17 m, x = 17, 19 m with the interface at x = 0 and source locations are shown by the closed circles. For receivers located in the low diffusive side, EGF could be reconstructed without any source being in the second medium which is not the case where receivers are in the opposite side of the interface.

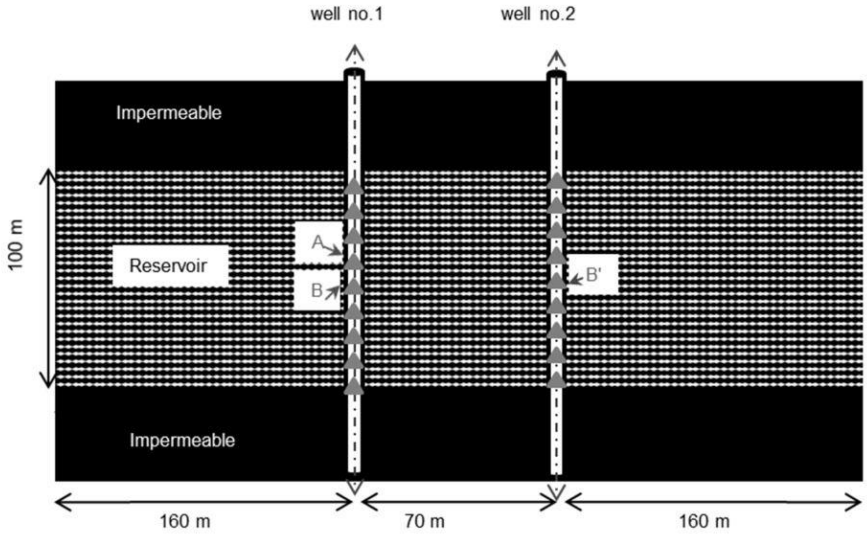

Figure 4.6: A synthetic model of a three-layered medium for a reservoir layer with hydraulic diffusivity of 100 m^2/hour between two impermeable layers (with diffusivity of $1m^2$/h). The gray triangles indicate receivers. 2-D time-series analysis was conducted for receivers A, B, and B' positioned at 45, 55, and 52 meters below the top of the reservoir, respectively due to impulsive sources (black dots) inside the reservoir layer.

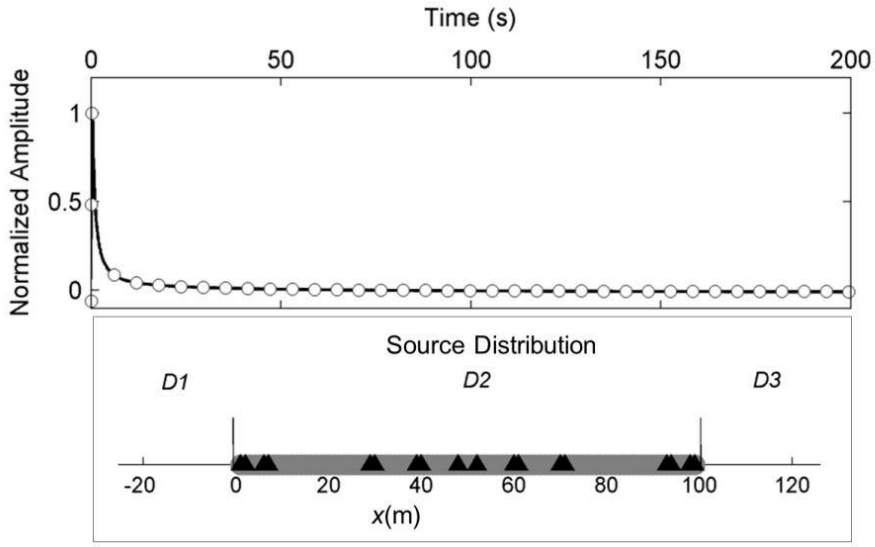

Figure 4.7: Time-domain analytic (solid black lines) and EGF (open circles) response of a three-layered medium in 1-D for receiver pairs being in the reservoir layer with diffusivity of D_2=100m^2/hour and D_1=D_3=1 m^2/hour (top figure). Layers are separated by vertical lines and receivers are demonstrated by black triangles (bottom figure). It is shown that EGF could be reconstructed with sources (closed circles) being in the middle layer only.

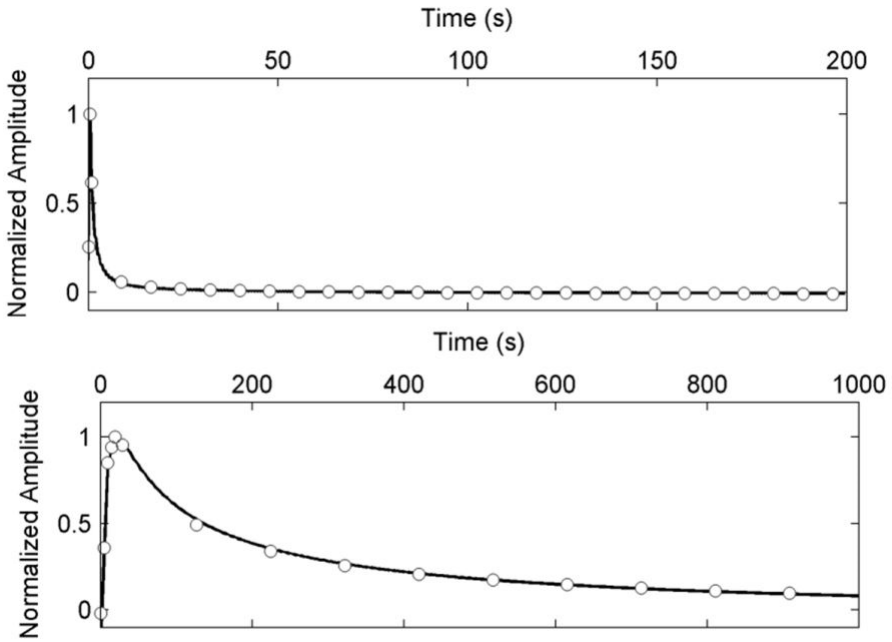

Figure 4.8: Time-series of single well (top) and cross well (bottom) analytic (solid black lines) and EGF (open circles) responses. Receiver geometries are taken from Figure (4.6, top and bottom, respectively).

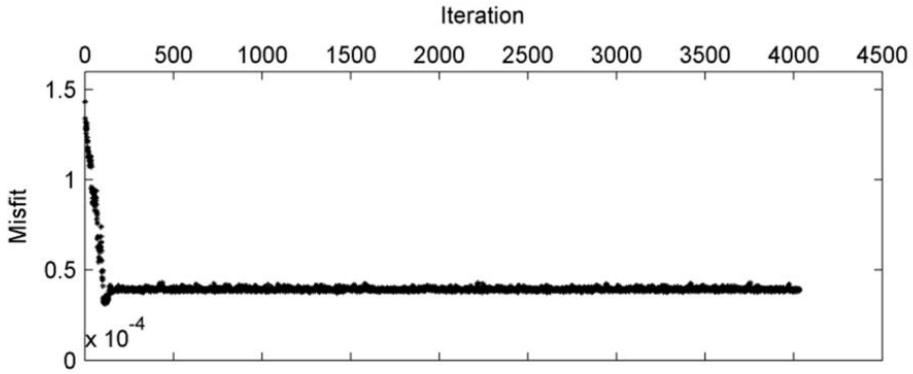

Figure 4.9: Convergence of data misfit in the MCMC algorithm.

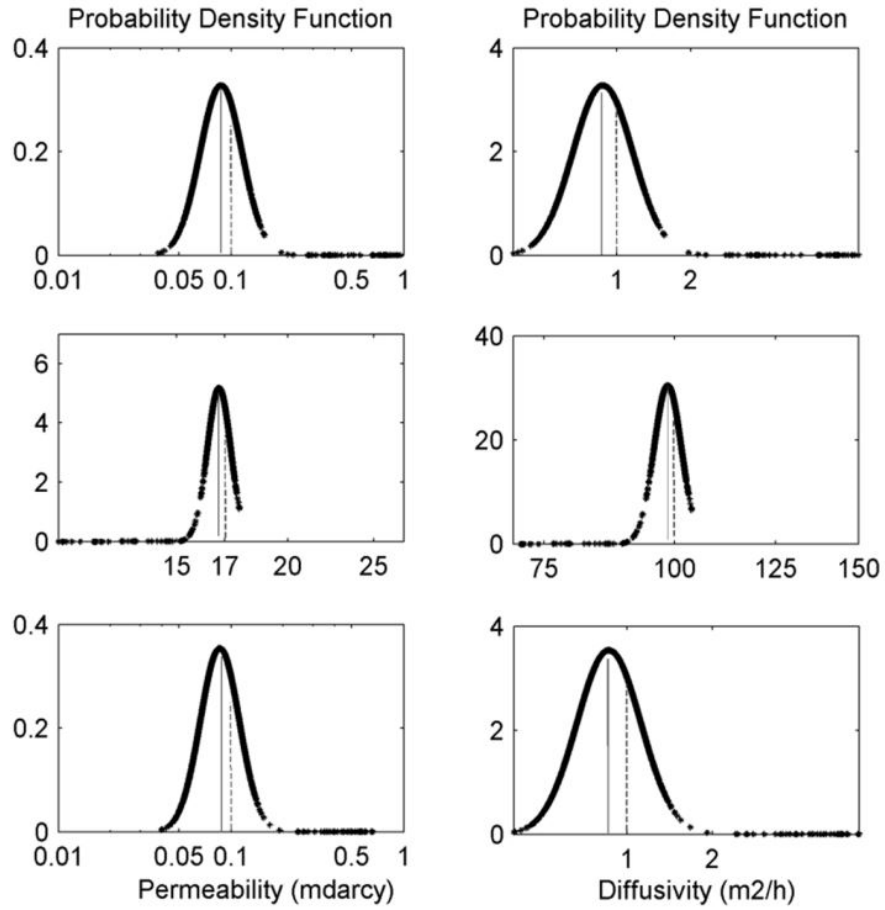

Figure 4.10: Posterior PDF of diffusivity (right) and corresponding permeability (left) for the 3 layers in Figure (4.7, single well configuration). Mean values shown by solid gray lines and actual values shown by dash gray lines.

Parameter	Value
Total compressibility β (Pa^{-1})	3×10^{-9}
Fluid viscosity η (Pa.s)	0.001
Reservoir thickness (m)	100
Porosity φ	0.1 (Impermeable layers) 0.2 (Reservoir)

Table 4.1: Parameters used to construct the synthetic three-layered model

References

Alpak, F.O., C. Torres-Verdin, and T.M. Habashy, 2004, Joint inversion of transient pressure and dc resistivity measurements acquired with in-situ permanent sensors: A numerical study: *Geophysics*, **69**, no. 5, 1173-1191.

Babour, K., A. K. Belani, and J. Pilla, 1995, Method and apparatus for long term monitoring of reservoirs: *United States Patent* **5**, 467, 823**.**

Bard, Y., 1974, Nonlinear parameter estimation: *Academic pres*s, New York.

Bryant, I. D., M. Y. Chen, B. Raghuraman, I. Raw, J.P. Delhomme, C. Chouzenoux, D. Pohl, Y. Manin, E., Rioufol, G., Oddie, D., Swager, and J. Smith, 2002, An application of cemented resistivity arrays to monitor waterflooding of the Mansfield sandstone: *SPE Reservoir Evaluation and Engineering*, Indiana, **5** , no. 6, 447–454.

Bauer, K., A. Schulze, T. Ryberg, S.V. Sobolev, M.H. Weber, 2003, Classification of lithology from seismic tomography: A case study from the Messum igneous complex, Namibia: *Journal of Geophysical Research-Solid Earth*, **108**.

Chen, J. G.M Hoversten, D. Vasco, Y. Rubin, Z. Hou, 2007, A Bayesian model for gas saturation estimation using marine seismic AVA and CSEM data: *Geophysics*, **72**, no. 2, WA85-WA95.

Fan, Y. & R. Snieder, 2009, Required source distribution for interferometry of waves and diffusive fields: *Geophysical Journal International*, **179**, 1232–1244.

Grandis, H., M. Menvielle, & M. Roussignol, 1999, Bayesian inversion with Markov chains–I. The magnetotelluric one-dimensional case: *Geophysical Journal International*, **138**, 757–768.

Green, P.J., 1995, Reversible jump Markov chain Monte Carlo computation and Bayesian model determination: *Biometrika*, **82**, no. 4, 711-732.

Hastings, W.K., 1970, Monte Carlo sampling methods using Markov Chains and their applications: *Biometrika*, **57**, no. 1, 97–109.

Jaynes E. T, 2003, Probability Theory: The Logic of Science: *Cambridge University Press*.

Jeffreys, H., 1924, The Earth, Its Origin, History and Physical Constitution: *Cambridge University Press*, second edition.

Jeffreys, H., 1939, Theory of probability: *Oxford University Press*, Oxford, U.K.

Kramers H.A., 1927, La diffusion de la lumiere par les atomes. Atti Cong. Intern: *Fisica, (Transactions of Volta Centenary Congress) Como* **2**, 545–557.

Kronig R. de L., 1926, On the theory of the dispersion of X-rays: *Journal of the Optical Society of America*, **12**, 547–557.

Lanczos, C., 1961, Linear differential operators: D. Van Nostrand Co. Ltd., London-Toronto-New York-Princeton, N.J.

Luccarini V., J. Saarinen, K. Peiponen, and E. Vartiainen, 2005, Kramers-Kronig Relations in Optical Materials Research: *Springer*, Berlin.

Malinverno, A. and C. Torres-Verdin, 2000, Bayesian inversion of DC electrical measurements with uncertainties for reservoir monitoring: *Inverse Problems*, **16**, no. 5, 1343-1356.

Malinverno, A., 2002, Parsimonious Bayesian Markov Chain Monte Carlo: *Geophysical Journal International*. 151, 675-688**.**

McGillivray, P. R., D.W. Oldenburg, R.G. Ellis, T.M. Habashy, 1994, Calculation of sensitivities for the frequency-domain electromagnetic problem: *Geophysical Journal International*, **116**, 1–4.

Metropolis, N., A. W. Rosenbluth, M.N. Rosenbluth, A.H. Teller, E. Teller, 1953, Equations of state calculations by fast computing machines: *Journal of Chemical Physics*, **21**, no. 6, 1087–1092.

Minsley, B.J., 2011, A trans-dimensional Bayesian Markov chain Monte Carlo algorithm for model assessment using frequency-domain electromagnetic data: *Geophysical Journal International*, **187**, no. 1, 252-272.

Mehrer, H., 2007, Diffusion in Solids – Fundamentals, Methods, Materials, Diffusion-Controlled Processes: *Springer*, Berlin Heidelberg, New York.

Morse, P. W. & H. Feshbach, 1953, Methods of theoretical physics: *McGraw-Hill*, New York, NY.

Mosegaard, K. & A. Tarantola, 1995, Monte Carlo sampling of solution to inverse problems: *Journal of Geophysical Research*, **100**, 12431-12447.

Oldenburg, D., 1990, Inversion of Electromagnetic Data – an Overview of New Techniques: *Surveys in Geophysics*, **11**, 231-270.

Ray, A. and K. Key, 2012, Bayesian inversion of marine CSEM data with a trans-dimensional self-parameterizing algorithm: *Geophysical Journal International*, **191**, no. 3, 1135-1151.

Robert, C. P. and G. Casella, 2004, Monte Carlo Statistical Methods: *Springer-Verlag*, New York.

Schuster, G. T. and M. Zhou, 2006, A theoretical overview of model-based and correlation-based redatuming methods: *Geophysics*, **71**, SI103-SI110.

Shamsalsadati, S. & C. J. Weiss, 2010, Retrieving the impulse response of the Earth due to random electromagnetic forcing: *Physical Review E*, **81**, 036603.

Shamsalsadati, S. and C. J. Weiss, 2012a, Empirical Green's function estimation for lossy systems: analysis of the volume of relevance for the origin of ambient fluctuations: *Geophysical Journal International*, **190**, no. 3, 1526-1532.

Shamsalsadati, S. and C. J. Weiss, 2012b, Time-series analysis of interferometry in diffusive systems: *SEG Technical Program Expanded Abstracts*, 1-6.

Slob, E. and K. Wapenaar, 2007, Electromagnetic Green's functions retrieval by crosscorrelation and cross-convolution in media with losses: *Geophysical Research Letters*, **34**, no. 5, L05307.

Slob, E. & C. J. Weiss, 2011, Lagrangian energy norms for retrieving the impulse response of the Earth due to random electromagnetic forcing: *Physical Review E*, **84**, 027601.

Snieder, R., 2006, Retrieving the Green's function of the diffusion equation from the response to a random forcing: *Physical Review E*, **74**, 046620.

Tarantola A., B. Valette, 1982, Inverse problems = quest for information: *Journal of Geophysics*, **50**, 159-170.

Tarantola A., 2005, Inverse Problem Theory and Methods for Model Parameter Estimation: *SIAM*, ISBN 978-0-89871-5729.

Toll J. S., 1956, Causality and the Dispersion Relation: Logical Foundations: *Physical Review*, **104**, 1760–1770.

van Kleef, R., R. Hakvoort, V. Bushan, S. Al-Khodhori, W. Boom, C. de Bruin, K. Babour, C. Chouzenoux, J. P. Delhomme, Y. Manin, D. Pohl, E. Rioufol, M. Charara, and R. Harb, 2001, Water flood monitoring in an Oman carbonate reservoir using a downhole permanent electrode array: Middle East Oil Show: Society of Petroleum Engineers, paper SPE 68078.

Wapenaar, K. & Fokkema, J., 2006. Green's function representations for seismic interferometry: *Geophysics*, **71**, SI 33–46.

Wapenaar, K., E. Slob, & R. Snieder, 2008, Seismic and electromagnetic controlled-source interferometry in dissipative media: *Geophysical Prospecting*, **56**, 419–434.

Woodruff, W.F., A. Revil, A. Jardani, Nummedal D., and Cumella, S., 2010, Stochastic Bayesian inversion of borehole self-potential measurements: *Geophysical Journal International*., **183**, no. 2, 748-764.

Chapter 5: Discussion and Future Work

5.1 Summary

One of the objectives of this dissertation was to develop the theory of interferometry using the cross-correlation method into the low-frequency electromagnetic fields where the wavefields are diffusive. A thorough literature review on the basics of interferometry and its augmentation in geophysics in the first section was followed by a brief summary of the work in low-frequency electromagnetic interferometry in the second chapter. Pore-pressure and low-frequency electromagnetic fields are two important diffusive wavefields to apply the theoretical findings. From the theoretical viewpoint, virtual source method in diffusive systems requires volumetrically distributed sources in an infinite domain. However, the existence of this condition doesn't seem realistic in real experiments. Consequently, an important question to answer is "what is the essential areas and distribution of sources that makes it possible to apply the theory in practice?" I attempted to answer this question in the third chapter through conducting numerical experiments of double half-pace models in one and two dimensions with a variety of receiver configurations and diffusivity contrasts between the layers using a single frequency.

On the other hand, diffusive systems often use multiple frequencies or operate in the time domain. Thus, the sensitivity analysis of sources was discussed in the fourth chapter through studying the problem in the time domain. A synthetic model of a three-layered Earth was then used to show how the data derived from interferometry fit with the actual source-receiver measurement. In this experiment, it was assumed that all exitations happen in the middle layer of a high diffuse (permeable) region while there were no sources in the two other impermeable

layers on the top and bottom of this reservoir layer. The system of diffusion equation in a layered system was solved analytically in the frequency domain. Note; however, that the numerical examination completed in the frequency domain gives the imaginary component of the EGF only. Thus, the Kramers-Kronig relations were used to reconstruct the real part. Then, the full signal was reconstructed in the time domain using Fourier transformation in the MATLAB environment.

The other objective of this project was to find diffusivity (and permeability) in the proposed three-layered model having the interferometry data. For this purpose, the synthetic interferometry data was used to find fluid diffusivity of each homogenous layer by applying the Bayesian inversion method. The results of this inversion described the predicted model in the form of a probability distribution that enables one to quantify the uncertainty associated with the model parameter in each layer.

5.2 Discussion

The theory of interferometry in seismology was introduced by Claerbout (1968) and was extended for the application in variety of exploration scenarios. This method has been also formulated to be utilized in electromagnetic geophysics (Sob & Wapenaar, 2007, 2007a; Slob et al., 2007b) where the sources are required to reside on some bounding surface wrapping the region of study. In addition, unified theories of EGF estimation have been proposed (Wapenaar et al., 2008) in which the EGF could be extracted for coupled electromagnetic fields. However, the problem was not addressed for decoupled electromagnetic fields where the quasi-static limit holds. The work presented in the second chapter of this dissertation (Shamsalsadati & Weiss, 2010) is the first demonstration of EGF estimation for magnetic fields in heterogeneous media

assuming the area of study is full of random point sources of current or time varying magnetization.

The interferometry method was well-suited for the systems that were invariant under time-reversal until Snieder (2006) proved that this method is also applicable to the diffusive media with losses where time-reversal invariant assumption is not fulfilled. The study described in the second chapter is similar to the Snieder's (2006) research in the pressure diffusive systems. The objective of this section was to develop the interferometry formula to find magnetic fields due to uncorrelated sources in low frequencies where the quasi-static limit holds. For this derivation, Maxwell equations were used to retrieve the Green's function for decoupled magnetic fields excited by ambient fluctuations. It was assumed that there is an infinitely large volume full of sources – either random noises or engineered sources – that encapsulates two receivers *A* and *B* lying inside this medium. For the electromagnetic problem, the sources must be spatially correlated with the electrical conductivity variations in the medium (Snieder, 2006); however, for the specific case of magnetic fields, it was shown that this constraint is not required. This constraint was relaxed by considering that the magnetic permeability of rocks does not change significantly (Shamsalsadati & Weiss, 2010). The result of the magnetic interferometry in the frequency domain demonstrated that the imaginary component of the Green's function projected at an arbitrary *s* direction and scaled by the power spectrum of the source for a virtual source located at the position of receiver *A* – which is measured by receiver *B* – can be retrieved by correlation of the observed fields measured at two receiver points. Note that all three components of the magnetic field are required to calculate the effect of the virtual source accurately (see Appendix A).

To verify the accuracy of the results, a 3-D numerical analysis has been done over an arbitrary volume representing a uniform 0.1 S/m layer underlying a 1 S/m homogenous region. The magnetic field throughout the volume was computed using the FDM3D finite difference code (Weiss & Constable, 2006) for magnetic dipole sources at points *A* and *B*, positioned at (206.25, 206.25, -6.25) m and (-206.25, -206.25, -6.25) m, respectively. The numerical study was conducted to find how the EGF kernel varies for these observation points encapsulated by volumetrically distributed sources. The results of the double half-space model revealed that there is symmetry between negative and positive amplitudes of the imaginary component of the EGF kernel (Figure A.1, top). Thus, these positives and negatives cancel out each other and only the real part of the cross-correlation kernel remains. Therefore, the right hand side of the Equation (A.2) calculates the imaginary component of the Green's function, and this is consistent with the theoretical findings. The numerical study was also shown that the actual measurement (active source and receiver) and the EGF are in general agreement (Figure A.2, bottom).

The development of the EGF estimation outlined in the second chapter does not consider any restriction on the type of magnetic and electric current source, other than is must be spatially impulsive. Most critical; however, is the need to quantify the breakdown of the method when the ambient sources are imperfect – that is, contaminated with spatial bias, anisotropy and correlated structure. The effect of correlated, heterogeneous, and anisotropic noise sources on the recovered EGF is an interesting question to be explored in depth.

For the purpose of this dissertation, the effect of source distribution for scalar diffusive fields was investigated since finding an area full of random and uncorrelated sources – required by the interferometry theory in diffusive systems – is not realistic in practice. Hence, the aim of the third chapter was to understand the required source distribution, or VoR (Volume of

Relevance), on the EGF retrieval through conducting numerical experiments. The effect of receiver position, its separation and also inhomogeneity in both one and two dimensions was examined to answer the question 'Where are the sources that contribute most to the Green's function estimate in diffusive, and lossy systems?' (Shamsalsadati & Weiss, 2012a).

Fan & Snieder (2009) investigated the problem for a homogeneous system with closely spaced receivers in 1-D and found that sources between the observation points and close to them contribute more to the Green's function estimate than the faraway sources. In the third chapter, the work started by Fan & Snieder (2009) was extended through exploring the effects of receiver separation and its location on the EGF kernel for double half-space systems in one and two dimensions. The study was initiated by reconstructing the work of the Fan & Snieder (2009) in the homogenous medium for receivers that stand at either side of the contact with a separation of 2 m using a fixed frequency of 0.02 Hz. The separation for receivers which were symmetric about the interface was also extended at various separations up to 20 m to inspect the VoR (Shamsalsadati & Weiss, 2012a). For a homogenous medium, illustration of the EGF kernel showed that as the receiver separation was increased, the VoR was constrained to be between the receivers which verified the results of Fan & Snieder (2009). It was shown analytically that the EGF kernel for the region between the observation points is a cosine function. Figure (3.1, left) illustrated that this kernel changes from a function with one extrema to a function with multiple exrema as the receiver separation increases. Consequently, the importance of the region between the receivers depends on their separation. For the particular occasion where the sensors are far apart by an integer of the wavelength λ, the EGF kernel is equivalently zero and those sources do not contribute to the EGF estimate (Shamsalsadati & Weiss, 2012a). On the other hand, the EGF kernel outside the area between the receivers follows an exponential decay function. Therefore,

for the 1-D homogeneous system, it is relevant that sources outside the receivers' range should be positioned sufficiently close to the receivers.

To analyze the problem for a double half-space, the system of diffusion equations was solved analytically in the frequency domain in 1-D and 2-D. The extension of the experiment in homogenous media for double half-space models showed that the general rule derived for the first experiment is not valid for the latter. The examination of double half-spaces demonstrated that the peak of the EGF kernel is skewed towards the low diffusivity region. Figure (3.1 center, right) illustrates that the EGF kernel in the high-*D* side has a heavy tail with gradual decay while in the low-*D* side it has fast decay with negative values. Numerical integration of the EGF kernel revealed that for receivers that are symmetric about the interface between regions of high diffusivity contrast, as receiver separation increases the VoR moves from the low-*D* region to the high-*D* region, and returns repeatedly. It was observed in both one and two dimensions that the repetition over which these shifts occur in the EGF estimation decreases as the diffusivity contrast increases. In the cases examined, for low receiver separations (up to a few tens of meters) in both 1 and 2-D – using a fixed frequency of 0.02 Hz – the sources in the low-diffusivity region contribute more to the EGF estimation. Note; however, that this is not a universal rule to determine the placement of VoR. The VoR's position depends on the frequency, receiver separation, and also diffusivity contrast between the layers. This numerical experiment resembles the scenario of a borehole experiment with a pair of sensors lying on both side of a lithological contact (Shamsalsadati & Weiss, 2012a).

For the occasion in which the receiver pair was rotated to be located on the interface, the rate of shifting between different regions was lower, and for medium and high diffusivity contrasts, the VoR remained on the more diffusive side over receiver separations up to two to

three skin depths. Therefore, for receivers located on the interface between two regions of high diffusivity contrast, or similarly high permeability difference, the EGF kernel was spatially deeper on the high diffusive (and permeable) side of the interface. Note that for simplicity the experiments designed based on the measurement of the pressure fields excited due to impulsive sources. Low-frequency electromagnetic induction in conductive media is also "diffusive" in lossy systems; thus, a similar approach could be used to derive the Green's function for electromagnetic fields. Although the relations for electromagnetic induction is more complicated than the case of the pressure field, the structure for both of them are similar, especially in low dimensions. Therefore, the electrical resistivity plays the same role as of the diffusivity and the findings suggest that for EGF estimation in surface-based experiments, sources located in the resistive region are more important than those located in the conductive region. Consequently, for surface-based experiments with receivers located on the surface "Air" region has much higher diffusivity than the "Earth" region; and hence; the VoR is extremely in the Air. This outcome is invaluable since majority of anthropogenic and natural sources exist in the Air.

Majority of the exploration problems in diffusive systems operate in the time domain; hence, EGF data in the time domain were analyzed to investigate the required width and density of sources for different source-receiver configurations and diffusivity contrasts between the layers. To derive the EGF in the time domain, the real component of the EGF in the frequency domain was recovered using Kramers-Kronig relations. Then, the full signal was Fourier transformed into the time domain. The results confirmed the previous findings in homogenous medium in which the width of source distribution needed to reconstruct EGF up to a desired time depends on the receiver separation and diffusivity of the medium (Fan & Snieder, 2009). For full construction of the EGF time-series, it was found that sources must be expanded further into

the high-*D* side of the double half-space in comparison to the low-*D* side of the model (Shamsalsadati & Weiss, 2012b). A derivation was also formulated for finding the required width of source distribution which depends on the diffusivity in each medium, their contrast, and the receiver separation. It was shown that source distribution need to be wider in the high-*D* side than in the other side. In general, for receivers located on either side of the interface, Δ' which is the distance between maximum width of sources in the high-*D* side and the receiver in that medium is proportional to $\sqrt{D_2/D_1}$ times the same distance (Δ) in the low-*D* side, Figure (4.2).

It was further demonstrated that for a higher receiver separation, an essential density of sources is lower. It was found that the density of sources should be changed such that two to three sources remain between the receivers which verified prior studies that sources between the receivers are more important than the other sources. The numerical experiments pointed out that, in the case of a close-spaced receiver pair far from the interface, sources are needed only in the region where the receivers exist; nonetheless, in the occasion where the sensors are close enough to the contact so that the wholespace response extends a distance *z* across the interface, the essential region beyond the contact enlarges by the factor of $\sqrt{D_2/D_1}$.

For a three-layered medium with a reservoir layer between two impermeable layers, the EGF was reconstructed due to impulsive sources in the middle layer. The numerical error due to EGF reconstruction depends on the receiver separation, frequency, and diffusivity of the medium and increases at the late times. Note that the time up to which the EGF could be reconstructed decreases for receivers close to the boundaries since, in this situation, there are not enough sources around the receiver pair. The results showed that the fit between the actual source and the receiver measurement and the EGF is not exactly identical. This is due to the fact that the

imperfect source distribution in addition to the Kramers-Kronig relation which was used for the full signal reconstruction introduces error. Note; however, that the majority of measurements in the hydrological or hydrocarbon studies are accomplished in the time domain. Hence, the alternative form of the EGF equation in the time domain (Snieder, 2006) could be used to reduce the numerical error caused by using Kramers-Kronig relations.

On the other hand, the aim of any data measurement in geophysical, petrophysical, or hydrological explorations – using either the active or the passive method – is to characterize subsurface properties. Electromagnetic, pressure, or seismic data are inverted to quantify different physical properties of the Earth such as electrical conductivity, density, porosity, and permeability. Thereupon, the final goal of this study was to show how we can find diffusivity by using the interferometry data derived for the proposed three-layered model. Furthermore, having the estimated diffusivity and also fluid parameters outlined in Table (4.1), information on the permeability in each homogenous layer was obtained.

In this dissertation, the statistical Bayesian inversion was used for the purpose of data inversion since it recognizes uncertainties in the model parameters. This is one of the advantages of this approach in comparison to the traditional methods which give a point estimate of the model parameters. The Bayesian statistical inversion was used to estimate fluid diffusivity (and permeability) from the EGF interferometry data. The last part in the fourth chapter discusses how to implement a nonlinear inversion on the data derived by interferometry in diffusive systems for a three-layered Earth in 1-D. Using Bayesian, the prior knowledge about the model parameters was combined with the likelihood of this model holding true for the observed data. In this study, the Metropolis-Hasting algorithm (Metropolis et al., 1953; Hasting, 1970) was used to sample models from the probability distribution using a proposal distribution with a tuning parameter

which was equivalent to the posterior's covariance. Implementing the posterior's covariance as a tuning parameter ensures that the acceptance rate is optimal (Gelman et al., 1996; Malinverno, 2002). At each iteration of this algorithm, this initial model was changed and tuned based on the posterior probability of the proposed model. Therefore, the MCMC chain was moved towards the area with high posterior probability. In this study, it was shown that the algorithm converges toward the model that is close to the true model starting with a simple prior model which was far from the true model (Figure 4.9, 10).

On the other hand, non-Bayesian inversion approaches do not consider probability distribution for the data or model; although their approach is inherently statistical. The Bayesian approach has an advantage over non-Bayesian approaches where there is a gap in the observed data and a prior knowledge of the model parameters is available. In addition, using this method, it is easier to describe the non-uniqueness part of the inversion while gradient based approaches provide a single model parameter without addressing ambiguities of the inversion. One of the challenges of this method is the difficulty of setting a prior which is used to tune the final model and regularize the posterior solution (Backus, 1988; Scale & Snieder, 1997; Ulrych et al., 2001; Malinverno, 2002). Nonetheless, Bayesian inversion is computationally more expensive than other methods which make it difficult to apply in higher dimensions.

Calculation of the Jacobian matrix for nonlinear inversion is one of the reasons the inversion algorithm is slow. To overcome this problem, a formula was suggested to reduce the computational costs of the Jacobian matrix. The relation introduced in Appendix B is an extension of the work started by McGillivray et al. (1994) in electromagnetics into the generic form of scalar diffusive fields.

5.3 Future Work

5.3.1 The Application Areas

The application of the interferometry method simulates a virtual source at the location of interest where it is not possible to use active as discussed by Schuster & Zhou (2006). On the other hand, this method is useful in the areas full of random noises where traditional geophysical methods are in limited use. Thus, these findings could be useful in exploring the way ambient background noise allows improvements to experiment design where conventional geophysics is constrained in urban areas, oilfields, and industrial facilities. These environments may be appropriate in examining the application of this method in practice.

The calculations in this dissertation were designed to consider a variety of geophysical, hydrological, and petrophysical examples, including borehole and surface-based experiment models. The findings elaborated in the third and fourth chapter could be applied to find fluid flow in the aquifer or hydrocarbon reservoirs. The method would also be useful in the evaluation of the concentration of contaminants in a fluid flow porous system as discussed by Snieder (2006). The possibility of implementing the method in the field for CSEM (Controlled Source Electromagnetic) exploration may yield a huge savings of time and energy since the ship would only be required to deploy receiver packages under ideal circumstances. Further study is required to quantify the survey and the environmental parameters in order to apply this method.

The findings of this study could also be useful when observing the electric or the pressure anomaly due to pumping fluids (oil or water) in a borehole (Wurmistch & Morgan, 1994). Pumping and injection in a porous medium changes both pressure and resistivity measurements

as it was examined by Alpak et al. (2004). Middleton et al. (2000) analyzed the magnetic field generated by displacement of water with oil in a porous medium. The anomalies generated by these types of experiments could potentially be utilized in an interferometry practice. On the other hand, Boleve et al. (2011) designed an experiment to locate the leak in a dam by injecting brine and measuring the streaming potential produced by the injection. In this case, the injection of the fluid generates both pressure and streaming potential anomalies and provides more information on subsurface properties. Developing the virtual source method for these problems would be useful in gaining information on electrical properties of the rocks and characterizing permeability of the reservoir.

There are varieties of electromagnetic or pressure fluctuations in the Earth and the possibility of using them for the application of virtual source method require further investigation. There is also a range of natural noises in the environment that can be used to apply interferometry therein. For instance, it was shown by many authors that the magnetic field is generated due to the stress change in crustal rocks. The variation of the magnetic field due the rupture adds extra information that might be helpful for Earthquake predictions (Stacey, 1964; Johnston, 1989; Johnston et al., 2001; Thomas et al., 2009).

As another example of natural sources, one may consider air bubbling which could be a source of both pressure and streaming potential anomalies (Revil et al., 1999). The authors discussed that the insulator bubbles carry charges on their surface and hence create streaming potential anomalies. Malama et al. (2009) also showed how overflow of a Geyser in a geothermal valley generates streaming potential signals. The authors described how the cavitation of gas bubbles during the upflow generates acoustic waves. They explained that the collapsing and merging of steam bubbles due to striking a barrier can generate strong acoustic

pulses. The investigation on the distribution and intensity of these sources is needed to find out if one can benefit from these types of fluctuations in the application of interferometry.

Jioa & Li (2003) investigated the reason for the appearance of cracks on the coastal pavement in Hong Kong. Numerical simulation conducted by the authors affirmed that the Air pressure fluctuation in coastal subsurface induced by the oceanic tide was the main reason for pressure fluctuations in the subsurface which resulted in the observed cracks on the surface. Hence, the oceanic tide in the coastal aquifers might be considered a source of natural fluctuations that could provide information on subsurface properties.

In either of the above examples, a thorough study on the type of source, its intensity, and power spectrum, other types of background fluctuations in the area, and the survey environment are required for the application of the virtual source method.

5.3.2 *An Alternative Approach to the Cross-Correlation Method*

The interferometry method benefits from using different mathematical tools such as cross-correlation, cross-convolution or deconvolution. Multidimensional deconvolution interferometry is an alternative approach to the cross-correlation method that allows contribution of sources with different properties (Wapenaar et al., 2008; Fan et al., 2010). The main advantage of the multidimensional deconvolution method is that the constraint imposed by the cross-correlation to have a volumetrically distributed source is relaxed. This method works for erratic source distribution and also where the bulk sources are not available. On the other hand, the multidimensional deconvolution is based upon the separation of the reference model from the observed data which sometimes makes using this method, challenging. In addition, this method is mathematically more expensive than the cross-correlation technique. For future study, it may

be beneficial to analyze the problem using the multidimensional deconvolution method to compare the findings with the outputs of the cross-correlation technique.

5.3.3 Improving the Inversion Results

Joint integration of different geophysical data sets provides more accurate results which cannot be obtained through using each method independently (Bedrosian, 2007). We can benefit from the strengths in one method for improving the weaknesses of the other one to characterize subsurface properties more accurately. For instance, electromagnetic methods are highly sensitive to fluid content. Prediction of the reservoir parameters using electromagnetic methods provide more reliable estimate of the water saturation in contrast to the porosity evaluation. In contrast, seismic exploration methods are more accurate tools for porosity estimation. Pressure data also provide more information on the permeability, which is useful to find out how pore spaces are connected to each other. The improvement of the inversion results may be obtained by combining these different data sets derived from various experiments.

Future joint-inversion studies remain to be conducted for various noisy data sets offered by interferometry to explore the power of Bayesian inversion in comparison to other inversion methods. In addition, consideration of the outcomes of different inversion approaches, such as cross-gradient, Bayesian, neural network, and fuzzy algorithms, could result in a more comprehensive understanding of the advantages and disadvantages of each method.

References

Alpak, F.O., Torres-Verdin, C. and Habashy, T.M., 2004. Joint inversion of transient pressure and dc resistivity measurements acquired with in-situ permanent sensors: A numerical study: *Geophysics*, **69**(5), 1173-1191.

Backus, G. E. , 1988. Comparing hard and soft prior bounds in geophysical inverse problems: *Surveys in Geophysics*, **94**, 249-261.

Bedrosian, P.A., MT+, 2007. Integrating Magnetotellurics to determine Earth structure, physical state, and processes: *Surveys in Geophysics*, **28**(2-3), 121-167.

Boleve, A., Janod, F. Revil, A. Lafon , A., Fry. J.-J., 2011. Localization and quantification of leakages in dams using time-lapse self potential measurements associated with salt tracer injection: *Journal of Hydrology*, **403**(3-4), 242-252.

Claerbout, J.F., 1968. Synthesis of a layered medium: *Geophysics*, **33**, 264–269.

Fan, Y. & Snieder, R., 2009. Required source distribution for interferometry of waves and diffusive fields: *Geophysical Journal International*, **179**, 1232–1244.

Fan, Y., Snieder, R., Slob, E., Hunziker, J., Singer, J., Sheiman, J., Rosenquist M., 2010. Synthetic aperture controlled source electromagnetics: *Geophysical Research Letters*, **37**.

Gelman, A., Roberts, G.O. & Gilks, w.r., 1996. Efficient Metropolis jumping rule, in Bayesian Statistics, 5, 599-607: *Oxford University Press*, Oxford.

Hastings, W.K., 1970. Monte Carlo sampling methods using Markov Chains and their applications: *Biometrika*, **57** (1), 97–109.

Jiao, J.J. and Li H., 2003.Tide-induced Air Pressure Fluctuation in Coastal Unsaturated Zones: *Proceedings of International Symposium on Water Resources and the Urban Environment*, Wuhan, P. R. China, 10-13.

Johnston, M.J.S, 1989. Review of magnetic and electric field effects near active faults and volcanoes in the U.S.A.: *Physics of the Earth Planetary Interiors*, **57**, 47-63.

Johnston, M. J. S., Byerlee, J. D. and Lockner, D. 2001, Rapid Fluid Disruption - A Source for Self Potential Anomalies on Volcanoes: *Journal of Geophysical Research*, **106**, 4327-4335.

Li, H., Bernardi, F. & Michelini, A., 2010. Surface wave dispersion measurementsfrom ambient seismic noise analysis in Italy: *Geophysical Journal International*, **180**, 1242–1252.

Lobkis, O.I.& Weaver, R. L., 2001. On the emergence of the Green's function in the correlations of a diffuse field: *Journal of the Acoustical Society of America*., **110**, 3011–3017.

Malama, B., Revil, A., and Kuhlman, K.L. 2009. A semi-analytical solution for transient streaming potentials associated with confined aquifer pumping tests: *Geophysical Journal International*, **176**(3), 1007-1016.

Malinverno, A., 2002. Parsimonious Bayesian Markov Chain Monte Carlo: *Geophysical Journal International*, **151.**

McGillivray, P.R., Oldenburg, D.W., Ellis, R.G., Habashy, T.M., 1994. Calculation of sensitivities for the frequency-domain electromagnetic problem: *Geophysical Journal International*, **116**, 1–4.

Metropolis, N., Rosenbluth, A.W., Rosenbluth, M.N., Teller, A.H., Teller, E., 1953. Equations of state calculations by fast computing machines: *Journal of Chemical Physics*, **21** (6) 1087–1092.

Middleton, M.F., Winkler, D., Bick, M., Sahli, T., 2000. Magnetic signatures produced by fluid flow in porous sediments: *Exploration Geophysics*, **31**, 413-417.

Revil, A., Schwaeger H., Cathles III L. M., Manhardt P.D., 1999. Streaming potential in porous media 2. Theory and application to geothermal systems: *Journal of Geophysical Research-Solid Earth*, **104**(B9), 20033-20048.

Sato, H., 2009. Green's function retrieval from the CCF of coda waves in a scattering medium: *Geophysical Journal International*, **179**, 1580–1583.

Sato, H., 2009a. Retrieval of Green's function having coda from the cross-correlation function in a scattering medium illuminated by surrounding noise sources on the basis of the first order Born approximation: *Geophysical Journal International*, **179**, 408–412.

Scales, J., and R. Snieder, 1997. To Bayes or not to Bayes?: *Geophysics*, **62**, 1045-1046.

Schuster, G. T. and Zhou, M., 2006. A theoretical overview of model-based and correlation-based redatuming methods: *Geophysics*, **71**, SI103-SI110.

Shamsalsadati, S. & Weiss, C.J., 2010. Retrieving the impulse response of the Earth due to random electromagnetic forcing: *Physical Review E*, **81**, 036603.

Shamsalsadati, S. and Weiss, C.J., 2012a. Empirical Green's function estimation for lossy systems: analysis of the volume of relevance for the origin of ambient fluctuations: *Geophysical Journal International*. **190** (3), 1526-1532.

Shamsalsadati, S. and Weiss, C.J, 2012b. Time-series analysis of interferometry in diffusive systems: *SEG Technical Program Expanded Abstracts*, 1052-3812.

Slob, E. and Wapenaar, K., 2007. Electromagnetic Green's functions retrieval by cross-correlation and cross-convolution in media with losses: *Geophysical Research Letters*, **34**(5).

Slob, E. & Wapenaar, K., 2007a. GPR Without a source: cross-correlation and cross-convolution methods: *IEEE Geoscience and Remote Sensing Society*, **45**, 2501–2510.

Slob E., K. Wapenaar and R. Snieder, 2007b. Interferometric electromagnetic Green's functions representations using propagations invariants: *Geophysical Journal International*, **169**, 60-80.

Slob, E., Snieder, R. & Revil, A., 2010. Retrieving electric resistivity data from self potential measurements by cross-correlation: *Geophysical Research Letters*, **37**, L04308.

Snieder, R., 2006. Retrieving the Green's function of the diffusion equation from the response to a random forcing: *Physical Review E*, **74**.

Stacey, F.D., 1964. The seismomagnetic effect. Pure Appl: *Geophys*ics, **58**(5).

Thomas, J.N., Love, Jeffrey J. and Johnston, M.J.S. 2009. On the Magnetic Precursor of the 1989 Loma Prieta earthquake: *Physics of the Earth and Planetary Interiors*, **173**, 207-215.

Ulrych, T.J., Sacchi, M.D. and Woodbury A., 2001. A Bayes tour of inversion: A tutorial: *Geophysics*, **66**(1), 55-69.

Wapenaar, K., Slob, E. & Snieder, R., 2008. Seismic and electromagnetic controlled source interferometry in dissipative media: *Geophysical Prospecting*, **56**, 419–434.

Weiss, C.J. and Constable S.C., 2006. Mapping thin resistors and hydrocarbons with marine EM methods, Part II: *Geophysics*, **71** (6).

Wurmstich B., and Morgan F. D., 1994. Modeling of streaming potential responses caused by oil well pumping: *Geophysics*, **59**, 46-56.

Appendices

Appendix A: Regenerating the Results in Chapter 2, Considering All Components of the Source Vector

In chapter 2, the integral containing the inner product for the curl of magnetic fields of Equation (23) was neglected. This equation was derived with the assumption that $s_A=s_B$; however, the vectors $\boldsymbol{s}$ demonstrate receiver orientations after reciprocity has been applied which needs to be independent of the required source directions (Slob & Weiss, 2011). Thus, despite the assumption made in the chapter 2 on the sufficiency of a single source vector component for the application of electromagnetic interferometry in low frequencies, vector $\boldsymbol{s}$ includes all components of the source orientation; thereupon, the equation

$$\int_{\Omega} \bar{\mathbf{h}}_B^{\,*} \cdot \bar{\mathbf{h}}_A \, d\Omega \approx \sum_i \bar{\mathbf{h}}_B^{\,*}(\mathbf{r}_i) \cdot \bar{\mathbf{h}}_A(\mathbf{r}_i) \, d\Omega_i \tag{A.1}$$

– the Equation (22) in chapter 2 – is rewritten as the following:

$$\int_{\Omega} \bar{\mathbf{h}}_B^{*} . \bar{\mathbf{h}}_A \, d\Omega \sim \int_{\Omega} (\mathbf{h}_z^{*}(\mathbf{r}_B)\mathbf{h}_z(\mathbf{r}_A) + \mathbf{h}_y^{*}(\mathbf{r}_B)\mathbf{h}_y(\mathbf{r}_A) + \mathbf{h}_x^{*}(\mathbf{r}_B)\mathbf{h}_x(\mathbf{r}_A)) \, d\Omega \tag{A.2}$$

Substituting Equation (24) into Equations (21, 22) – in chapter 2 – and considering all of the components of the sources term, the final expression for Green's function in the frequency domain would be equivalent to:

$$\left[\bar{\mathbf{h}}_B^*(\mathbf{r}_A) - \bar{\mathbf{h}}_B(\mathbf{r}_A)\right] \left| f(\omega)\right|^2 = 2j\omega\mu_0 \left\langle [\boldsymbol{s}\cdot\mathbf{h}^*(\mathbf{r}_B)]\cdot[(\boldsymbol{s}\cdot\mathbf{h}(\mathbf{r}_A)]\right\rangle \tag{A.3}$$

where $< \cdot >$ denotes the expectation value (Slob & Weiss, 2011). Inspection of Equation (A.3) reveals that the difference between Green's function for the magnetic field and its complex conjugate projected in one direction and scaled by the power spectrum of sources is given by the correlation of the fields measured at two distinct points. These sources are required to be uncorrelated and volumetrically distributed due to the excitation in all directions. Transforming this expression into the time domain, the product between spectral power density and Green's function becomes a convolution operation, whereas the term $j\omega$ converts into a time-derivative. Hence, in the time domain, Green's function for magnetic field $\bar{\mathbf{H}}(\mathbf{r}, t)$ could be retrieved using

$$\left[\bar{\mathbf{H}}_B^*(\mathbf{r}_A,-t) - \bar{\mathbf{H}}_B(\mathbf{r}_A,t)\right] * F(t) = 2\mu_0 \frac{\partial}{\partial t}\left\langle [\boldsymbol{s}\cdot(\mathbf{H}(\mathbf{r}_B,t)] \otimes [\boldsymbol{s}\cdot\mathbf{H}(\mathbf{r}_A,t)]\right\rangle \tag{A.4}$$

in which *F(t)* is the autocorrelation of the noise. The symbols $\otimes$ and * denote correlation and convolution, respectively.

Figure (A.1, bottom) illustrates the imaginary component of the cross-correlation, or the EGF kernel in the right hand side of the Equation (A.3) for the double half-space model discussed in chapter two. The isocontours in blue and red demonstrate the positive and negative amplitudes of the EGF kernel, respectively. The figure shows that there is symmetry between positive and negative values; and thus, the amplitudes cancel out each other when summed over the sources. Therefore, only the real part of the cross-correlation shown in Figure (A.1, top)

remains in the summation. This confirms the theoretical findings summarized in Equation (A.3), since both sides of this equation leads to calculation of the imaginary components.

The numerical results in the second chapter sketched in Figure (1) are regenerated using the modified equations for the Green's function estimation. Figure (A.2, top) shows the contribution of sources as a function of distance for a line that connects the two receivers. In Figure (A.2, bottom), the numerical output of the EGF for a source located at *A* which is measured by receiver *B* is measured similar to the calculations shown in Figure (1, bottom).

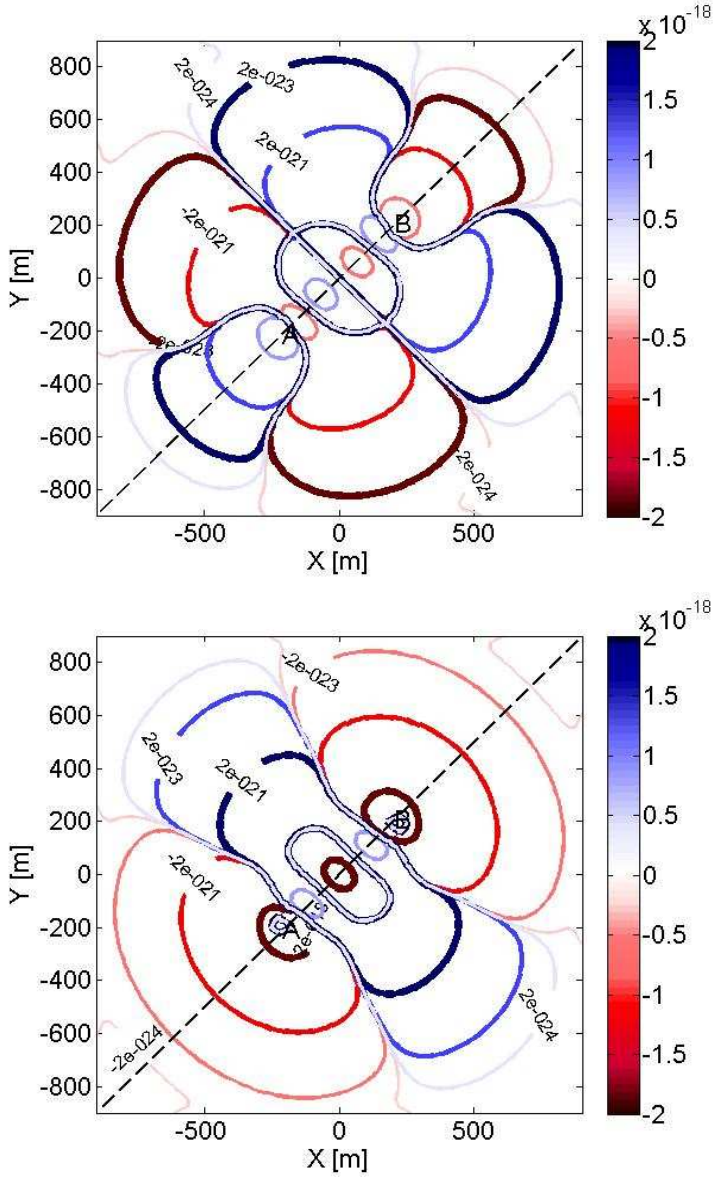

Figure A.1: Isocontours, represent those parts of the double half-space system whose co-located random sources contribute most to the EGF calculation for imaginary (top) and real (bottom) parts where receivers are located at $(-206.25, -206.25, -6.25)_A$ and $(206.25, 206.25, -6.25)_B$. The magnetic field throughout the area is computed using the FDM3D finite difference code developed by Weiss and Constable (2006).

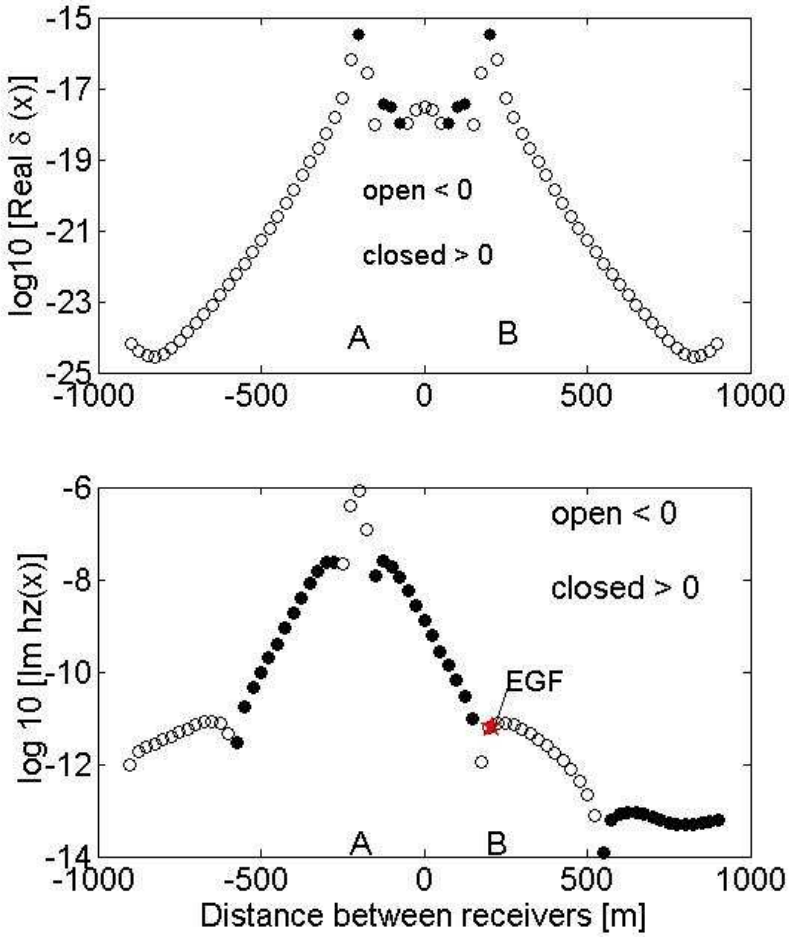

Figure A.2: (top) Relative contribution of noise sources δI to EGF estimation as a function of position along a line passing through two passive receiver locations *A* and *B*. (bottom) Finite difference (FD) (circle) and EGF (red star) calculated values of the vertical magnetic field at *A* due to a source $\mathbf{M_s} = \hat{z}\delta(\mathbf{r}\text{-}\mathbf{r}_B)$. Open and closed circles indicate FD-computed h_z at z = -6.25 m. Figures reproduced from the revised relation given in Slob & Weiss (2011).

Appendix B: Reducing the Computational Cost of the Jacobian for Diffusive Scalar Wavefields

Consider the general form of the diffusion equation given by Equation (4.2) defined in a finite domain where the Green's function G is replaced by the scalar wavefield u. Let's assume that the model parameter is equal to $\sum m_n\psi_n(x)$ which $\psi_n(x)$ is some basis function defined in terms of position x. I substitute $D(x) = \sum m_n\psi_n(x)$ in the Equation (4.2) and differentiate the equation with respect to the m_n:

$$-\frac{\partial}{\partial x}\left[\psi_n \frac{\partial u(x,\omega)}{\partial x} + \left(\sum_n m_n\psi_n\right)\frac{\partial}{\partial x}\left(\frac{\partial u(x,\omega)}{\partial m_n}\right)\right] + j\omega\frac{\partial u(x,\omega)}{\partial m_n} = 0. \qquad \text{(B.1)}$$

Following the development in McGillivray et al., (1994), the auxiliary form of the equation is considered as:

$$-\frac{\partial}{\partial x}\left[\left(\sum_n m_n\psi_n\right)\frac{\partial \tilde{u}(x,\omega)}{\partial x}\right] + j\omega\tilde{u}(x,\omega) = \tilde{s}(x,\omega). \qquad \text{(B.2)}$$

I multiply Equations (B.1) and (B.2) by the auxiliary function $\tilde{u}$ and $\partial u/\partial m_n$, respectively. Subtraction of these two equations from each other yields the following:

$$\frac{\partial}{\partial x}\left[\tilde{u}\,\psi_n\frac{\partial u(x,\omega)}{\partial x} + \tilde{u}\left(\sum_n m_n\psi_n\right)\frac{\partial}{\partial x}\left(\frac{\partial u(x,\omega)}{\partial m_n}\right) - \left(\sum_n m_n\psi_n\right)\frac{\partial \tilde{u}(x,\omega)}{\partial x}\frac{\partial u(x,\omega)}{\partial m_n}\right]$$
$$= \tilde{s}\frac{\partial u(x,\omega)}{\partial m_n} + \psi_n\frac{\partial u(x,\omega)}{\partial x}\frac{\partial \tilde{u}(x,\omega)}{\partial x}. \qquad \text{(B.3)}$$

Integrating this equation over $a < x < b$ results in the:

$$\left\{ \tilde{u}\,\psi_n \frac{\partial u(x,\omega)}{\partial x} + \tilde{u}\left(\sum_n m_n \psi_n \right) \frac{\partial}{\partial x}\left(\frac{\partial u(x,\omega)}{\partial m_n} \right) - \left(\sum_n m_n \psi_n \right) \frac{\partial \tilde{u}(x,\omega)}{\partial x} \frac{\partial u(x,\omega)}{\partial m_n} \right\} \Bigg|_{x=a}^{b}$$

$$= \int_a^b \left(\tilde{s} \frac{\partial u(x,\omega)}{\partial m_n} + \psi_n \frac{\partial u(x,\omega)}{\partial x} \frac{\partial \tilde{u}(x,\omega)}{\partial x} \right) dx. \qquad \text{(B.4)}$$

Letting a, $b \rightarrow \pm\infty$, respectively, the left hand-side of this equation vanishes. Hence, the Jacobian for the field u at a location x_0 ($\tilde{s}=\delta(x-x_0)$) is derived as

$$\frac{\partial u(x_0,\omega)}{\partial m_n} = -\int_a^b \psi_n \frac{\partial u(x,\omega)}{\partial x} \frac{\partial \tilde{u}(x,\omega)}{\partial x}\ dx. \qquad \text{(B.5)}$$

Therefore, the Jacobian for a scalar field u can be estimated through solving two forward calculations. Thus, the number of derivatives one needs to calculate increases with the number of data and is independent of the model size. Consequently, using these formulae reduces the cost of inversion which is especially important when large numbers of model parameters are desired.